Michigan Department of Transportation	MDOT Michigan Department of Transportation
Michigan Asphalt Paving Association	M A P A

DETERMINING THE CAUSES OF TOP-DOWN CRACKS IN BITUMINOUS PAVEMENTS

Michigan State University
Pavement Research Center of Excellence
Department of Civil and Environmental
Engineering
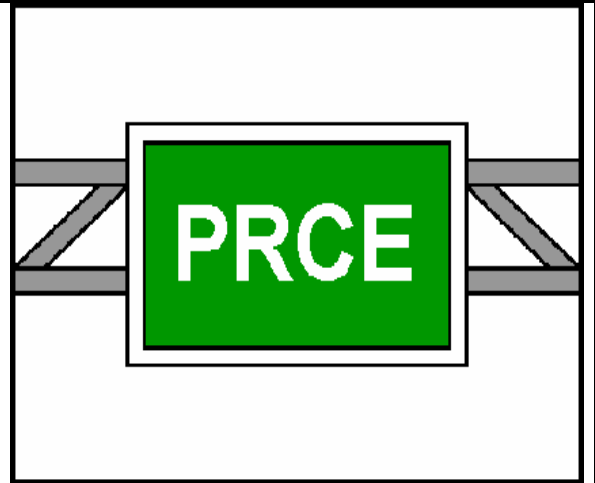East Lansing, Michigan 48824-1226
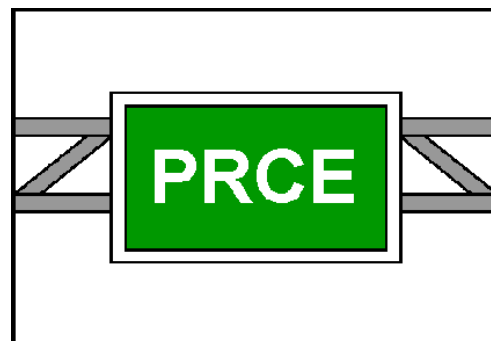
PRCE

August 2003

PAVEMENT RESEARCH CENTER OF EXCELLENCE Michigan State University Department of Civil and Environmental Engineering East Lansing, Michigan 48824-1226 (517) 355-5147 Fax (517) 432-1827 baladi@egr.msu.edu <u>Final Report</u>	PRCE

Report Number MDOT - PRCE - MSU -2003 -110	Contract Number)

Title and Subtitle **DETERMINING THE CAUSES OF TOP-DOWN CRACKS IN BITUMINOUS PAVEMENTS**	Report Date June 2002
Authors Gilbert Y. Baladi, Ph.D., P.E. Michael Schorsch Tunwin Svasdisant	TAG Chairperson Vernon T. Barnhart
Sponsoring Agencies Michigan Department of Transportation Construction and Technology Division Michigan Asphalt Paving Association	

Abstract

Top down cracks (TDC) are longitudinal or transverse cracks that initiate at the pavement surface and propagate downward and outward. They have been observed with increasing frequency on roads in Michigan. In this study, field and laboratory investigations were conducted to determine the factors that affect the load-induced tensile stresses at the pavement surface and the tensile strength of the AC mixes, and hence, affect the susceptibility of the pavement surface to TDC potential. Results of laboratory testing indicate that the AC mixtures used as surface courses in Michigan may be weakened by moisture damage. Further, segregation increases the susceptibility of the AC mixtures to moisture damage, and hence, increases TDC potential. Finally, a crack propagation model was developed as a function of pavement age and degree of segregation based on distress survey data.

Key Words: asphalt pavements, top-down cracks, asphalt mix, nondestructive deflection tests, segregation, and moisture damage.

ACKNOWLEDGEMENTS

TABLE OF CONTENTS

CHAPTER 4

DATA ANALYSIS 104

CHAPTER 5

SUMMARY CONCLUSIONS AND RECOMMENDATIONS........................217

REFERENCES 222

LIST OF TABLES

LIST OF FIGURES

CHAPTER 1

INTRODUCTION

1.0   BACKGROUND

Top-down cracks (TDC) are longitudinal and/or transverse cracks that initiate at the surface of asphalt pavements and propagate downward. They have been increasingly observed in flexible pavements throughout the state of Michigan. TDC are usually manifested as longitudinal cracks appearing just outside the wheelpaths. Over time, they form an extensive network of longitudinal cracks connected by short transverse cracks, which ultimately reduce the life of the pavement.

TDC are receiving increased attention throughout the world, in general, and in Michigan in particular. Some existing asphalt pavement design methods address conventional fatigue cracks, which initiate at the bottom of the asphalt layer and propagate upwards. No design method is capable of predicting or analyzing top-down cracking potential. Since TDC adversely affect pavement performance, understanding the factors that enhance their potential would be the first step that needs to be taken to improve the service life of the pavements.

2.0   OBJECTIVES

The objectives of this research are:

1. Identify the causes of TDC and the factors affecting top-down cracking potential.

2. Compare top-down and bottom-up cracking potentials.

3. Develop a model to describe the rate of TDC propagation.

To accomplish the above stated objectives, a research plan was designed and is presented in section 4.0 below.

3.0 HYPOTHESIS

Based on literature review and field observations of TDC, the following hypotheses were developed:

1. TDC are longitudinal and/or transverse cracks caused by high stress ratios at the AC surface course. Therefore, top-down cracking potential is affected by all the factors influencing the magnitude of the induced tensile stress and the tensile strength of the AC mix.

2. Mechanistic analysis can be used to ascertain the factors that result in high tensile stress at the pavement surface, while laboratory investigation can be used to determine the factors that result in low tensile strength of the mix.

To accomplish the study objectives and to verify the hypotheses, a research plan was drawn and is presented in the next section.

4.0 RESEARCH PLAN

To verify the hypotheses and to accomplish the objectives of this study, a research plan was developed and is shown in Figure 1.1. A detailed summary of each activity is presented below.
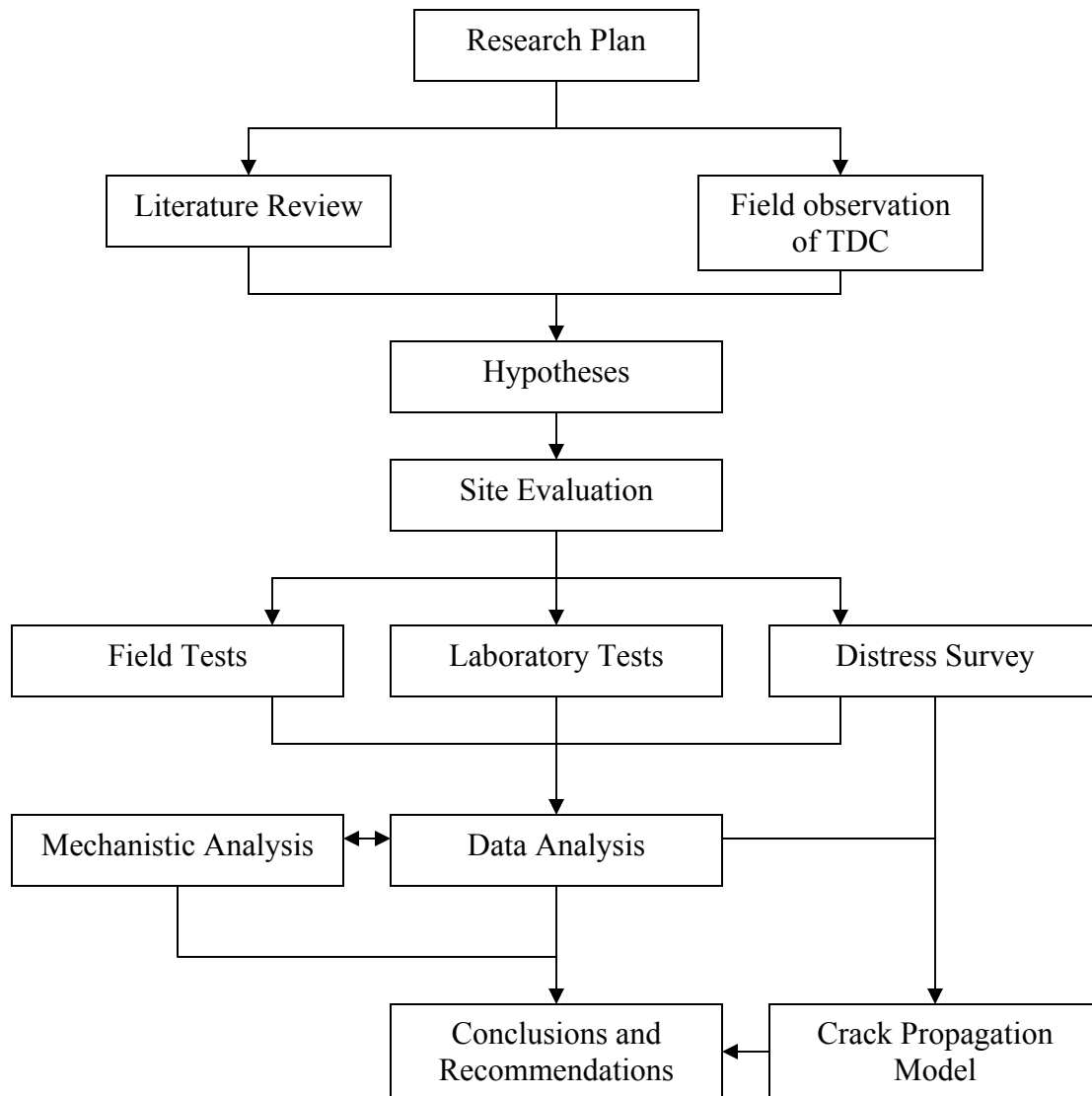
Figure 1.1 Flowchart of the research plan

4.1   Literature Review

A comprehensive literature review was conducted to determine the types of research activities that were undertaken to study the factors that affect the initiation and propagation of top-down cracking. Said review is presented in Chapter 2.

4.2   Field Investigation

The field investigation activities include:

1. Test Site Selection – In this activity, various pavements were examined to determine if they were possible candidates for the study. From the pool of candidates, 18 test sites were selected for evaluation.

2. Test Site Evaluation – The test site evaluation consisted of the following:

   ➢ Distress Survey – Included length and location of potential top-down cracks and cores taken over cracks to determine the types of cracks. Also cataloged other distresses to determine if top-down cracking occurs in conjunction with other distresses. On several test sites, multiple surveys were conducted over time to determine the rate of propagation of top-down cracks.

   ➢ Field Tests – The field tests included non-destructive deflection tests using the MDOT falling weight deflectometer (FWD), nuclear density measurements, core extraction, subsurface investigation (using hand augers) and measurements of the asphalt layer temperature, as a function of depth.

4.3   Laboratory Investigation

Laboratory testing consisted of sawing the cores to obtain test specimens, and subjecting those specimens to a battery of laboratory tests. These tests include the following:

1. Examining each pavement core and measuring its dimensions, including the thickness of each AC course, and the depth and width of cracks, if any. The total AC layer thickness was then calculated as the sum of the thicknesses of the AC courses. The results were used for the backcalculation of the pavement layer moduli.

2. Conducting specific gravity tests to determine the density of the individual asphalt courses in the pavement. The test results were used to observe density variation along and across the pavement.

3. Performing indirect tensile cyclic load tests (ITCLTs) to determine the laboratory resilient moduli of the AC courses, when possible. The test results were used to observe variations in moduli along and across the pavement as well as through the AC layer thickness.

4. Conducting indirect tensile strength tests (ITSTs) to obtain the indirect tensile strength of the AC courses, when possible. The results were used to calculate the applied stress to strength ratios.

5. Determining the asphalt content of the AC courses and the aggregate gradation of the various AC mixes using sieve analyses. The asphalt content and the recovered aggregate were obtained by incinerating the asphalt binder.

Additional tests were conducted in support of the above battery of tests (for example, theoretical maximum specific gravity tests to calculate the percent air voids of laboratory compacted specimens).

4.4   Data Analysis

Two fold analyses were conducted in this study; backcalculation of layer moduli using the measured FWD deflection data and mechanistic analyses of flexible pavements.

4.4.1   Analysis of the Measured FWD Deflection Data

The measured deflection data were analyzed in two ways as follows:

1. Determine the variations in the deflection data along and across the pavement at each test site. Results of the analyses were used to indicate the degree of uniformity in the structural capacity of the pavements.
2. Backcalculate the pavement layer moduli using the measured pavement deflections and cross-section data. The range of the resulting modulus values were used in the mechanistic analysis of the pavement structures.

4.4.2   Mechanistic Analysis of Flexible Pavements

Mechanistic analyses of flexible pavements were conducted to assess:

1. The temperature-induced tensile stresses in the AC layer.

2. The sensitivity of the load-induced tensile stresses in the AC layer to the factors affecting top-down and bottom-up cracking potentials. The results are used to compare the crack initiation potentials at the top and at the bottom of the AC layer.

3. The influence of various factors affecting the tensile strength of the AC mixes.

4.5 Validation of the Results of the Analyses

Results of the analyses were validated as follow:

1. The accuracy of the MICHBACK computer program was checked using forward and backward mechanistic analyses.

2. For the same pavement sections and load conditions, results of the analyses obtained from finite element programs (ABAQUS and MICHAPVE) were compared to those obtained from a well accepted closed form solution program (CHEVRONX).

3. The locations of the maximum tensile stress obtained from the analyses were compared to locations of TDC observed in the field.

4.6 Conclusions and Recommendations

Based on the results of the field and lab investigations, analyses, and the understanding obtained from the literature, the proper conclusions and recommendations will be made.

5.0 REPORT LAYOUT

This report is composed of five chapters:

Chapter 1 – Introduction

Chapter 2 – Literature Review

Chapter 3 – Field and Laboratory Investigation

Chapter 4 – Data Analyses

Chapter 5 – Conclusions and Recommendations

CHAPTER 2
LITERATURE REVIEW

1.0   INTRODUCTION

Considerable literature regarding the design and performance of asphalt pavements is available, most of which has been directed toward determining the pavement cross-section (design) and predicting pavement roughness, rutting and the conventional bottom-up fatigue cracking. Recently, top-down cracks (TDC) in flexible pavements have been widely reported by various researchers and highway agencies. Numerous studies were conducted to determine the causes of TDC. The researched topics included the effects of tire-pavement interaction, pavement cross-section, axle load, and the environment on top-down cracking potential.

This review of literature covers the following topics:

1. The causes and propagation of TDC in flexible pavements.

2. The factors affecting tensile stresses induced in the AC layer.

3. The factors affecting tensile strength of the AC mixtures.

2.0   TOP-DOWN CRACKS IN FLEXIBLE PAVEMENTS

Top-down cracks (TDC) are longitudinal and/or transverse cracks that initiate at

the pavement surface and propagate downward and outward as shown in Figure 2.1.

Based on examination of pavement cores, various researchers have reported that TDC

may propagate only within the AC surface course or throughout the entire depth of the

AC layer (Myers et al, 1998, Gerristsen et al, 1987, Uhlmeyer et al, 2000, Niederquell et

Figure 2.1 Top-down cracks in a rubblized pavement (US-131)

al, 2000, and Svasdisant et al, 2002). Field investigation has shown that most longitudinal TDC are located in the vicinity of the wheel paths (Myers et al, 1998, Gerristsen et al, 1987, Matsuno and Nishizawa, 1992, Niderquell et al, 2000, and Svasdisant et al, 2002). Also based on field observations, Svasdisant et al (2002) have divided the development of TDC into three stages as shown in Figure 2.2. The first stage consists of a single short longitudinal crack or cracks appearing just outside the wheel path. Over time, the second stage develops where the short longitudinal TDC grow longer and new sister cracks develop parallel to the original crack. Finally, the TDC evolve into the third stage where the parallel longitudinal TDC are connected via short transverse TDC.

TDC have been investigated and reported as a prominent distress in flexible pavements in various countries including Japan, Kenya, South Africa, France, and the Netherlands (Matsuno and Nishizawa, 1992, Wambura et al., 1999, Hugo and Kennedy, 1985, Duzauts and Rampal, 1987, and Gerritsen et al, 1987). In the United States, TDC are increasingly reported as a major distress in flexible pavements and either are being investigated or have been investigated in several states including Florida, Michigan and Washington (Meyers, 1998, 1999, 2001, Svasdisant, 2001, Neiderquell, 2000, and Uhlmeyer, 2000). Most of the investigations are related to the causes of TDC in flexible pavements while few address the propagation of TDC. These two topics are reviewed in the sections below.

3.0   CAUSES OF TDC

Several causes of TDC have been studied and reported in the literature. These
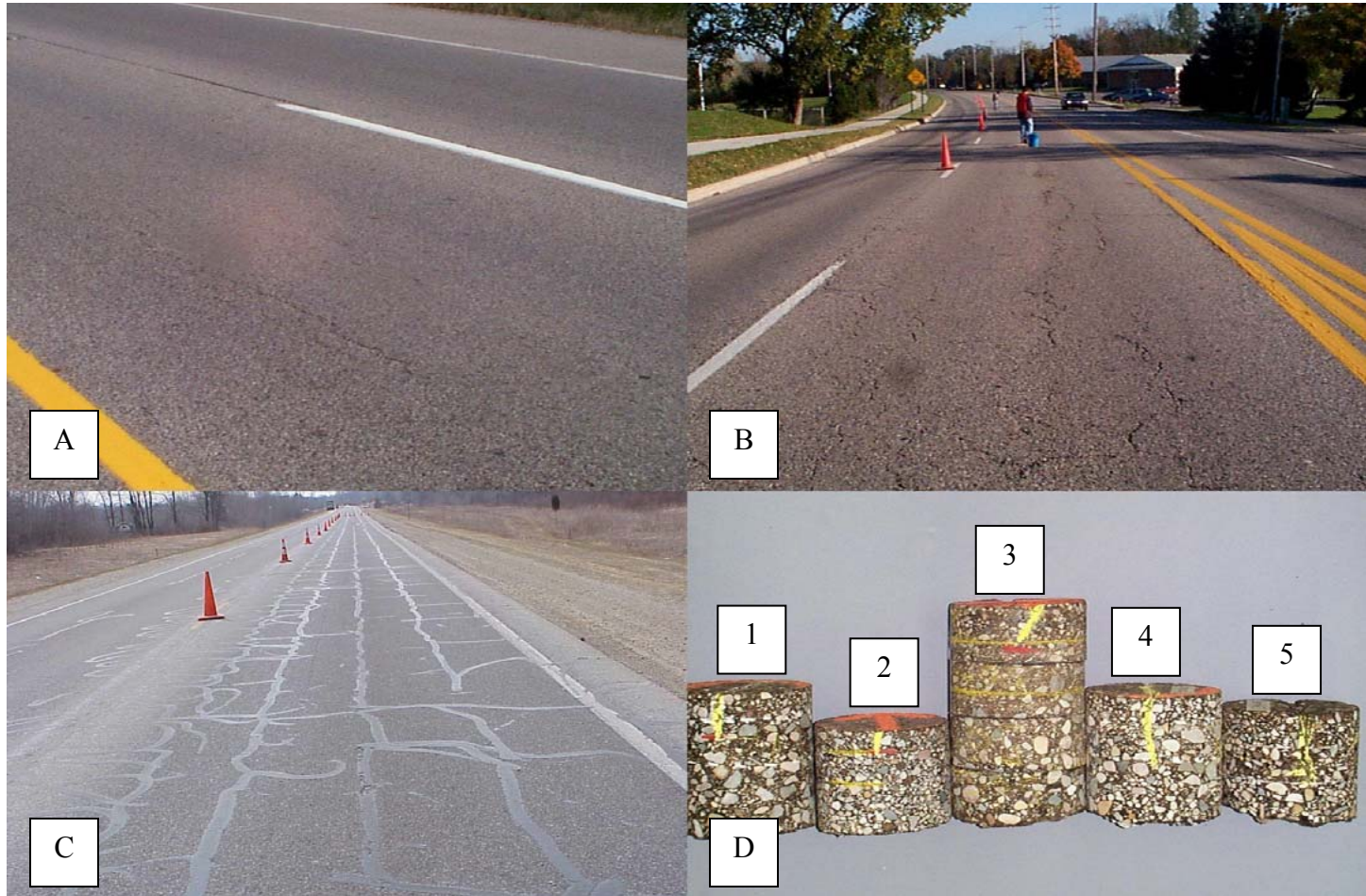
Figure 2.2 Photographs showing the development of Top-Down Cracking (A = Stage 1, B = Stage 2, C = Stage 3) and cores showing TDC, core 1- I-96, 2- M-20, 3- Marsh Road, 4- M-37, and 5- I-194

include:

1. Load-induced stresses and strains.

2. Thermal stresses.

3. Aging of the AC binder.

4. Segregation in the AC mix.

Various researchers including Myers et al (1998) concluded that TDC are caused by tensile stress rather than shear stresses. Since the majority of the longitudinal TDC are found in the vicinity of the wheel paths, the load-induced tensile stresses and strains in the vicinity of the tire-pavement contact areas are the most commonly studied causes of TDC.

Molenaar (1984) used the CIRCLY multi-layer computer program to analyze the effects of tire-pavement vertical and lateral contact stresses (inward shear stresses) on TDC. He concluded that high surface tensile strains induced at the edge of the tire are the cause of TDC. Further, his results indicated that thicker and softer AC layer (at high temperatures) on top of a stiffer base layer increases top-down cracking potential. Similarly, in the Netherlands, Gerritsen et al (1987) used the CIRCLY computer program to analyze the tensile stresses induced at the pavement surface due to vertical and lateral contact stresses. They have found that the load-induced tensile strains at the edge of the tire in pavements with bound bases (stiff base) are high enough to initiate TDC. They added that thermal stresses and aging of the AC binder could also enhance top-down cracking potential.

Groenendijk (1998) used the 3-Dimensional (3-D) finite element computer program, CAPA, to analyze the load-induced surface tensile stresses at the pavement

surface. He employed the three components of the tire-pavement contact stresses; vertical, lateral, and longitudinal contact stresses, to simulate different loads and different inflation pressures. He concluded that the combined influence of the non-uniform tensile contact stress and the aging of the AC at the surface could result in critical tensile stress at the surface rather than the bottom of the AC. Note that, the values of the contact stresses used in Groenendijk's analyses were measured in South Africa using the Vehicle-Road Surface Pressure Transducer Array (VRSPTA). More details of the South African measurements are presented in the tire-pavement interaction section.

The effects of the vertical and lateral contact stresses of radial and bias ply tires on the induced tensile stresses at the tire-pavement contact areas were studied by Myers et al (1998, 1999 and 2001). They concluded that:

1. Lateral contact stresses (inward shear stresses) induce high surface tensile stresses in the pavement at the edges of bias ply tires and cause TDC, Myers et al (1998). This conclusion was based on shear stresses data that were measured by Jacobs' (1996) for bias ply tires.

2. Lateral contact stresses (outward shear stresses) at the outer ribs of radial tires induce high surface tensile stresses under the outer ribs, which are the causes of TDC, Myers et al (1998). This conclusion was based on shear stresses data that were measured by Pottinger (1992) for radial tires. The difference in this and the first conclusion regarding the direction of the shear stress and its locations stems from the fact that Myers et al used two different sets of data. According to Myers et al (1999), the later conclusion is more accurate. Note that the data presented in Myers et al (1999) indicate that the maximum surface tensile stress occurs under

the center of the outer rib.

3. The tensile stresses under the tire ribs are localized phenomenon at the AC surface and they dissipate rapidly throughout the depth of the AC layer. Hence, the pavement structural characteristics such as moduli of the AC and base layers have insignificant effects on the magnitude of the induced surface tensile stresses, Myer et al (1998) and (1999). This also supports the conclusion made by Matsuno and Nishizawa (1992) (as stated in the next paragraph).

4. Radial and wide-base radial truck tires induce higher surface tensile stresses relative to bias ply tires. As a result, they are more detrimental to the pavement than the bias ply tires, Myers et al (1999).

5. Load-induced tensile stresses away from the edges of the tire are the driving mechanism for the propagation of TDC. The pavement layer stiffnesses and the location of the tire relative to TDC have significant impact on the magnitude of the load-induced tensile stresses away from the tire, Myers et al (2001).

In Japan, Matsuno and Nishizawa (1992) reported that longitudinal TDC were found mostly along the wheel paths and they are absent in shadowy areas (such as under bridges). They conducted finite element analysis of flexible pavements at high temperatures and made the following two conclusions:

1. The load-induced tensile strains at the edge of the tire cause TDC initiation. This conclusion supports that of Molenaar (1984) and Gerritsen et al (1987).

2. The pavement cross section had little effect on the surface tensile strains, which agrees with the conclusion made by Myers et al (1998), Myers et al (1999) and contradicts that of Uhlmeyer et al (2000), which is stated below.

Uhlmeyer et al (2000) studied of the causes of TDC in conjunction with the Washington State Department of Transportation. They observed that TDC occur in and around the wheel paths in pavements 3 to 8 years old with AC thickness of more than 6.3-inch (16-cm). Hence, they concluded that pavement thickness has an effect on the initiation of TDC, which contrasts the conclusions made by Myers et al (1998), Myers et al (1999), and Matsuno and Nishizawa (1992).

A different mechanism of top-down cracking was reported by Bensalem et al (2000). They used a finite element model to analyze the load induced stresses and strains in the pavement. They reported that:

1. The load-induced shear strains at the edge of the wheels in the vertical plane are higher than the load-induced lateral tensile strains at the same location on the pavement surface. Therefore, the shear strains on the vertical plane play an important role in TDC initiation and propagation.

2. The magnitude of the shear strains on a vertical plane at the edge of the wheel path decreases rapidly with depth. This explains some of the field observations that TDC propagate through the upper AC courses.

3. Decreasing the thickness of the AC layer results in increasing the load-induced shear strains. Hence, thinner AC layers are more vulnerable to TDC. This is in contrast with the conclusions of Uhlmeyer et al (2000) stated above.

4. Differential stiffness in the AC layer due to temperature gradient and thermal tensile stresses may have important roles in the initiation and propagation of TDC.

Note that, the first three conclusions represent a new view of the causes of TDC.

The commonly agreed on causes of TDC initiation and depth are the load-induced tensile stresses or tensile strains at the edge of the wheel paths on the pavement surface, thermal stress and aging of the asphalt binder (Myers et al, 1999, Molenaar, 1984, De Beer et al, 1997), and that TDC were more likely to initiate in pavements with relatively thick AC layer (Uhlmyer, 2000, and Molenaar 1984). In addition, field data collected during the field investigation of this report and other studies (Myers et al, 1998) do not support the first two conclusions of Bensalem et al (2000). Cracks caused by shear failure along a vertical plane should be inclined at an angle from the vertical plane. The cracks found in numerous cores extracted from 18 different test sites in this study showed vertical crack alignment.

The agreements and contradictions regarding the effect of the pavement cross-section on the induced tensile stress at the pavement surface were further scrutinized by examining the types of analyses conducted by various researchers. Eventually, all sides have made the proper conclusions relative to their input data and results. To clarify, the tensile stress induced at the pavement surface due to the inward/outward shear is independent of the pavement cross-section. However, the vertical load-induced tensile stress at the pavement surface is a function of the pavement cross-section. The above implies that when only the effects of the vertical contact stress are analyzed, the results would show a significant role of the pavement cross-section. On the other hand, analyses of the inward and outward shear stresses would result in an opposite conclusion.

Thermal stresses and strains were also investigated as possible causes of TDC. Dauzats and Rampal (1987) reported that most of the TDC found in their test sections in southern France were located on the centerline side of the slow lane. They calculated thermal stresses, strains, and tensile strength of the AC using equations developed by Shahin (1977). Results of their study indicated that the surface tensile strains due to low temperatures could initiate TDC after a number of repeated

33

temperature cycles. Similarly, Roque and Ruth (1990) used MEAPs/CRACK3 computer program to study TDC initiation potential in flexible pavements due to thermal and load-induced stresses. They concluded that the combination of thermal and load-induced stresses is the cause of TDC, especially under critical conditions such as fast cooling rate or spring thaw with more emphasis placed on the former condition than the latter one.

In South Africa, Hugo and Kennedy (1985) also investigated thermal stresses as a possible cause of TDC. They calculated the thermal stresses in the AC layer using the CRACK computer program. They also studied the impact of several AC mix characteristics including aggregate gradation, air voids, and asphalt cement contents on the aging of the AC mix. They concluded that TDC could initiate due to load-associated or non-load associated causes (thermal stress and/or aging) or combination thereof.

In Kenya, Wambura et al (1999) tested cores obtained from pavements exhibiting TDC. They concluded that the recent AC mix design procedure in Kenya allowed high air voids in the mix at the time of construction. As a result, the AC binder experienced severe aging, which caused the initiation of TDC at the AC surface. Similarly, Malan et al (1988) related aging of the AC binder to TDC initiation. They studied premature surface cracking in South Africa and concluded that gap-graded AC mixes are more vulnerable to aging and TDC than dense graded mixes. They also reported that viscosity of the AC binder has a significant influence on TDC potential. They stated that TDC potential decreases when high viscosity binders are used for low traffic loads and low viscosity binders are used for high traffic loads.

To this end, it becomes obvious that there is no consensus in the literature regarding the causes of TDC in flexible pavements. Several factors that have been hypothesized as the causes of TDC are summarized in Table 2.1. As can be seen, the noted causes of TDC can be summarized into two categories as follows:

1. High tensile stresses and strains induced by load, temperature, and other factors

    such as construction.

2. Low tensile strength or fatigue resistance of the AC materials due to the AC mix

    properties, aging or hardening of the AC binder and poor construction practice

    such as compaction.

Some researchers only emphasized the effects of one category while others emphasized the combined effects of some factors from both categories. In the study for this report at Michigan State University, it was hypothesized that TDC are fatigue cracks caused by high stress ratios (high tensile stresses and/or low tensile strength) at the AC surface. Hence, to determine the causes of TDC, it is necessary to address the factors that affect the tensile stress and the tensile strength at the AC surface. In addition, this study addresses the potentials of fatigue crack initiation at the top, as well as, at the bottom of the AC layer. Hence the induced tensile stresses and the available tensile strengths at the bottom and at the top of the AC layer are considered. Therefore, in the next sections, available literature addressing the factors affecting tensile stresses and tensile strengths in the AC layer are reviewed.

Table 2.1 A summary of conclusions made by various investigators

References	Conclusion
Svasdisant et al (2002)	TDC are located at the edge of the wheel path and they develop in three stages
Molenaar (1984) Gerritsen et al (1987) and Matsuno and Nishizawa (1992)	➢ The tire-pavement vertical and lateral contact stresses cause TDC. ➢ Soft AC surface on top of stiff base causes TDC.
Matsuno and Nishizawa (1992)	The pavement cross section had little effect on the surface tensile strains
Uhlmeyer et al (2000)	TDC occur in and around the wheel paths in pavements 3 to 8 years old with AC thickness of more than 6.3-inch (16-cm).
Myers et al (1998), (1999) and (2001)	➢ Lateral contact stresses (inward shear stresses) induce high surface tensile stresses under the first tire rib at the edges of radial tires and cause TDC. ➢ The pavement structural characteristics such as moduli of the AC and base layers have insignificant effects on the magnitude of the induced surface tensile stresses. ➢ Radial and wide-base radial truck tires induce higher surface tensile stresses relative to bias ply tires. ➢ Load-induced tensile stresses away from the edges of the tire are the driving mechanism for the propagation of TDC.
Groenendijk (1998)	The combined influence of the non-uniform tensile contact stress and the aging of the AC at the surface could result in critical tensile stress at the AC surface instead of at the AC bottom.
Dauzats and Rampal (1987)	Surface tensile strains due to low temperatures could initiate TDC after a number of repeated temperature cycles.
Roque and Ruth (1990)	The combination of thermal and load-induced stresses is the cause of TDC especially during fast cooling rate and the critical spring thaw condition.
Hugo and Kennedy (1985)	TDC initiate due to load- or non-load associated causes (aging) or combination.
Wambura et al (1999) and Milan et al (1988)	Severe aging causes the initiation of TDC at the AC surface.
Malan et al (1988)	➢ Gap-graded AC mixes are more vulnerable to aging and TDC than dense graded mixes. ➢ Viscosity of the AC binder has a significant influence on TDC potential.

4.0   FACTORS AFFECTING THE TENSILE STRESS IN THE AC LAYER

In this section, the following factors affecting the load-induced tensile stress in the AC layer are reviewed:

1. Thickness and modulus of each AC course and each pavement layer and the differential stiffness between the AC courses and the pavement layers.

2. Wheel load and configuration (single and dual).

3. Tire-Pavement Interaction

4. Temperature.

4.1   Thickness and Modulus of Each Pavement Layer

Flexible pavement designs are accomplished by using either empirical or mechanistic-empirical approaches or both. Some empirical procedures (such as the AASHTO 1993) are based on the ride quality (serviceability index) whereas most mechanistic-empirical procedures are based on limited rut depth and pre-determined fatigue life. The common output of all pavement design methods is that thicker pavements are required for higher traffic levels or longer performance period. The implication of this is that the pavement layer thicknesses (especially the AC layer thickness) affect the ride quality, rutting and fatigue cracking. For example, higher AC layer thicknesses reduce the tensile stress/strain at the bottom of the AC layer and the compressive stress/strain at the top of the subgrade thereby causing increases in the fatigue life and decreases in rut potential. Similarly, the moduli and thicknesses of the AC and the other pavement layers have significant impact on pavement performance relative to fatigue life, rut depth and ride quality.

In reality, pavement performance is affected by numerous factors that can be divided into various categories as follows:

1. Pavement design factors such as layer thicknesses and their properties.

2. Construction factors.

3. Environmental factors.

4. Traffic factors, which are typically accounted for in the pavement design phase.

While the last three factors are addressed elsewhere in this chapter, the pavement layer thicknesses and moduli are addressed below.

The effects of the AC layer thickness on the load-induced stresses vary and depend on the type of the contact stresses. For example, the tire-induced transverse and longitudinal shear stresses are independent of the thicknesses and moduli of the pavement layers including the AC layer (Myers et al, 1999 and Molenaar, 1984). On the other hand, the effects of the vertical contact stress on the induced tensile, shear and compressive stresses in the pavement layers are a function of the thicknesses and moduli of the pavement layers and the modulus ratios between the AC courses and between the pavement layers (Myers et al, 1999).

Svasdisant et al (2002) used 3-D finite element analyses to study the induced tensile stress at the pavement surface due to vertical contact stress. He concluded that high modulus ratios between the AC surface and the AC base courses (high differential stiffness in the AC layer) result in higher induced tensile stress at the pavement surface. Such differential stiffness could be the product of the asphalt mix design practice, aging, temperature gradient or a combination thereof. The idea of higher differential stiffness or modulus ratio was mentioned several times by other researchers; some mentioned it as

the differential stiffness within the AC layer (Roque et al, 2002) and some others

mentioned it as the differential stiffness between the AC layer and the aggregate base

(Molenaar, 1984). Roque et al (2002) concluded that differential stiffness (higher

modulus at the pavement surface) in the AC layer due to temperature gradient and aging

results in higher tensile stresses at the crack tip. They concluded that temperature

gradients accelerate the TDC propagation rate. Molenaar (1984) has shown in his

analyses (using the CIRCLY computer program) that high modulus ratio between the

base and AC, or stiff base layer, could result in the shift of the maximum load-induced

tensile strain from the bottom of the AC layer to the pavement surface.

4.2   Wheel Load and Configuration

In conventional flexible pavement designs and analyses, the wheel load is
assumed to be vertical and uniformly distributed over a circular area and the resulting
tire-pavement contact stress is assumed to be equal to the tire inflation pressure
(Yoder and Witczak, 1975 and Huang, 1993). Based on the two assumptions,
numerous articles have been published addressing the sensitivity of the pavement
responses to variations in the wheel load and the tire inflation pressure.

Researchers such as Bensalem et al (2000) and Huang (1993) addressed the

effects of single and dual wheel loads on pavement responses. Their results, which

agreed with numerous other researchers, indicate that a single wheel load induces higher

stresses and strains at the surface and at the bottom of the AC layer relative to dual wheel

load. Other researchers studied the effects of non-uniform tire-pavement contact stresses

and the shape of the contact area on pavement responses. Still others incorporated tire-

pavement interaction (vertical, transverse and longitudinal stresses) into the analyses of

flexible pavements, De Beer et al (1997) Molenaar (1984), Groenendijk (1998), and

Myers et al (1998) and (1999). Their general conclusions are presented in section 4.3 of

this chapter. One significant conclusion was that made by DeBeer et al (1997) who stated that, for conventional flexible pavement design and analyses, the uniformly distributed vertical contact stress assumption is adequate when the AC layer is relatively thick (more than 4- in). This conclusion is based on the observation that the effects of non-uniform vertical contact stress on the tensile stress at the bottom of a thick AC layer are not significantly different than that of uniform vertical contact stresses.

4.3   Tire-Pavement Interaction

Almost all vehicles use rubber-based pneumatic tires. The principal functions of a rubber tire include (Clark, 1981):

1. Transferring the load from the vehicle to the pavement.

2. Providing wear resistance by being tough and minimizing cuts, tears and cracks by being resilient.

3. Providing good friction between the tire and the pavement surface.

4. Resisting the bruising impacts due to defects on the roadways.

The truck fleets in the United States and other countries use a wide variety of pneumatic tires. Unless otherwise specified, in the rest of this report the technical term "pneumatic tire" is referred to as "tire".

Previous research has focused on the effects of tire imprint on the stress/strain in the pavement. These analyses, which were summarized in section 4.2, concentrate on the stress and strain at the bottom of the AC layer, or in several cases, the stress and strain at the surface of the pavement due to various tire contact areas. Directly under the tire however, significant stress/strain may be induced by the interaction of the tire structure

with the pavement. The tire structure varies between different types of tires and includes variations in size, inflation pressure, structure, tire-treads and grooves, and tire stiffness. In general, two tire types are heavily used; radial and bias ply with a high percentage of the truck fleet using radial tires.

According to Myers et al (1999), the differences in the structures between the radial and bias ply tires include:

1. The tire-tread structure of radial tires is more rigid than the bias ply tires.

2. The wall structure of the bias ply tires is more rigid than the radial tires.

The factors affecting tire-pavement contact area and contact stresses, and their effects on the pavement responses (stresses, strains and deflections) are presented in the next subsections. Note that the term "tire-pavement interaction" refers to the following:

1. The shape and size of the tire-pavement contact area.

2. The magnitude and distribution of the tire-pavement contact stresses including the vertical contact stress, the lateral or transverse contact stress (perpendicular to the tire traveling direction), and the longitudinal contact stress (parallel to the tire traveling direction).

Unless otherwise specified, in the rest of this report, the term "contact stresses" is used to reference all three contact stresses between the tire and the pavement.

4.3.1   Tire-Pavement Contact Area

The shape and size of the tire-pavement contact area is affected by various factors including tire type (e.g., radial versus bias ply), tire inflation pressure, axle load, carcass stiffness, the number and dimensions of the ribs and grooves, vehicle speed, steering, and the pavement micro and macro textures (Clark, 1981). De Beer and Fisher, (1997) obtained tire-prints of bias, radial and wide-base

radial tires at different loads and inflation pressures. Figure 2.3 shows the tire

imprints of the bias, radial and wide based tires measured by De Beer and Fisher .

Examination of their tire prints indicates that:

1. For radial tires, the shape of the contact area can be simulated by a
    rectangle with almost a constant width and a variable length. The constant
    width is equal to the tread width whereas the length increases with
    increasing wheel load and decreasing inflation pressure.

2. For bias ply tires, the shape of the contact area is rectangle with rounded
    ends. The width and the length are variables and function of the wheel
    load and inflation pressure.

3. The tire print area of both tire types can be divided into two zones; the
    actual contact area under the ribs and the non-contact area under the
    grooves.

Groenendijk (1998) made similar observations regarding the shape of the

contact area of radial tires.
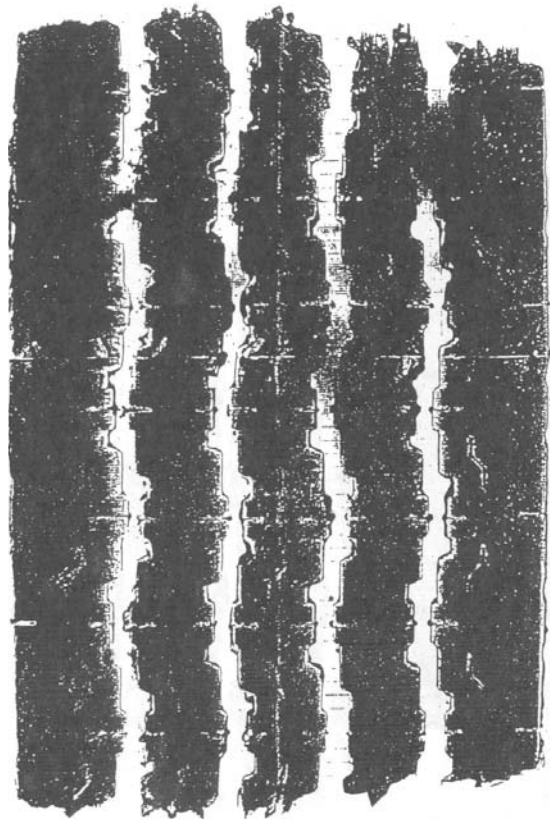
a) Tire print of a radial tire   b) Tire print of a bias-ply tire
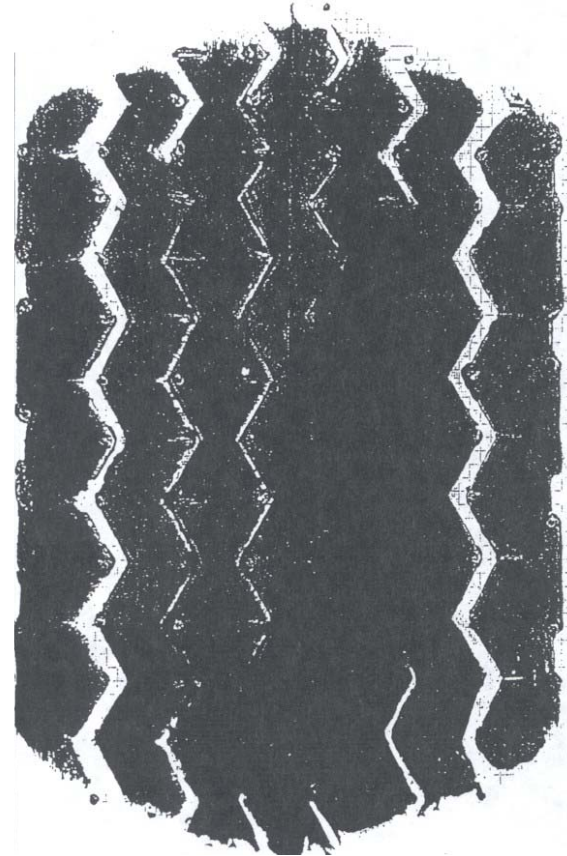
Figure 2.3 Tire prints of a radial and a bias ply tire having 9.2-kip wheel load and 104-psi inflation pressure (De Beer and Fisher, 1997); (the scale is in mm)

4.3.2   Tire-Pavement Contact Stresses

Numerous researchers have studied the tire-pavement contact stresses using several approaches including:

1. Theoretical approach based on tire mechanics (Clark, 1981, Teilking and Roberts, 1987, and Schapery and Teilking, 1977)

2. Finite element analyses (Schapery and Teilking, 1977, and Roque et al, 2000)

3. Measurement of the contact stresses (Markwick and Starks, 1940, De beer et al, 1997, Himeno et al, 1997, and Teilking and Abraham, 1994)

Results of their studies indicated that the tire-pavement contact stresses are affected by various parameters including:

1. Tire type and structure

2. Wheel load and inflation pressure

3. Tire motion (stationary or rolling)

The effects of the above factors are addressed below.

As stated earlier, one of the functions of the pneumatic tire is to transfer load from the vehicle to the pavement. The load can transfer to the tire-pavement interface through the tire wall at the edge of the tire and through the pressurized air over the tire tread as shown in Figure 2.4. Since a bias ply tire has a more rigid wall than a radial tire, a higher portion of the load is transferred through its wall than through the wall of a radial tire. Such difference in the load transfer mechanisms affects the distribution of the tire-pavement contact stresses.

Load transferred through wall structure

Load transferred through wall structure

Tire wall

Tire inflation pressure (IP)

Tire grooves

Tire tread

Tire ribs

Pavement surface

Vertical contact stress (VCS)
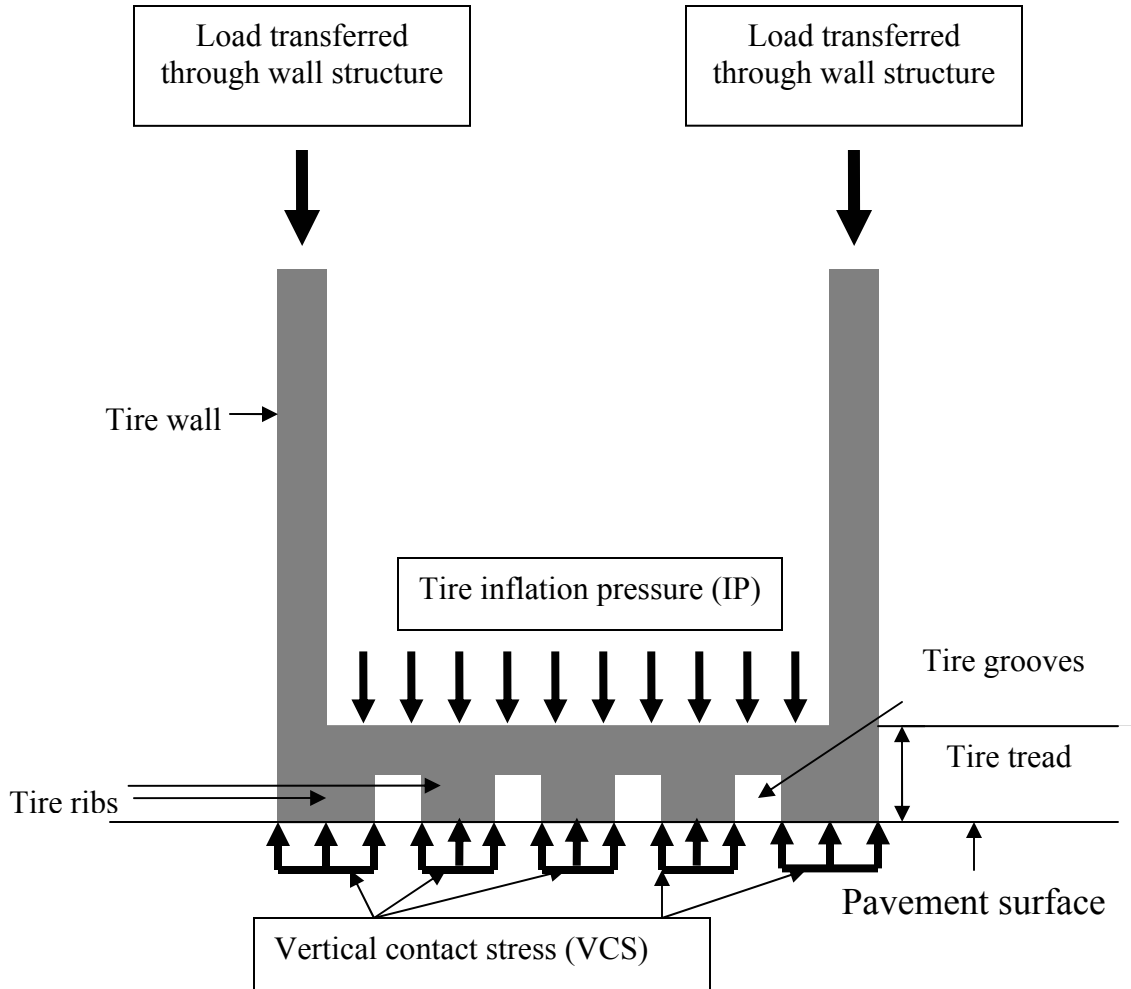
VCS ~ (IP)*(Total tire imprint area/Total contact area of the ribs)

Figure 2.4 Load transfer mechanisms of a tire

Myers et al (1999) addressed the effect of the structures of bias ply and radial tires on the tire-pavement contact stresses. They stated that the relatively rigid wall and flexible tread structures of the bias ply tires allow the tire ribs to pull in toward the center of the tire inducing inward shear stress at the pavement surface. The tire industry refers to this phenomenon as the pneumatic effect of the tire. The pneumatic effect of radial tires is much less than that of bias ply tires because of the relatively rigid tread structures and the flexible wall of the radial tire. Such horizontal rib expansion away from the radial tire center induces an outward shear stress at the pavement surface. Myers et al (1999) referred to this phenomenon as the "Poisson effect" of the tire tread structure. A schematic showing the stresses under a truck tire are shown in Figure 2.5. Due to the more rigid tread structure, the Poisson effect is more prevalent in radial tires than in bias ply tires. This agrees with the findings by Markwick and Starks (1940). They reported that the rib-hardness has significant impact on the friction properties between the tire and the pavement and hence on the inward and outward shear stresses. Harder ribs produce higher contact stresses. It is also important to note the effect of these behaviors on pavement stresses and strains. The pneumatic effect tends to cause compressive radial stresses at the pavement directly underneath the tire. Radial tensile stresses are created at the edge of the tire by the tendency of the pavement to be pulled towards the center of the tire. In contrast, the Poisson's effect has the tendency to pull the pavement apart under the ribs of the radial tire. Therefore, areas of high tensile stress are generated under the imprint of the tire.

Tire grooves

Tire ribs

Tire inflation pressure

Transverse inward shear
(Toward the center of the tire)

Transverse outward shear
(Away from the center of the rib)

Transverse inward shear
(Toward the center of the tire)
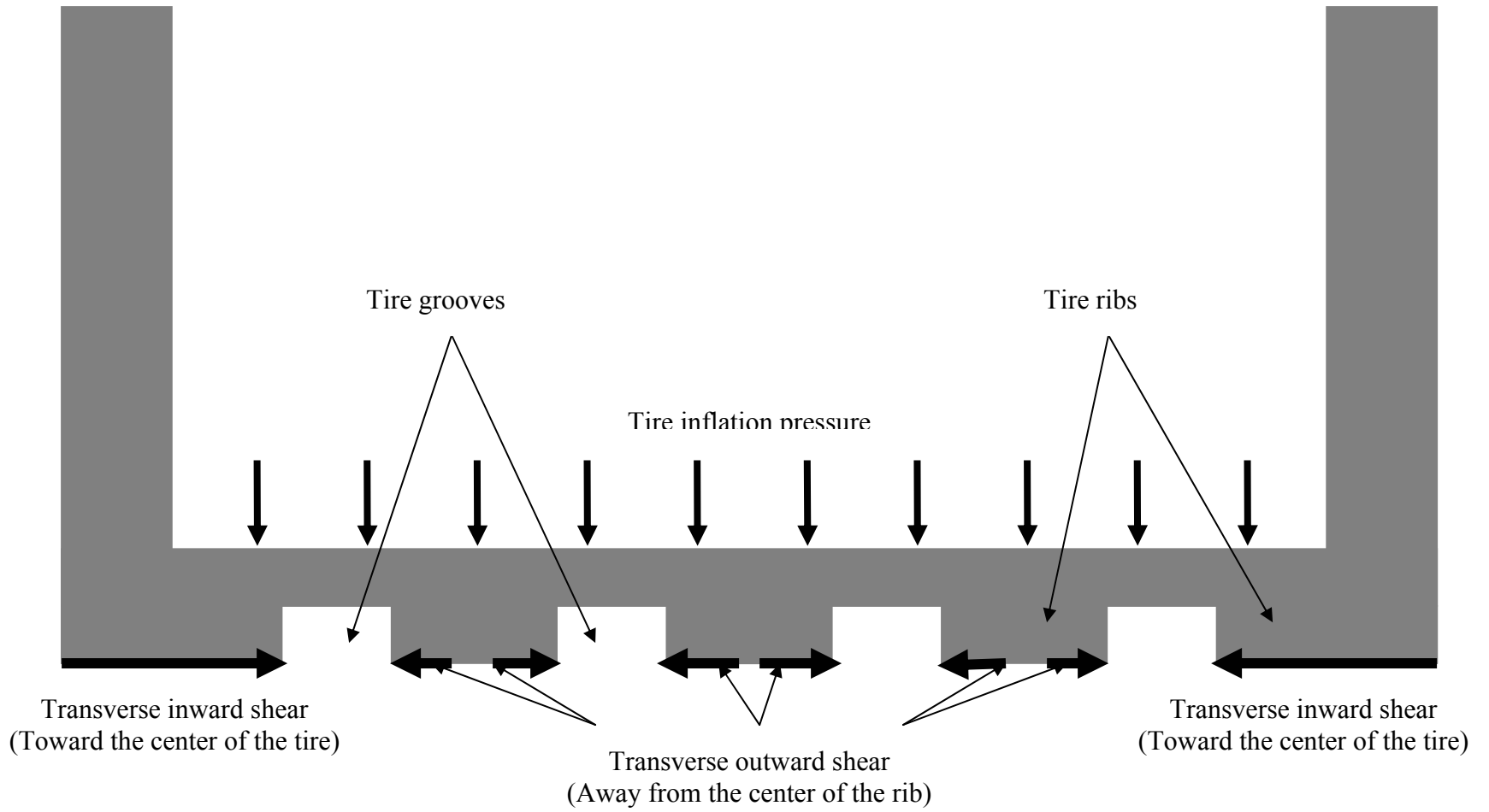
Figure 2.5 Detail of stresses induced by truck tire treads

In the Netherlands, Groenendijk (1998) investigated the contact stresses of new, used and trimmed (smooth tire/no groove due to tire wear) radial tires. His findings relating to new radial tires are similar to those of Myers et al (1999). Relative to trimmed radial tire, Groenendijk reported that the maximum induced shear stress is an inward shear located at the tire edge.

Roque et al (2000) used the ABAQUS finite element computer program to model the structure of a radial tire and analyze the tire-pavement contact stresses. They reported that:

1. The calculated contact stresses were similar to those that were measured earlier using actual radial tire and sensors.

2. The magnitudes of the transverse contact shear stress are highest at the outer ribs near the edge of the tire.

3. The transverse contact shear stress is not affected by the thickness of the AC layer and the modulus ratio of the AC and aggregate base layers.

Many researchers have investigated the effects of wheel load and inflation pressure on the contact stresses. Tielking and Abraham (1994) measured the vertical contact stresses of radial and wide-base radial truck tires with different wheel loads and inflation pressures. Their measurements indicated that both higher wheel load and higher inflation pressure result in overall higher contact pressure but minimal increase in the vertical contact stress at the center of the tire.

Markwick and Starks (1940) measured the contact stresses of stationary and rolling tires. They concluded that the maximum vertical contact stresses are about 1.5 times higher than the inflation pressure. They explained that the tire-

carcass stiffness and the reduced contact area due to the tire grooves are the causes of the increase in the vertical contact stresses relative to the inflation pressure.

Similar results regarding the location of the maximum vertical contact stresses were found by De Beer et al (1997). They measured tire-pavement contact stresses due to slow rolling smooth tires (no grooves) using Vehicle-Road Surface Pressure Transducer Array (VRSPTA). Their results indicated that:

1. The vertical contact stresses were neither equal to the tire inflation pressure nor uniformly distributed throughout the contact area.

2. The maximum vertical contact stresses were found to be a function of both the tire inflation pressure and the wheel load. The tire inflation pressure controls the vertical contact stress at the tire center whereas the wheel load control the contact stress at the tire edges.

3. Overloaded and/or under inflated tire cause high vertical contact stress at the tire edge, which may exceed the inflation pressure by a factor of three.

4. The direction of the measured transverse (lateral) contact stress is toward the tire center; inward shear stress

5. The longitudinal (parallel to the wheel traveling direction) contact shear stress is the lowest among the three contact stresses.

De Beer and Fisher (1997) also measured the contact stresses of bias and radial truck tires with various wheel loads and inflation pressures. Their results indicated that:

49

1. The average vertical contact stress is higher than the tire inflation pressure by about 20 percent.

2. The vertical contact stress is higher than the transverse and the longitudinal shear stresses as shown in Figures 2.6 through 2.8. These findings regarding the magnitude of the contact stresses agreed very well with the measurements made by De Beer et al (1997).

3. The maximum contact stresses (vertical, lateral and longitudinal) of both bias ply and radial tires are highly related to the wheel load. They showed no relationship with the tire inflation pressure as shown in Figures 2.6b and 2.7b. Himeno et al (1997) made a similar conclusion by stating that the vertical contact stress is more sensitive to the wheel load than to the tire inflation pressure.

4. The maximum lateral contact stress of the bias ply tire is higher than that of a similar size radial tire having the same inflation pressure and carrying the same load as shown in Figure 2.8. This finding contradicts that of Myers et al (1999) who concluded that radial tires induce greater lateral contact stresses relative to bias ply tires. Groenendijk (1998) also measured the contact stresses of new and used radial tires with various wheel loads and tire inflation pressures using the VRSPTA. Based on his measured data, he concluded that:

    1. The contact area is rectangular in shape with a constant width equal to the tire tread width.
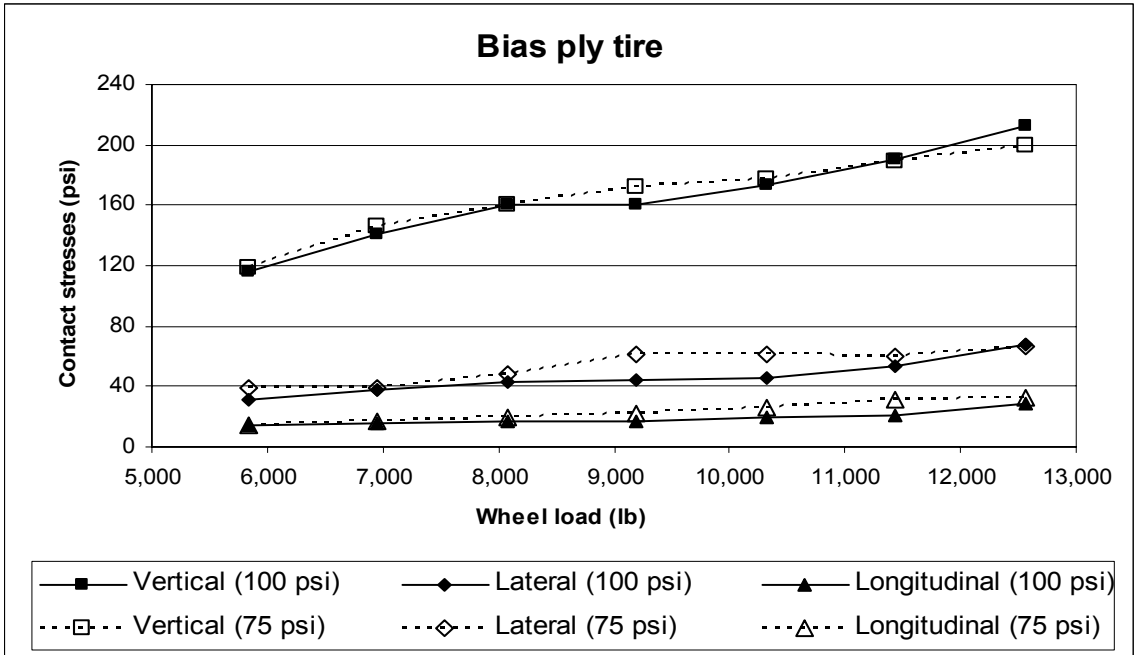
a) Various wheel loads
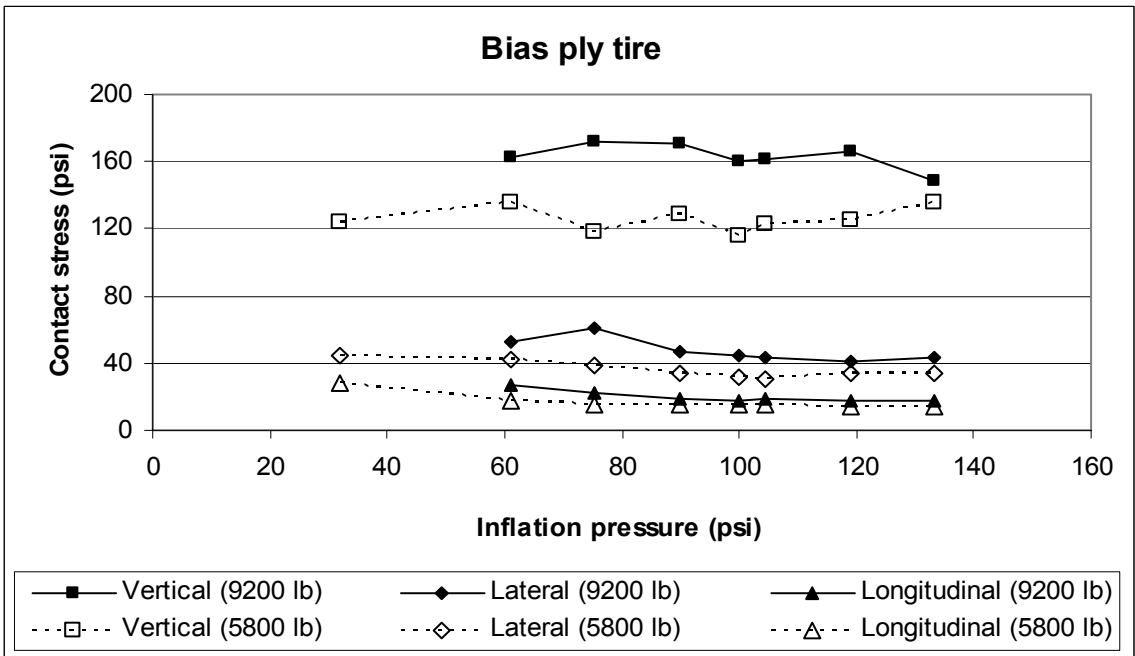
b) Various inflation pressures

Figure 2.6 Plots of vertical, lateral and longitudinal contact stresses of a bias ply tire with various wheel loads and inflation pressures (De Beer et al, 1997)
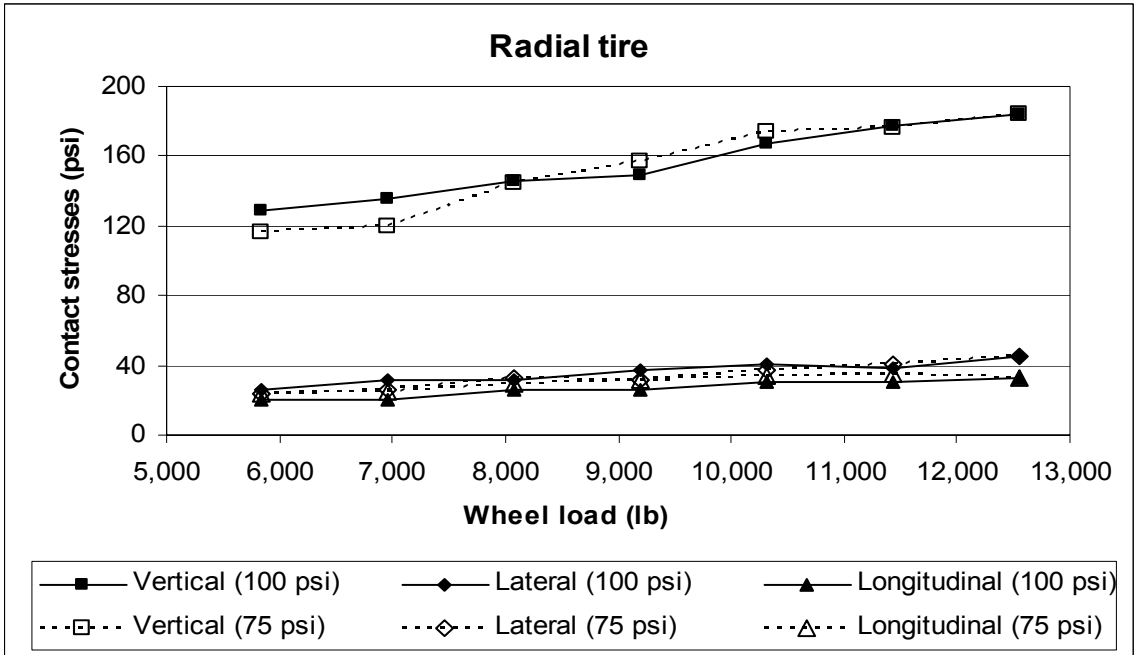
a) Various wheel loads
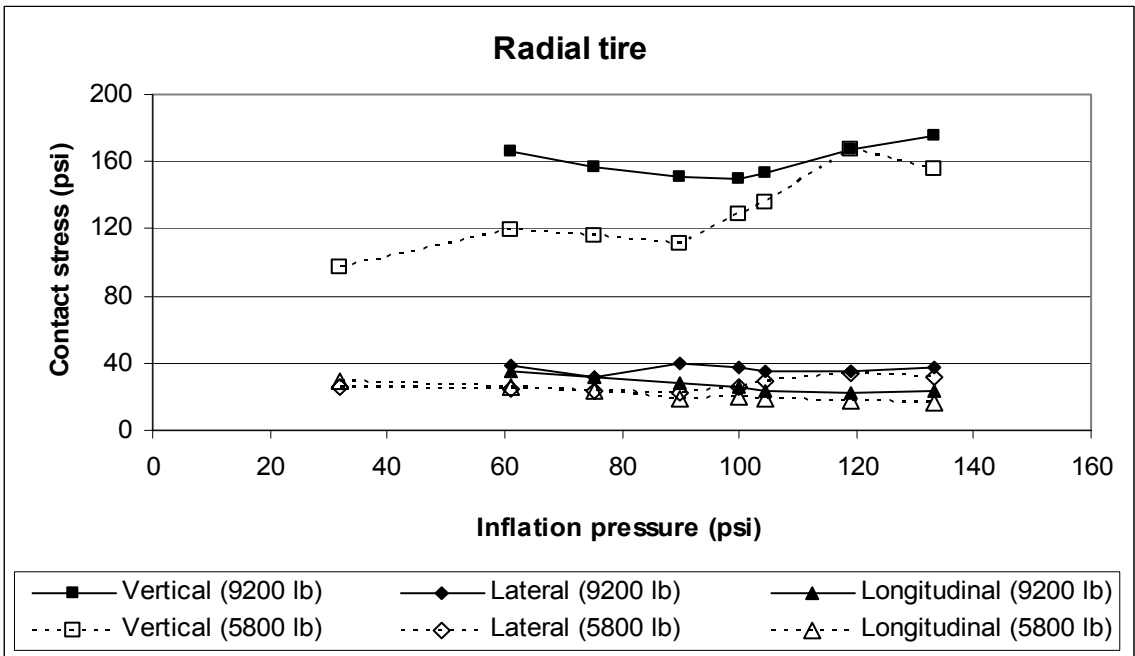
b) Various inflation pressures

Figure 2.7 Plots of vertical, lateral and longitudinal contact stresses of a radial tire with various wheel loads and inflation pressures (De Beer et al, 1997)
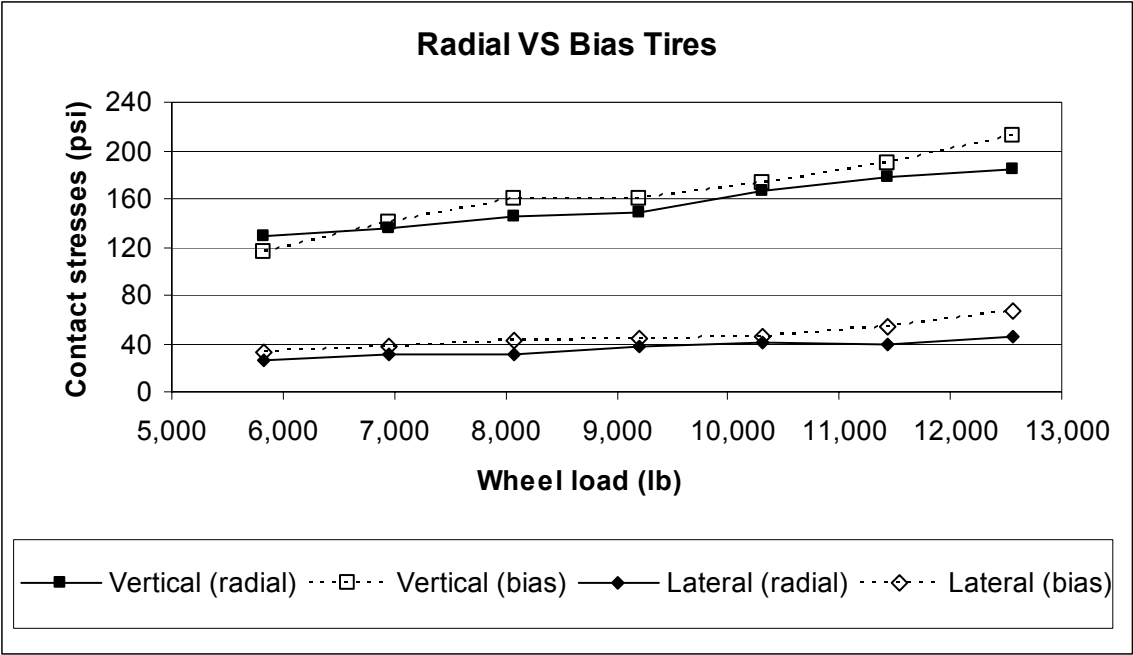
a) Various wheel loads
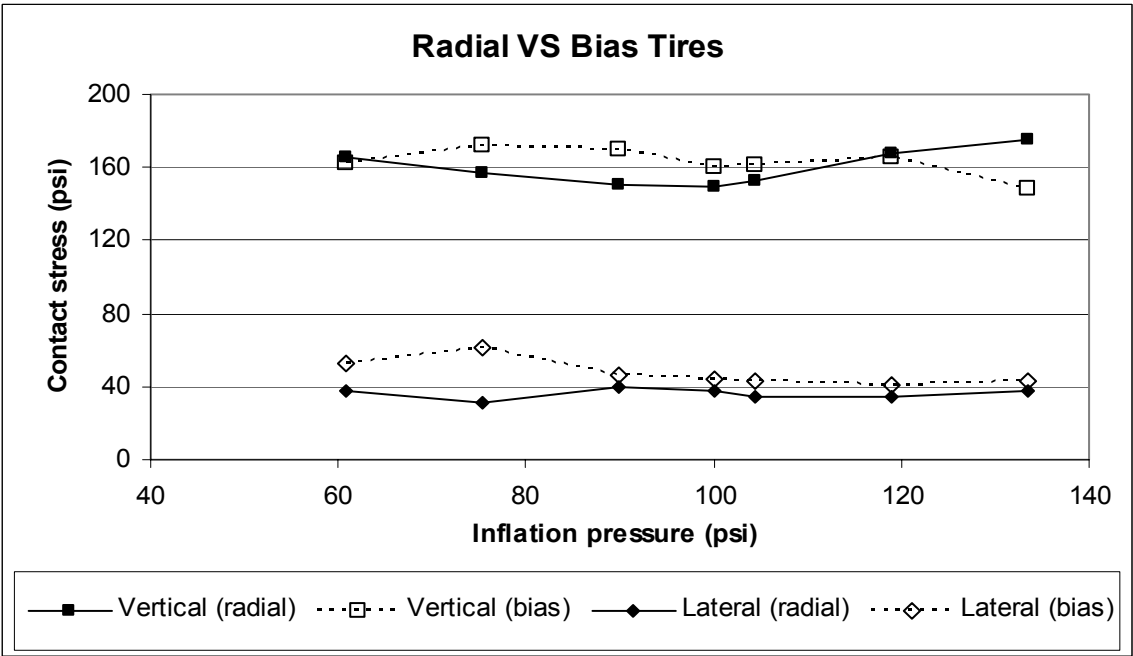
b) Various inflation pressures

Figure 2.8 Comparisons between the vertical and lateral contact stresses of a radial tire and of a bias ply tire at various wheel loads and inflation pressures (De Beer et al, 1997)

2. The maximum shear stresses were only 20 percent of the maximum vertical contact stresses.

3. The maximum shear stress could be higher than 50 percent of the tire inflation pressure.

4. In most cases, the maximum transverse (lateral) shear stress was an outward shear stress under each rib located in the middle of the tire.

5. For tires whose ribs were trimmed to a groove depth of 1.5 mm or less, the maximum transverse shear stresses were inward shear located at the edge of the tire.

The differences in the tire-pavement contact stresses of stationary and rolling tires were addressed by Markwick and Starks (1940). They stated that under a stationary tire, the shear stresses are symmetrical around the center of the tire. The shear direction is toward the center of the tire and its values decrease to zero at the center of the tire. Under a rolling tire, the shear stresses are no longer symmetrical. The resultant shear force on the pavement is in the opposite direction of the vehicle traveling direction.

Schapery and Teilking (1977) applied the mechanics of pneumatic tires in finite element analyses and developed various computer programs (TIRELOAD, TIRETRAN, TIREFOUR and TIREFRIC) that are capable of analyzing the tire-induced contact stresses, braking forces (parallel to the traveling direction) and sliding force (perpendicular to the traveling direction) due to maneuvering of the vehicle. The required program inputs include various properties of the pneumatic

tire. This made the programs very difficult to use since the tire industry considers such data as proprietary information.

4.3.3   Pavement Responses

Bonaquist et al (1989) also studied the effect of different tire inflation pressures on the pavement responses using the accelerated load testing facility (ALF). They reported that increasing tire pressures by 20 percent causes a 2 to 10 percent increases in the pavement surface deflections and in the strains at the surface and at the bottom of the AC layer.

Huhtala et al (1989) used strain gauges and pressure cells to measure the pavement responses due to different tire types and tire inflation pressures. They concluded that:

1. As the tire inflation pressure increases, the stresses and strains induced in the pavement increases thereby delivering higher damage to the pavement.

2. The tire-pavement contact pressure is highest at the center of the tire for truck tire and at the edges of the tire for passenger car tires.

3. The sensitivity of the pavement responses to tire types and tire pressures is inversely proportional to the thickness of the AC layer.

The effects of tire motion on the pavement responses were also investigated by Siddharthan and Sebaaly (1999) using the 3D-MOVE computer program, which is capable of analyzing flexible pavement responses due to moving wide-base tires. Their results indicated that the load-induced strains in the AC layers decrease significantly due to moving-loads. These results agreed with the field

measurements conducted by Chatti et al (1996) and (1997) and Dai et al (1997) that the measured strains at the mid- depth and at the bottom of the AC layer decrease as the truck speed increase.

Siddharthan et al (2002) also used the 3D-MOVE computer program to analyze pavement responses due to wide-base tires. They concluded that incorporation of the inward shear stresses in the analyses does not significantly affect the pavement responses. Note that, the magnitude of the inward shear stresses used in their analyses were about 12 to 16 percent of the magnitude of the maximum vertical contact stresses which is lower than the 20 percent reported by Groenendijk (1998).

4.3.4   Pavement Temperature

Thermal stresses are results of the contraction of the AC layer due to low pavement temperatures and the restraining force caused by the friction between the AC and base layers (Zubeck and Vinson, 1996). Based on the above explanation, it can be seen that the maximum thermal stress is a function of the contraction force of the AC due to cold temperatures and the frictional force between the AC and base layers. Shahin (1977) developed a design system to minimize the asphalt concrete thermal cracks. In his calculation, Shahin (1977) used the following equation to predict the thermal stresses.

$$\Delta\sigma(t,\Delta T) = S(t,\Delta T) * \alpha(\overline{T}_\Delta) * \Delta T \qquad (2.1)$$

Where: $\Delta\sigma(t,\Delta T)$ = the increase in a thermal stress for a given loading

time t and a temperature interval of ΔT,

$S(t,\Delta T)$ = asphalt concrete modulus at a given time t and the

mean value of a temperature interval of ΔT, and

$\alpha(\overline{T}_\Delta)$ = thermal coefficient of contraction of the asphalt concrete

at the mean value of the temperature interval ΔT.

As can be seen from the equation, Shahin predicted thermal stress based on the contraction force in the AC, which is a function of the properties of the asphalt binder, temperature and the cooling rate. Note that the thermal coefficient of contraction and expansion of the asphalt concrete is not a constant value and it varies with the temperature of the asphalt (Littlefield, 1967). The value of the coefficient of thermal contraction of asphalt mixtures at any temperature can be obtained from the equation reported by Hiltunen and Roque (1994) and is a function of the properties of the AC binder and aggregate and their volumetric relationship as shown in equation 2.2 below.

$$\alpha_{MIX} = \frac{VMA * B_{AC} + V_{AGG} * B_{AGG}}{3 * V_{TOTAL}} \qquad (2.2)$$

Where: α_{MIX} = linear coefficient of thermal contraction of the asphalt

mixture $(1/^{\circ}C)$

B_{AC} = volumetric coefficient of thermal contraction of the asphalt

cement in the solid state $(1/^{\circ}C)$

B_{AGG} = volumetric coefficient of thermal contraction of the

aggregate $(1/^{\circ}C)$

V_{MA} = percent volume of voids in the mineral aggregate

V_{TOTAL} = 100 percent

Temperature and the properties of the AC mix affect the magnitude of the thermal stress induced in the pavements. In their study of thermal and load-induced stresses as possible causes of TDC in flexible pavements, Roque and Ruth (1990) concluded that low temperatures and fast cooling rates could result in high thermal stress. Further, in the same study, they also concluded that the high thermal stresses combined with load-induced stresses can result in TDC initiation in flexible pavements.

5.0   TENSILE STRENGTH OF AC MIXTURES

The tensile strengths of the AC mixtures are affected by several factors including:

- ➢ the AC mix design;

- ➢ temperature and temperature gradient within the AC layer;

- ➢ particle segregation;

- ➢ compaction; and

- ➢ stress state (confinement).

The effects of each of these factors on the tensile strengths of AC mixtures are presented in the subsections below.

5.1   AC Mixture Design

To improve the ride quality, decrease noise and bleeding/flushing potential, the AC surface course is typically designed to have smaller maximum aggregate size (higher aggregate surface area) and slightly lower asphalt binder content relative to other AC courses. The lower AC content and smaller aggregate sizes results in thinner asphalt film coating the aggregates and hence, higher stress concentration in the AC film (Harvey and Tsai, 1996). This leads to lower overall tensile strength of the AC mix. Furthermore, the low AC content tends to increase the percent air voids, which also results in low tensile strength (Button et al, 1990). Similarly, Jung and Vinson (1993)

showed that the fracture strength of asphalt mixtures is most sensitive to the air void contents and aggregate types, and Zubeck and Vinson (1996) showed that the tensile strength of an AC mix is a direct function of its fracture strength.

Brown and Bassett (1990) studied the effect of the maximum aggregate size on the properties of AC mixes by conducting several tests including indirect tensile strength tests. They concluded that increasing the maximum aggregate size resulted in increased tensile strengths of the AC specimens.

In a study by Baladi and Harichandran (1987), the relationship between the indirect tensile strength of the AC mix with AC mix design parameters was investigated. One hundred and twenty six AC specimens were subjected to indirect tensile strength test using a newly designed indirect tensile test apparatus. In all 126 indirect tensile strength tests, the test variables were:

1. Percent air voids of the test specimens (AV); the value of AV ranged from three

    to about seven percent.

2. Kinematic viscosity of the asphalt binder (KV); the value of KV was 159, 212, or

    270 centistokes.

3. Gradation of the aggregates (GRAD); the value of GRAD was 1 for gradation A

    or 2 for gradation B.

4. Aggregate angularity (ANG); the value of ANG was 2 for rounded aggregates, 3

    for 50/50 mix of round and crushed limestone, and 4 for crushed limestone.

5. Test temperature (TT); the tests were conducted at temperatures of 44, 77 or 140

    ^{o}F.

Equation 2.3 presented below was developed for indirect tensile strength (INTS) from the test results using regression analysis. Equation 2.3 has a coefficient of correlation (R^2) of 0.997 and standard error of 0.078.

$$\ln(\text{INTS}) = 8.0160 - 0.03363\text{TT} - 0.2605\text{AV} + 0.0509\text{ANG} + 0.0007676\text{KV} \quad (2.3)$$

Based on the above equation, it can be seen that the tensile strength of the AC mix is a function of the properties of the AC binder (KV), aggregates (ANG) and how the two materials were combined in the AC mix (AV). It can also be concluded, from equation 2.3 and from other literature, that AC surface courses are typically (but not intentionally) designed to possess lower tensile strength than AC base courses. Note that the above equation also shows that tensile strength of the AC mix is also affected by temperature of the AC. Further discussion regarding the effect of the temperature on the tensile strength of AC mix is presented below.

5.2 Compaction

Rickards et al (1999) summarized the objectives of compaction of asphalt mixtures as follows:

1. Achieve optimum density.

2. Achieve aggregate particle contact to provide adequate deformation (shear) resistance.

3. Minimize air void contents.

4. Provide crack-free pavement surface to reduce permeability of the AC layer.

The second objective (increasing the AC mix resistance to shear deformation) can be achieved, if and only if, the tensile strength of the AC mix is increased. Marker (1967) explained that by moving aggregates particles closer together, the compaction helps the asphalt film around the aggregates to develop the inter-particle cohesion force. The increase in particle cohesion force results in increasing tensile strength of the AC mix.

5.3 Particle Segregation

Segregation of the asphalt concrete mixtures in pavements may lead to premature distress, such as stripping, raveling, rutting, and longitudinal and fatigue cracking. These distresses are usually caused by the decreased tensile strength or durability of the mix. Segregation may occur during stock piling and handling, hot mix asphalt production, truck loading and unloading, transportation and/or lay down operations. The amount of segregation that occurs may be exacerbated by such factors as aggregate type and mixture design (Khedaywi and White 1996, Williams et al 1996).

Chang (2000) stated that particle "segregation refers to the separation of coarse and fine aggregates in an asphalt mix. The mechanism of segregation is based on the motion of aggregates. Whenever aggregates are moved, there is a tendency for segregation to occur." He adopted the following Michigan Department of Transportation definition of particle segregation "areas of non-uniform distribution of coarse and fine aggregate particles in a bituminous pavement that are visually

identifiable or can be determined by other methods." He defined three degrees of segregation as follows:

1. Light – The fine matrix in place, more stone than the surrounding mat.

2. Medium – Lack of surrounding fine matrix, significantly more stone than the

   surrounding mat.

3. Heavy – Stone against stone, little or no fine matrix.

Khedaywi and White (1996) conducted laboratory investigations on segregated mixture that they had manufactured in the laboratory. They conducted indirect tensile strength tests and fatigue tests, and noted that the tensile strength and fatigue life are adversely affected as the segregation becomes more severe, i.e., the gradation becomes coarser. Brown et al (1989) conducted a similar study on segregation of asphalt mixtures in Georgia. The results of their indirect tensile strength tests correlated well with those conducted by Khedaywi and White. In both cases, the increase in segregation results in high air voids. In both studies however, the levels of segregation of the mixes tested were very severe. Differences of up to 75% passing the 3/8-in sieve were present in the mixes, as are visible on Figures 2.9 and 2.10.

Chang (2000) investigated 25 test sites located along various pavement projects exhibiting segregation. At each test site, his investigation consisted of:

1. Conducting nuclear density tests to determine the density and asphalt content of

   the asphalt mats using the one minute readings.

2. Extracting pavement cores and determining their densities in the laboratory.

3. Mapped the boundaries of the various degrees of segregation and segregation-

   related distresses. For some sites, the distress surveys were conducted 6 times

   within a 30-month period while for other sites, 5 distress surveys were conducted.
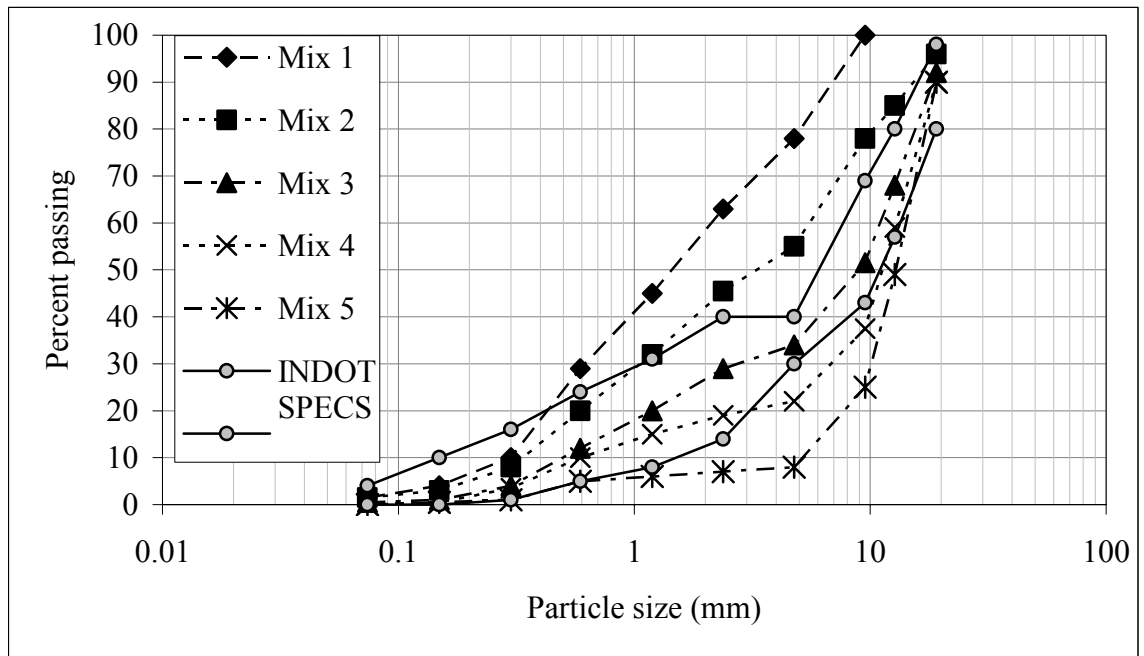
Figure 2.9 Gradations for different levels of segregation (after Khedaywi and White, 1995)
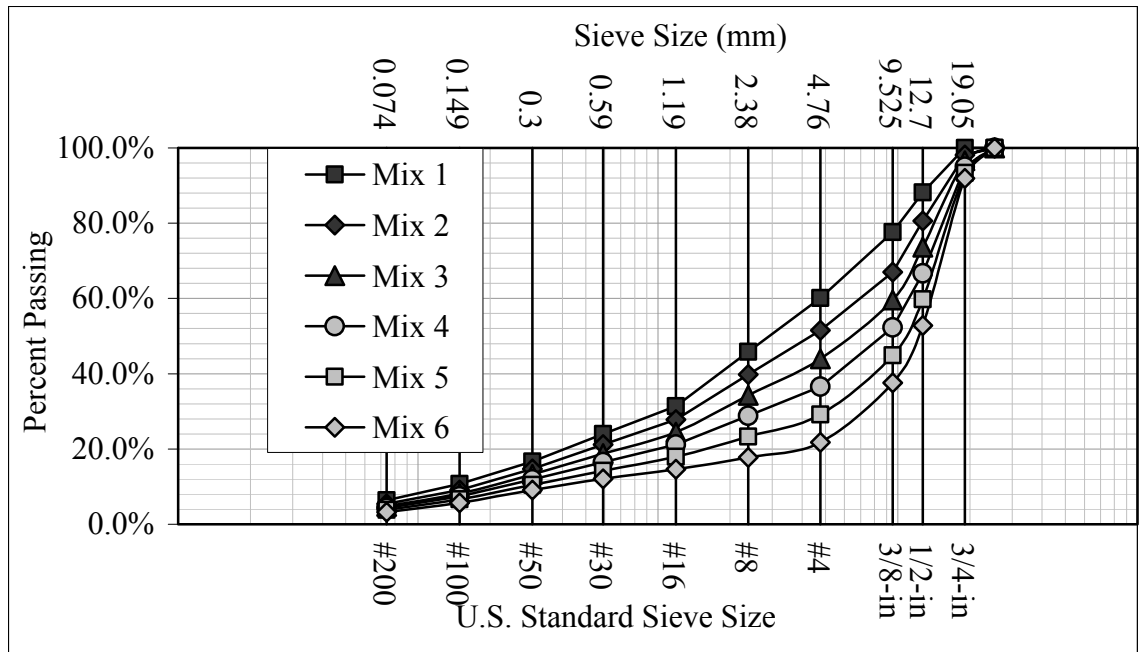
Figure 2.10 Gradations used by Brown et al (1989) for different levels of segregation

His data indicated that raveling and cracking are segregation-related distresses, which results in reduction in the pavement service life. He reported that areas exhibiting medium to heavy degrees of segregation can be expected to lose 56 to 73 percent of their design life due to raveling and cracking. More recently, Svasdisant et al returned to the sites investigated by Chang, and through coring, confirmed that these cracks were TDC (Svasdisant et al 2001). The reduction in the pavement life is mainly due to the low asphalt contents and high percent air voids of the segregated mix. These factors reduce the tensile strength and the fatigue lives of the mixtures. Brown et al (1989), and Khedaywi and White (1995) also drew similar conclusions that the tensile strengths of the AC mixtures decrease with increasing segregation. Again, it should be noted that the gradations observed in the field by Chang deviated from the mix design, even in the most severe cases, by a significantly lesser degree than those mixes tested by Khedaywi and White and Brown et al.

Williams et al (1996) use the PURWheel tracking device to test AC mixtures experiencing various degrees of segregation. They used the techniques employed by Khedaywi and White (1995) to produce in the laboratory five levels of mixture segregation: very fine, fine, control, coarse, and very coarse and made the following conclusions:

1. The asphalt content decreases and the percent air voids increases significantly

    from very fine to very coarse segregation.

2. Segregated mixtures exhibit significant loss in performance when tested in the

    PURWheel tracking device.

These conclusions were expected based on prior literature.

Ultimately, segregation provides and ideal situation in which TDC can initiate and propagate. In regards to the material itself, other researchers have linked TDC to gap graded mixes, low tensile strength, and aging of the asphalt binder. Each is present on segregated pavements where the gradation has unintentionally been made coarser, the tensile strength has been lowered, and the low density and high air voids promote accelerated aging and decreased durability.

5.4   Temperature and Temperature Gradient

It is well known that asphalt binders and AC mixtures are temperature susceptible materials and their properties including viscosity, elastic modulus and tensile strength vary with temperature. Mohammad and Paul (1993) manufactured specimens using different AC binders and levels of compaction effort, and conducted indirect tensile strength tests at varying temperatures. Their results indicate that lower temperatures and the higher densities result in higher indirect tensile strengths of the AC mixtures.

Chapuis and Gatien (1995) conducted four-point flexion tests to investigate the effect of temperature on the tensile strength of conventional and polymer modified AC mixtures. Their results indicated that the tensile strengths of the polymer modified AC mixtures are significantly higher than the conventional asphalt mixtures and the tensile strength of both conventional and polymer modified asphalt (PMA) mixtures increases with decreasing temperatures.

The results of the studies by Mohammad and Paul (1993) and Chapuis and Gatien (1995) as presented above agree with the correlation between the temperature and the tensile strength in equation 2.3. Such correlation between the tensile strength and the temperature of the AC has a limit at a certain temperature, however. During the development of prediction models for low temperature crack spacing, Zubeck and Vinson (1996) conducted low temperature cracking test of AC mix Thermal Stress Restrained Specimen Test (TSRST). Their TSRST results indicated that the tensile strength of the AC increases as the temperature decreases until the temperature reaches the glass transition point. As the temperature decreases further below this point, the tensile strength of the AC decreases. Equation 2.4 below was presented by Zubeck and Vinson to calculate the tensile strength of the AC mix at the temperature below glass transition temperature.

$$\text{Tensile Strength} = \frac{(S_1 - FS)}{(T_1 - FT_{org})}(PT - CT) + FS \tag{2.4}$$

Where $\qquad$ S_1 = tensile strength (MPa) measured at temperature T_1 (^{o}C),

$\qquad$ FS = fracture strength (MPa),

$\qquad$ FT_{org} = fracture temperature of un-aged AC sample (^{o}C),

$\qquad$ PT = pavement temperature (^{o}C), and

$\qquad$ CT = cracking temperature of AC in the field (^{o}C), which is the same as TSRST fracture temperature.

A simplified relationship between the tensile strength and the pavement temperature was also presented by Zubeck and Vinson (1996) as follows:

$$\text{Tensile Strength} = \frac{250}{6}(PT - CT) + FS \tag{2.5}$$

Similar conclusions regarding the relationship between tensile strength and temperature were made by Heukelom (1966). His test results indicate that the tensile strength of AC mixtures increase as the stiffness of the asphalt cement increases (as a result of different temperatures and loading times) up to a certain value and then decreases as the stiffness of the asphalt cement increases.

5.5 Stress State

The load-induced stress state in the AC layer varies from one point to another as shown in Figure 2.11. The pavement surface at the tire edges is subjected to load-

induced horizontal tensile stresses whereas the bottom of the AC layer under the tire is subjected to load-induced vertical compressive and horizontal tensile stresses. Further, the bottom of the AC layer is also subjected to confining stresses due to the overburden pressure and the frictional force between the AC and the aggregate base layers (Zubeck and Vinson, 1986). The different states of stress between the top and the bottom of the AC layer impact the total tensile strengths at both locations. The total tensile strength herein is defined as "the true tensile strength of the AC mix, which could be the same at the top and bottom of the AC layer, and the added apparent strength due to the overburden pressure and friction." It should be noted that the total, not the true strength, controls cracking potential.

6.0   TOP-DOWN CRACK PROPAGATION MODELS

While fairly extensive literature exists on the causes of TDC, relatively little

addresses TDC propagation. Most of the literature that exists addresses the method of

propagation of the cracks. Myers and Roque (2002) incorporated the effect of the

temperature gradient on the differential stiffness in the AC layer in their analyses of

tensile stresses at the crack tip using the finite element method. They reported that the

Truck tire

AC layer

Horizontal tension   Horizontal tension

Base layer

Vertical compression and
horizontal tension
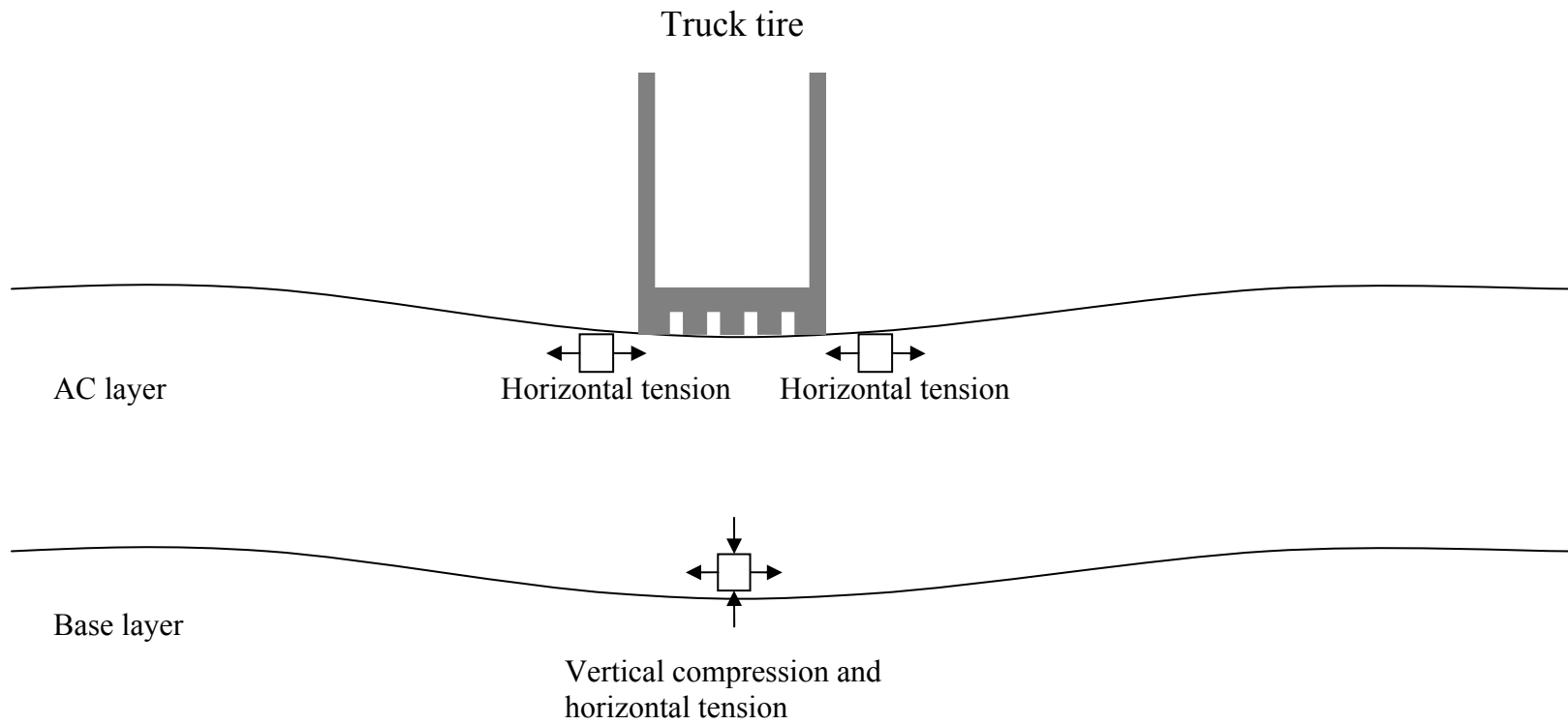
Figure 2.11 Load-induced different stress state at the top and bottom of the AC layer

differential stiffness in the AC layer results in higher tensile stresses at the crack tip. As a result, they concluded that the temperature gradient accelerates the propagation rate of TDC. Further, they concluded that the crack propagation rate is not constant throughout time, but is divided into three phases as follows:

1. During the crack initiation, the cracks propagate at a relatively fast rate

2. The crack propagation rate slows for a certain period of time. Myers and Roque (1998) have suggested the time of slow propagation is the window of opportunity for TDC identification and rehabilitation.

3. After a period of slow growth, TDC propagate at an accelerated rate until they propagate throughout the AC layer.

Jacobs et al (1992) studied crack propagation through flexible pavements with an AC overlay on the original cracked AC surface. In the study, they conducted uniaxial tensile tests of notched AC specimens to study the behavior of crack growth in asphalt concrete. They concluded that the cracking process in AC material can be simplified and analyzed using a single crack propagation model. Further, they used CRACKTIP, a 2-D finite element computer program, to calculate mode I (opening) and mode II (shearing) stress intensity factors in front of the crack tip in the AC layer. Combining the two stress intensity factors, they calculated the equivalent mode I stress intensity factor ($K_{I,eq}$), which varies with the crack length during the crack propagation. They used the $K_{I,eq}$ to calculate the effective stress intensity factors (K_{eff}), which is constant, and used their prediction model (equation 2.5) for the number of load repetitions that crack required to propagate throughout the AC overlay.

$$N_{tot} = \frac{h_0}{AK_{eff}^n} \qquad (2.6)$$

Where N_{tot} = the number of load repetitions

            h_0 = the overlay thickness (mm)

            K_{eff} = the effective stress intensity factors

            A,n = material constant in Paris' law

The above equation was developed based on the Paris' law crack propagation model as

presented below.

$$\frac{dc}{dN} = AK^n$$ (2.7, Jacobs et al, 1992)

Where: c = crack length (mm) per loading cycle, N

            K = stress intensity factor (N/mm$^{1.5}$)

            A,n = crack propagation coefficients (material constant)

Similarly, Molenaar (1984) and Jacobs (1996) modified Paris' law in their crack

propagation analyses such that crack propagation coefficients ("A" and "n") can be

determined using simple static tests and master curves. They reported, however, that their

models contain some errors due to the simplifications and the discrepancies of the linear-

elastic and homogeneous material assumptions and the actual asphalt mix characteristics.

Similarly, Dauzats and Rampal (1987) used the finite element method to calculate the

stress at the crack tip, and developed a propagation model of TDC based on Paris' law.

They concluded that their propagation model has some drawbacks including the two-

dimensional stress analyses and the exclusion of the elastoplastic calculation. The

accuracy of the above TDC propagation model developed by the above mentioned

researchers could not be verified or calibrated because their historical TDC data is not

available in any State Highway Agency database.

Nevertheless, there is at least one TDC propagation model that was developed

based on TDC historical data. Schorsch et al (2003) conducted field investigation of

segregated and non-segregated pavements as a part of their study of TDC initiation and propagation in segregated areas. Based on TDC propagation data obtained during their study and historical distresses data on the same pavements collected by Chang (2000), they developed TDC crack propagation model in the segregated area as shown below.

$$PC = 0.0602\,DS + 0.0093\,DS\ln(t) \qquad (2.8)$$

Where: PC = Percent (TDC) cracking from segregated areas = Crack length within

an area showing certain degree of segregation / Length of the area

showing that degree of segregation * 100%

DS = Numerical value of degree of segregation (Light = 2.5, Medium =

7.5, Heavy = 10)

t   = Pavement surface age (months)

Further, Schorsch et al (2003) rearranged the preceding equation to calculate the service life of the pavement from TDC based on areas experiencing different degrees of segregation. Their modified equation is stated is follows:

$$SL = \exp\left(\frac{PC_{th} - 0.0602\,DS}{0.0093\,DS}\right) \qquad (2.9)$$

Where: SL = Service Life of the pavement (months)

PC$_{th}$ = Percent cracking threshold at which RSL equal zero

By comparing the design life with estimated service life, it is possible to determine the reduction in the design life due to TDC in segregated areas.

CHAPTER 3

FIELD AND LABORATORY INVESTIGATION

1.0   GENERAL

The laboratory and field investigations were designed to identify the causes of TDC and their propagation rates. The investigations consisted of:

1. Selecting pavements showing TDC.

2. Coring, to confirm the presence of TDC and to provide material for laboratory testing.

3. Conducting falling weight deflectometer (FWD) tests on selected pavement test sections to determine the moduli of the pavement layers.

4. Examining the pavement surface to document the types of distress and possible particle segregation in the AC mat.

5. Conducting a battery of laboratory tests such as specific gravity, indirect tensile cyclic load tests (ITCLT), indirect tensile strength tests (ITST), aggregate extraction, and particle size (sieve) analyses to:

    ➢ Determine the physical and engineering characteristics of the asphalt mixes.

    ➢ Assess the effects of segregation and moisture conditioning on the indirect tensile strength of the asphalt mixes.

2.0   SELECTION OF PAVEMENT SECTIONS

The 13 flexible and 5 rubblized pavement test sections listed in Table 3.1 were

selected by MDOT and PRCE personnel for field and laboratory investigations. The

only

Table 3.1 Summary of the test sections and test sites selected for field and laboratory

investigations

Route	Control section	Test lane	Test section/ Test site	Designation number	Pavement type
US-27	37014	SB	1-1	20273-11	Flexible
US-41	7013	NB	1-1	20411-11	
US-41	7013	NB	1-2	20411-12	
M-20	37022	EB	1-1	30202-11	
M-20	37022	EB	1-2	30202-12	
M-42	83041	EB	1-1	30422-11	
M-50	23052	EB	1-1	30502-11	
M-50	23052	EB	2-1	30502-21	
M-52	33051	NB	1-1	30521-11	
M-52	76011	NB	2-1	30521-21	
M-55	72022	EB	1-1	30552-11	
M-55	72022	EB	1-2	30552-12	
Marsh Road[1]		SB	1-1	Marsh	
I-194	13033	NB	1-1	10941-11	Rubblized
I-194	13033	NB	1-2	10941-12	
I-75	16092	SB	1-1	10753-11	
I-75	16092	SB	1-1	10753-12	
M-15	25092	SB	1-1	30153-11	

1. Marsh Road is owned and maintained by Ingham County Road
Commission

criterion used in the selection process is the presence of longitudinal TDC in the vicinity of the wheel paths.

3.0 FIELD INVESTIGATION

The various activities of the field investigation are detailed in the next six subsections.

3.1 Test Layout

Within each selected pavement, a 280-ft long and 12-feet wide test section was established. The test section was subsequently divided into two 90-ft long test sites separated by a 100-ft gap. Figure 3.1 shows the two typical layouts of the test sites within a test section for divided highway and 2-lane road.

At each test site, the FWD and core locations were marked on the pavement surface based on nine transverse and seven longitudinal grid lines as shown in Figure 3.2. The (Xs) in the figure designate FWD test locations whereas the (Os) designate core locations.

Each test site was designated using seven-digit number as follows:

➤ The first digit represents the road type (1 = Interstate, 2 = U.S., 3 = Michigan).

➤ The second through the fourth digits represent the highway/route number.

➤ The fifth digit represents the traffic direction (1 = North, 2 = East, 3 = South, 4 = West).

➤ The sixth digit expresses the test section number.

➤ The seventh digit represents test site number.

vii
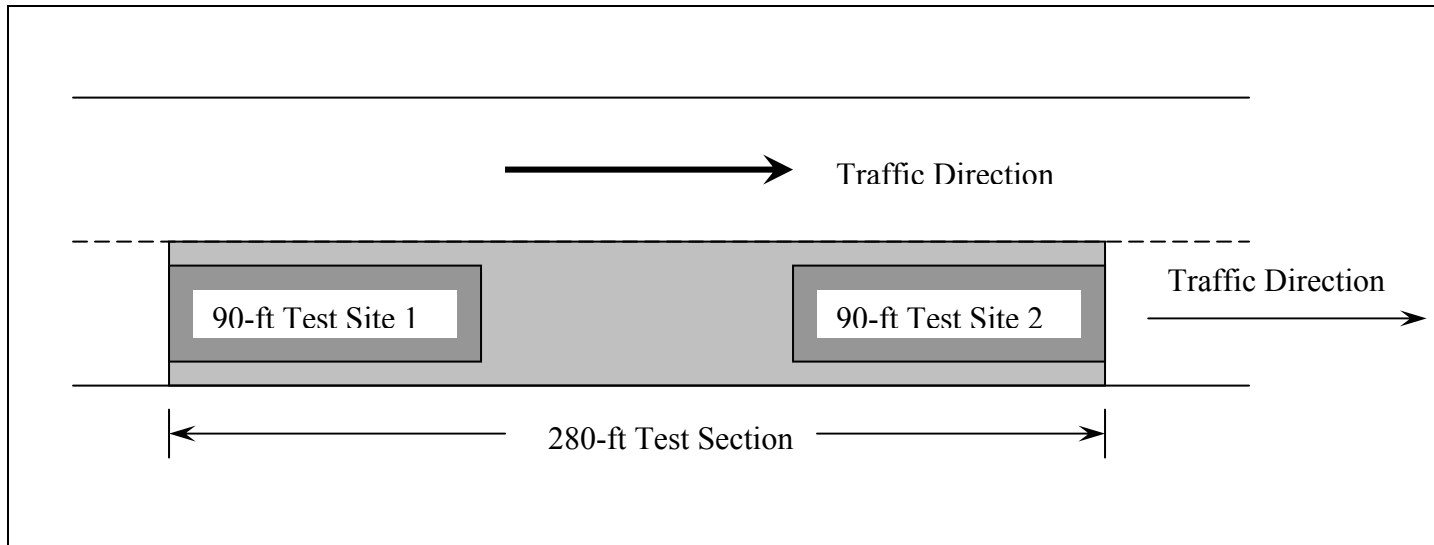
(a) Layout of a test section on a divided highway

Traffic Direction

Traffic Direction

90-ft Test Site 2
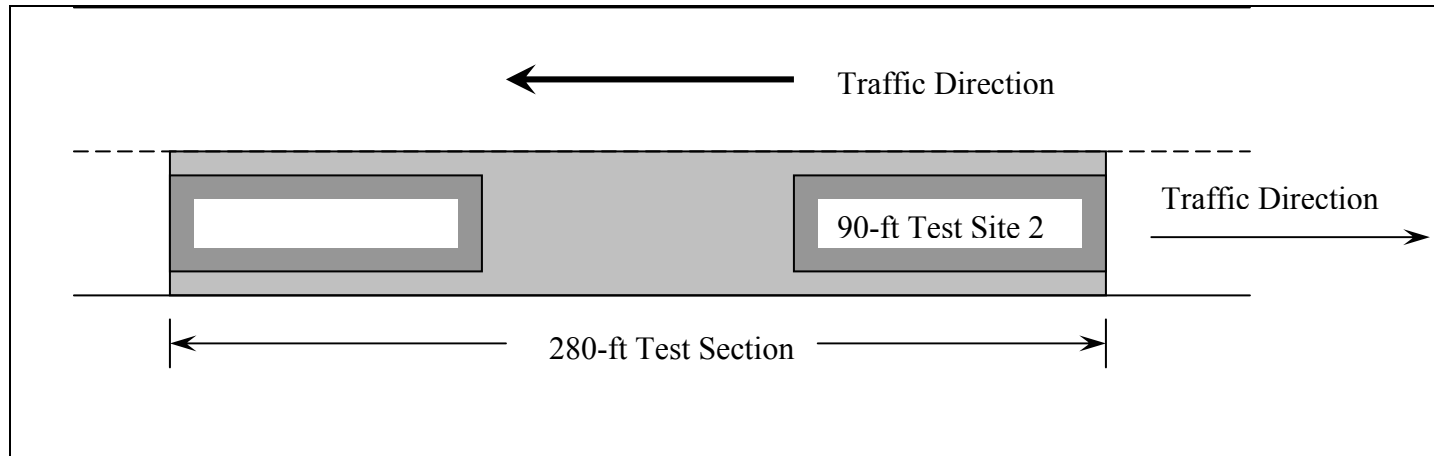
280-ft Test Section

(b) Layout of a test on 2 lane (one lane in each direction) road

Figure 3.1 Typical layouts of test sections and test sites

Road
Centerline

Edge of
shoulder

40 30 26 22 18 14 10

10'

39 09

38 08

37 29 25 21 17 13 07

36 06 **Traffic
Direction**

35 05

34 28 24 20 16 12 04

33 03

32 02 Longi-
tudinal
Direction

**3'
Fixed**

31 27 23 19 15 11 01

1'

Transverse Direction
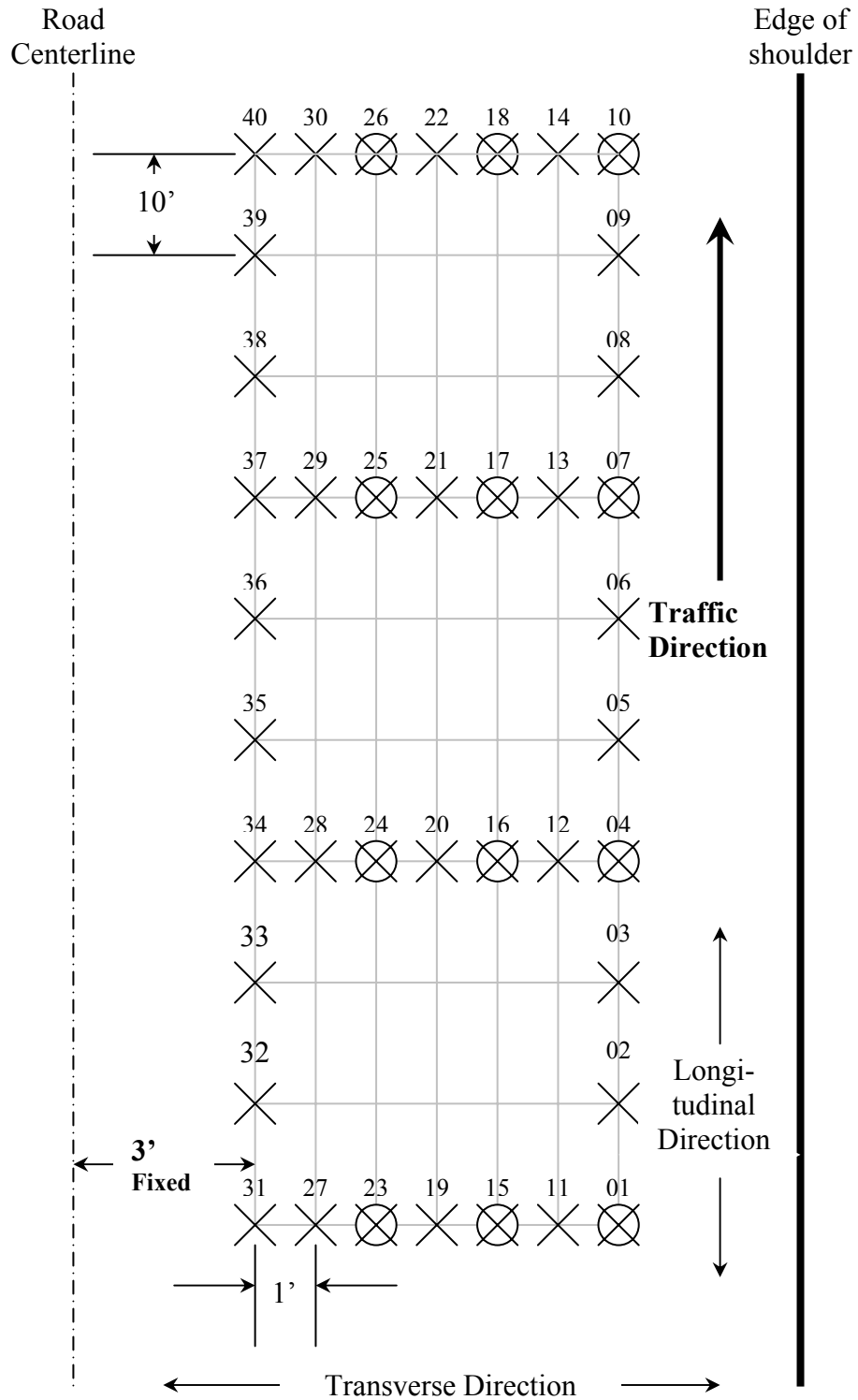
Figure 3.2 Typical test site layout showing FWD tests (X) and core locations (O)

For example, a designation number of 11941-12 implies route I-194, northbound test section 1 test site 2. In addition, the two digit numbers shown in Figure 3.2 that designate the FWD test location number was added to the right-hand side of the test designation number. Hence, the code that identifies test location consists of 9 digits. For example, a test conducted at location 23 on test site 1 of test section 1 located on the south-bound lane of M-15 would be designated 30153-1101. At some test sites, additional FWD tests were conducted and cores were extracted at special points of interest not shown in Figure 3.2. For these cases, the test number for each point was assigned starting at 50, and its location was referenced by the longitudinal and transverse distance from test point 1.

3.2   Distress Survey

During the field investigation, detailed distress maps were developed at selected test sections. Early in the study, the criteria for selecting the test sections were based on the extent of cracking observed at the time of field investigation. For example, a pavement that exhibited cracks at the earliest stages of initiation was selected because it was assumed that periodic distress surveys could be conducted to assess the rate of crack propagation. As the field investigation progressed however, distress maps were developed for each test site. The purposes of these maps were 3 fold:

1. To catalog the general appearance of TDC.

2. To identify any distresses that may generally be associated with TDC.

3. To determine crack growth over time and therefore determine the rate of crack propagation.

The distress maps were developed by measuring the coordinates of the crack ends relative to the test grid. In addition to mapping distress, visually identifiable segregation areas were also mapped. The two maps were used to visually identify those cracks that fell within the segregated areas. Additionally, each visually identified segregated area was assigned a degree of segregation based on the apparent severity of segregation. The definitions of each degree of segregation are the same as those developed by Chang (2000) and are listed below:

1. Light – The fine matrix in place, more stone that the surrounding mat.
2. Medium – Lack of surrounding fine matrix, significantly more stone than the surrounding mat.
3. Heavy – Stone against stone, little or no fine matrix.

3.3 FWD

During the course of this study, nondestructive deflection tests (NDT) were conducted on all test sites using the MDOT falling weight deflectometer (FWD). The objectives of the tests were to:

1. Measure the variation in the pavement deflections along and across the pavement.
2. Backcalculate the moduli of the pavement layers.
3. Assess the linearity of the pavement response to load.

The configuration and spacing of the 9 FWD deflection sensors are shown in Figure 3.3.

All deflection data were recorded by an on-board computer to within 0.01-mils (0.00001-in). At each FWD test location, the pavement and air temperatures were also measured and the data were recorded. After the FWD tests were completed, pavement
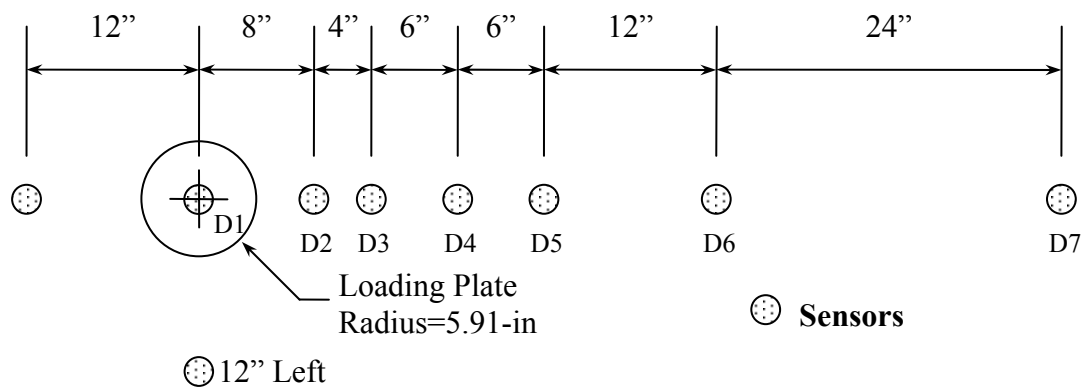
Figure 3.3 Top view of the sensor configuration of the MDOT FWD

cores were extracted and the thickness of each core was measured. The thickness data were used as input to the backcalculation program. The deflections from sensors D1 through D7 (see Figure 3.3) were used to backcalculate the layer moduli using the MICHBACK computer software.

All FWD tests consisted of 4 drops. The first drop was used to seat the load plate on the pavement surface, and therefore the deflection data from this first drop were not recorded whereas the data from the next three drops were recorded. Most tests were conducted at the target load of 9000-lb. At some test sites, about ten additional FWD tests were conducted at each of four load levels to assess the repeatability of the deflection data and the linearity of the pavement response to load.

3.4   Nuclear Density

After the test locations were marked on the pavement surface at each test site, one-minute nuclear density measurements were made using a Troxler nuclear density meter shown in Figure 3.4. The purpose of the nuclear density readings was to confirm the observed level of segregation. The level of segregation was confirmed by analyzing differences in nuclear density between visibly segregated and non-segregated areas using the computer program MBITSEG202 (Chang, 2000).

3.5 Coring

After all non-destructive tests had been completed, cores were extracted at the designated locations using a power rotary drill as shown in Figure 3.5. Each core was numbered according to the system previously discussed in section 3.1.

Figure 3.4 Troxler nuclear density meter

Figure 3.5 Drilling cores using a power rotary drill

3.6   Boreholes

At most test sites, when coring was completed, boreholes were drilled to a maximum depth of 4-ft using a hand auger. The extracted material was then examined to estimate the thickness and material types of the base and subbase and the type of the roadbed soil.

4.0   LABORATORY INVESTIGATION

Laboratory testing was conducted to determine the physical and engineering characteristics of the AC mixes exhibiting TDC. The testing program consisted of the following activities.

1. core preparation;

2. specific gravity tests;

3. indirect tensile cyclic load Tests (ITCLT);

4. indirect tensile strength tests (ITST); and

5. aggregate extraction by incineration and sieve analysis.

4.1   Core Preparation

Cores were prepared for testing as soon as they arrived in the laboratory. Each core was washed to remove excess aggregate or any other material contamination that may have occurred during coring or handling. The total thickness of each core was measured to the nearest 0.1-mm at four points located at the opposite ends of two orthogonal diameters. Then, the thickness of each asphalt course within the core was

measured. Once all measurements were completed, the lowermost portion of the core that had been contaminated by the base material (typically the lowermost 0.5-in) was removed by sawing. The core was then marked with the appropriate designation number.

4.2   Specific Gravity Tests

Once the cores had been prepared as discussed in section 4.1, they were subjected to specific gravity tests, according to ASTM standard test procedure D-2726 (ASTM 1994). The test results were used to determine the bulk specific gravity of the cores using the following equation:

$$G_{sb} = \frac{A}{B-C} \qquad (3.1)$$

Where: A = mass of the dry specimen in air (g)

B = mass of the saturated surface-dry specimen in air (g); and

C = apparent mass of the specimen in water (g)

G_{sb} = Bulk specific gravity from equation 3.1

After the specific gravity tests of the cores were completed, each core was sawed into test specimens according to predetermined thicknesses. These specimens were again subjected to the preparation procedure discussed in section 4.1 and to the specific gravity tests discussed above.

4.3 Indirect Tensile Cyclic Load Test

After sawing, test specimens from each test site were subjected to ITCLT. In this
test, a cyclical load pulse is transmitted across the vertical diameter of a cylindrical
specimen using a 0.5-in wide loading strip. The resultant deformations in the vertical,
horizontal, and longitudinal directions were measured. The deformations at the 500th load
cycle were used to determine the resilient modulus and Poisson's ratio of the specimen.
After sawing the test specimen and measuring its specific gravity, the ITCLT was
conducted using the following steps:

1. All moving parts and the two loading strips of the ITCLT loading device were
    cleaned and lubricated.

2. The ITCLT loading device was placed on the MTS loading frame such that the
    center of the device corresponded with the center of the MTS actuator and the
    center of the load cell.

3. The test specimen was placed on the loading frame and five linear variable
    differential transducers (LVDT) were placed in their respective positions as
    shown in Figure 3.6. The accuracy and range of the LVDTs are shown in Table
    3.2. In addition, a sixth LVDT placed inside the MTS actuator was also used to
    measure the test specimen deformation along the vertical diameter.

4. The position of each LVDT on the specimen holder was adjusted by moving the
    LVDT core toward or away from the test specimen using two position adjustment
    nuts until the LVDT signal indicates that the core position would allow the use of
    a high percentage of the LVDT range.

5. A 50-lb sustained load was placed on the test specimen by lowering the actuator of the MTS. The resulting test specimen deformations were recorded.

6. When the rate of deformation due to the sustained load was small enough (not measurable), a 250-lb cyclic load was applied to the test specimen at a frequency of 2 Hz. Each cycle consisted of 0.1-second of load-unload and 0.4-second
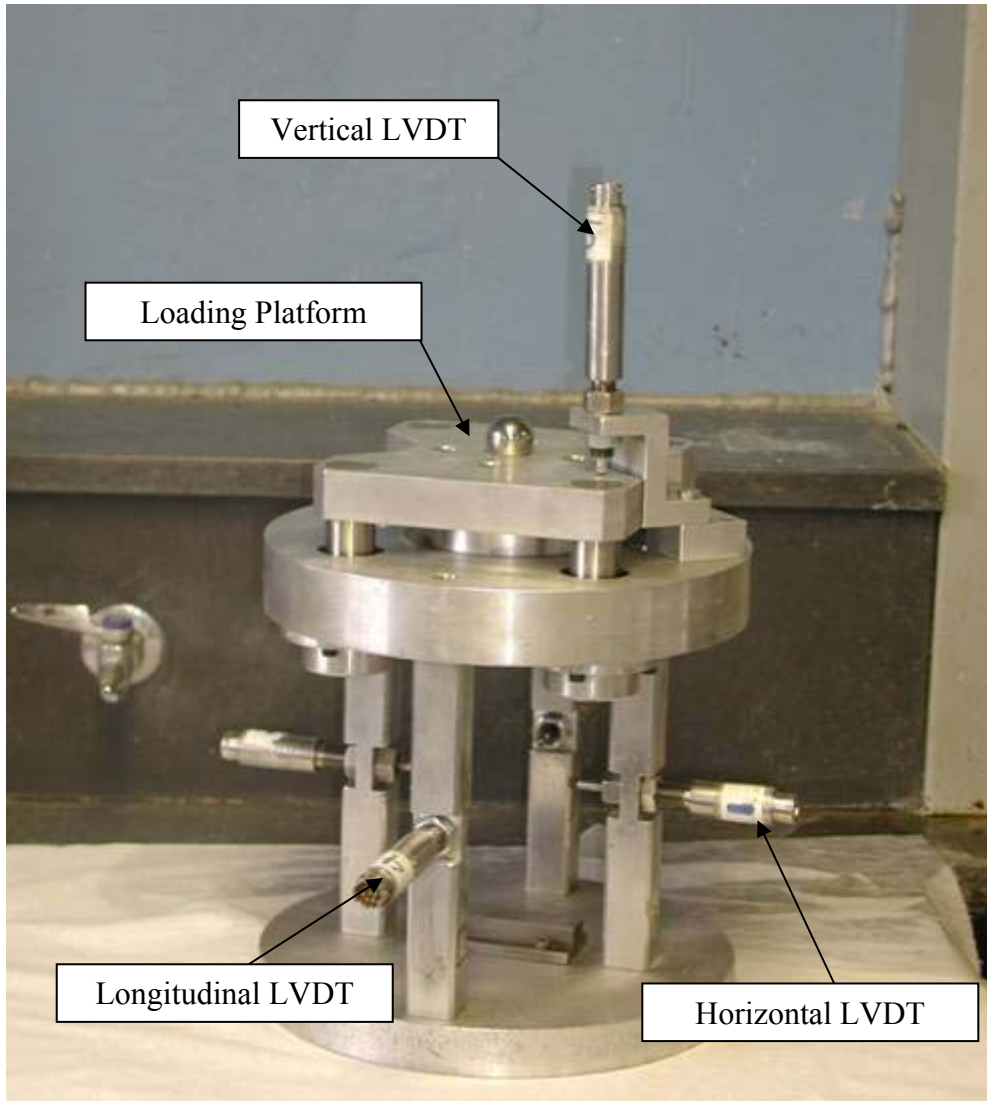
Figure 3.6 ITCLT and ITST specimen holder for a 6-in diameter and 3-in thick test specimen

Table 3.2 Sensitivity of LVDTs used in the ITCLT apparatus

Number of LVDT	Position	Range (in)	Accuracy (in)
2	Horizontal diameter	$\pm$0.125	0.00005
2	Specimen thickness	$\pm$0.100	0.00001
1	Vertical diameter	$\pm$0.250	0.00010

relaxation periods. Figure 3.7 illustrates a plot of one load cycle as a function of time.

7. Each test specimen was subjected to a minimum of 700 load cycles. At certain specified cycles (e.g., the 200 and 500 cycles), the load magnitude and the deformations of the test specimen in three directions were recorded for three sequential cycles. The rate of data collection was set at one set of deformation readings every 0.0004-second. Hence, 250 deformation readings were collected by each LVDT during the load-unload cycle and 1,000 readings during the rest period. Note that the load data were collected using a 1000-lb capacity load cell located under the ITCLT loading frame (see Figure 3.8).

8. The test was terminated and the data was downloaded for analysis.

The load and deformation data corresponding to load cycles 499, 500 and 501 were used to calculate the resilient modulus of the test specimen using one- and three-dimensional analyses as follows:

a) **One-Dimensional Analysis** – The resilient modulus of the test specimen was calculated using the deformation measured along the vertical diameter of the test specimen, equation 3.3 (Harichandran and Baladi, 1987). In this calculation, since the impact of Poisson's ratio on the value of the resilient modulus is insignificant, a Poisson's ratio of 0.3 was assumed for all test specimens.

$$MR_v = \frac{P(4.085950 - 0.0417333\ \upsilon)}{LD_v} \tag{3.3}$$

Where: MR_v = Resilient modulus based on vertical deformation (psi);

P = peak cyclic load (lb);

ν = Poisson's ratio;

25
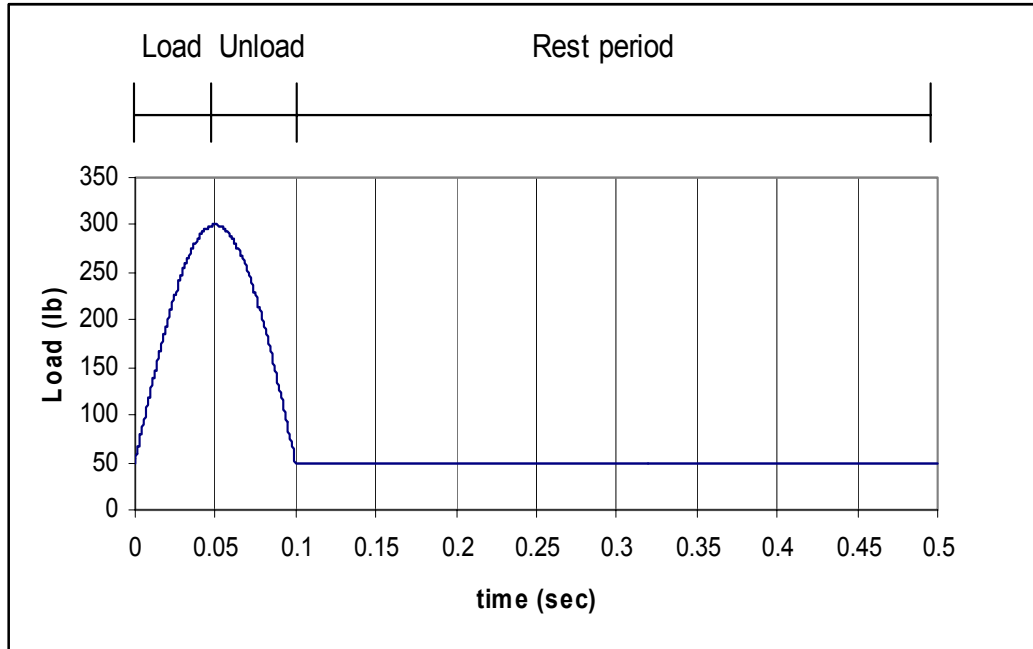
Figure 3.7 One load cycle consisting of 0.1-second load-unload period and 0.4-second relaxation period
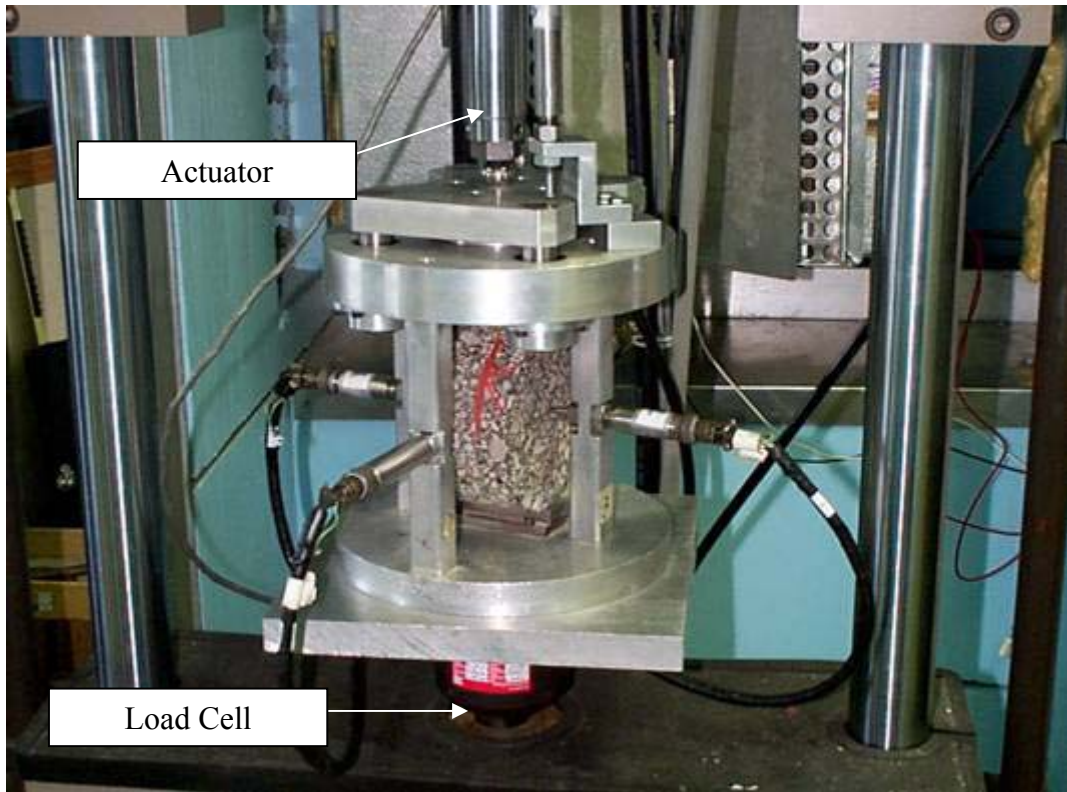
Figure 3.8 Test specimen in the specimen holding device during an ITCLT test

L = thickness of the test specimen (in); and

D_v = the deformation of the test specimen along the vertical

diameter (in).

b) **Three-Dimensional Analyses** - The resilient moduli of the test specimens

were calculated using the deformations measured along the vertical and

horizontal diameters and along the thickness of each test specimen using the

equations below (Harichandran and Baladi, 1987).

$$MR_{3D} = \frac{(0.1832585H + 4.2817159V - 0.0215089A)}{D} \tag{3.4}$$

$$D = 1.0468779\left(H^2 + V^2 + A^2\right) - \left(H - 0.0417333V + 0.212453A\right)^2$$

$$H = \frac{D_h * L}{P}; \quad V = \frac{D_v * L}{P}; \text{ and } A = \frac{D_l}{P}$$

Where: MR_{3D} = Resilient modulus based on 3-D deformations (psi);

L = thickness of the test specimen (in);

P = peak cyclic load (lb);

D_h = the horizontal deformation = the sum of the displacements

measured by the two LVDT along the horizontal diameter of the

test specimen (in);

D_v = the deformation of the test specimen along the vertical diameter

(in); and

D_l = the longitudinal deformation = the sum of the displacements

measured by the two LVDT along the thickness of the test

specimen (in).

Note that, the vertical deformation used in equations 3.3 and 3.4 was that obtained from the LVDT placed inside the MTS actuator. The reason is that the actuator and the LVDT were positioned at the center of the test specimen. The outside mounted LVDT was positioned at the corner of the top plate of the ITCLT device which may be affected by the rocking motion of the test specimen during the cyclic load test. The resilient moduli obtained from equations 3.3 and 3.4 were compared. Detailed data (measured deformations in three dimensions, test specimen thickness, and the resilient moduli calculated using equations 3.3 and 3.4) for each core are presented and discussed in chapter 4.

4.4   Indirect Tensile Strength Tests

All specimens tested in the ITCLT mode were subsequently subjected to indirect tensile strength tests. In this test, the load is applied across the diameter of the specimen at a constant 2-in/min rate until failure. The peak load measured is the load required to fail the specimen, and the vertical deformation corresponding to that load is the deformation at failure. By utilizing the geometry of the specimen, the tensile strength of the specimen was determined.

A Reinhart analog device was used in conducting the tests. Since the output was not recorded digitally, there is a certain degree of subjectivity involved in interpreting the results. Therefore, a standard procedure for reading the output graphs was developed. The procedure is as follows.

1. After initial contact is made between the loading head and the specimen, the load increases in a roughly linear fashion. This linear portion of the load/deformation curve was extrapolated backwards to the load datum (P=0-lb). This point was taken as zero deformation for the specimen (d_o).

2. The peak load P_f (also referred to as the load at failure) was determined for the specimen. The deformation corresponding to this load was defined at the deformation at failure (d_f).

3. A third point, at a load approximately half of the peak-load, was located on the curve. The load and deformation at this point (P_m and d_m respectively) were recorded.

The strain at failure was calculated as follows:

$$\varepsilon_t = \frac{d_f}{D} \tag{3.5}$$

Where: ε_t = Strain at failure (in/in)

d_f = Specimen deformation at failure (in)

D = Specimen diameter (in)

The tensile strength of the specimen was determined as follows:

$$S_t = \frac{2 \cdot P_f}{\pi \cdot D \cdot t} \tag{3.6}$$

Where: S_t = Tensile strength of the specimen (psi)

P_f = Peak load (lbs)

D = Specimen diameter (in)

t = Specimen thickness (in)

29

From the load/deformation curve of the specimen, an equivalent modulus (ITST) could be calculated as follows:

$$E_{EQ} = \frac{P_m}{t \cdot d_m}(4.08595 - 0.041733v) \qquad (3.7)$$

Where: E_{EQ} = ITST equivalent modulus (psi)

P_m = Approximate half-peak load (lbs)

d_m = Approximate half-peak deformation (in)

t = Specimen thickness (in)

v = Poisson's ratio (assumed = 0.3)

4.5 *Extraction of Aggregate*

After the preceding tests had been completed, the aggregate was extracted by ASTM standard test procedure D-5444, which allowed sieve analysis to be conducted on the recovered cores. All extraction tests were conducted using a forced air ignition furnace preheated to 450°C. Each sample specimen was evenly placed within a basket which was placed in the furnace and burned until the internal scale stabilized, indicating that the extraction process was complete. The aggregate was then retrieved and subjected to sieve analysis. By measuring the weight of the sample prior to and after incineration, the asphalt content could be determined by the following computation.

$$\%AC = \frac{A - B}{B} \times 100\% \qquad (3.8)$$

Where: A = Mass of the specimen in air prior to incineration (g), and;

B = Mass of the specimen in air after incineration.

Once the aggregate and fine material left from the extraction process had cooled, the particle size distribution was determined by sieve analysis. The sieves used and the corresponding sieve openings are listed in Table 3.3.

5.0   MANUFACTURED TEST SPECIMENS

During the field investigation, TDC were observed to initiate in segregated areas. Therefore, it was desirable to obtain the engineering characteristics of the segregated mixture in particular to assess if a correlation existed. Conducting the required tests on field specimens is hampered by several problems which are listed below:

1.   The segregated areas were frequently deteriorated or cracked. This made obtaining segregated material suitable for

laboratory investigation difficult.

2.   The segregated areas were only visible in surface course, which, in most case, was approximately 1-in thick. Several of the

tests employed required specimen thicknesses of at least 2.2-in. Therefore, it was impossible to obtain test results of pure

segregated material. This situation is shown in Figure 3.9.

In an attempt to circumvent these problems, segregated asphalt mixture was manufactured in the lab to determine if there was any difference in the engineering characteristics between the segregated and non-segregated mixtures. The basic goal of producing manufactured specimens was to produce a pure specimen of material that closely matched the gradation and asphalt content of segregation in the field, and then performing the above mentioned battery of tests to determine if the properties of the segregated mixture were significantly different than those of the non-segregated mixture.

Table 3.3 Sieves and corresponding opening sizes used in the sieve analysis

Sieve Size	Opening (mm)	[Opening (mm)]$^{0.45}$
0.75-in	19	3.76
0.50-in	12.5	3.12
0.375in	9.5	2.75
No. 4	4.75	2.02
No. 8	2.37	1.47
No. 16	1.18	1.08
No. 30	0.60	0.79
No. 50	0.30	0.58
No. 100	0.15	0.43
No. 200	0.075	0.31

2.2" Required Thickness

1 11/16"

2 ¼"

2 9/16"

2 3/8"
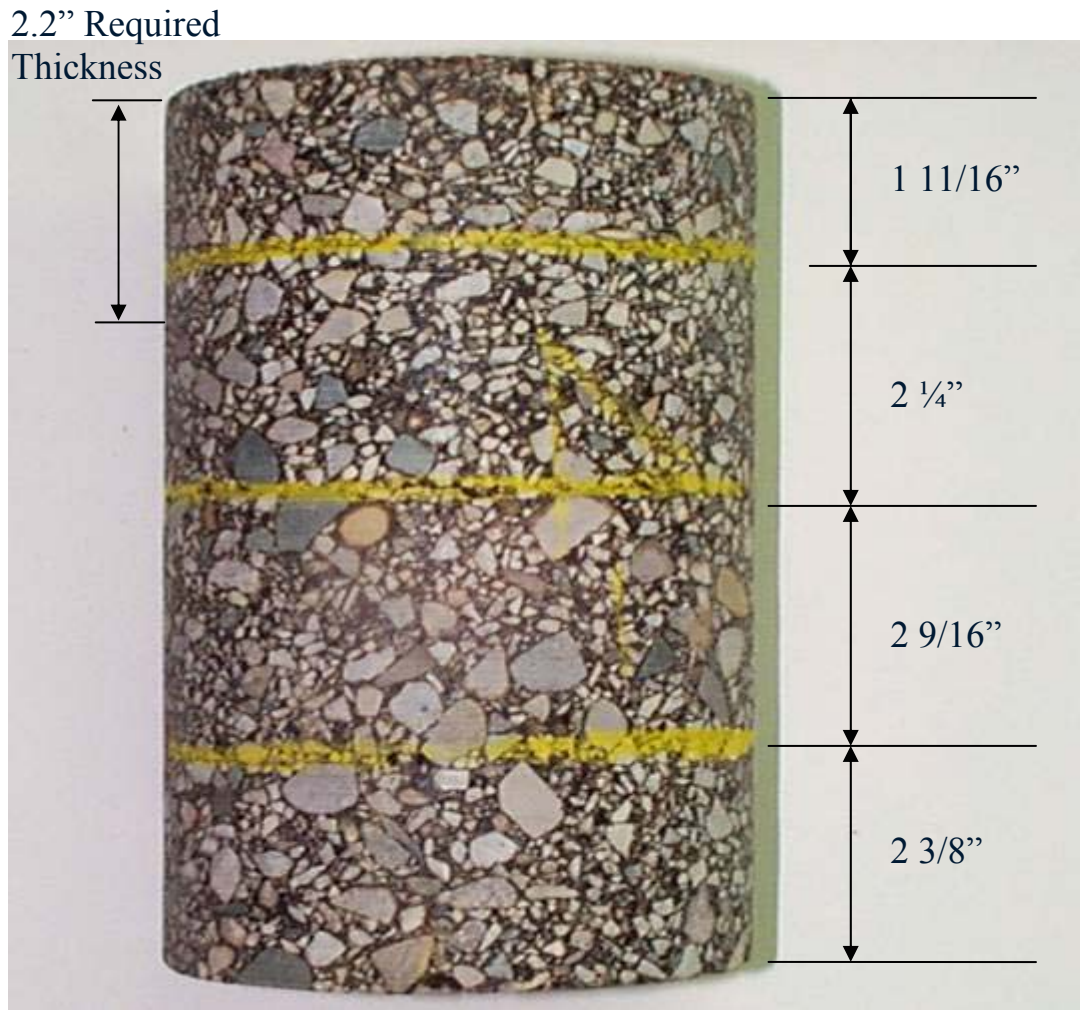
Figure 3.9 Relationship between actual core thicknesses and required minimum thickness for ITCT and ITST testing

5.1 Manufacture of Specimens

The gradation and asphalt content of the segregated mixtures was determined by incinerating cores obtained from cracked and non-cracked areas by the method outlined in section 4.5. Specimens were then fabricated according the following process.

1. Fresh aggregates and asphalt cement were obtained from Spartan Asphalt Paving Company in Lansing, MI. The aggregates used were manufactured sands and gravels, and the binder used was a SUPERPAVE PG 64-22.

2. The aggregates were dried and separated into the required sizes by sieving. The materials used were those retained on the ½-in, 3/8-in, #4, #8, #16, #30, #50, #100, #200 sieves and the pan, respectively.

3. Aggregates retained on the ½-in, 3/8-in, #4, #8, #16, #30, and #50 sieves were washed to remove any dust. The aggregates were then placed in an oven heated to 90°C to dry.

4. The oven dry aggregates were combined by weight to create several specimens having gradations matching those of segregated or non-segregated pavements in the field as well as the mix JMF. The combined aggregates were then placed in an oven and heated to 124 °C.

5. The asphalt content was calculated based on the incineration data from recovered cores. In cases where the asphalt content was not obtained from incineration of the original cores, the asphalt content was calculated based on equivalent binder film thickness of the JMF (Roberts et al, 1991).

6. The prescribed weight of asphalt cement (heated to 140°C for not more than 12-hours) was added to the aggregate. The mixture was then transferred to a mixing bowl (heated to 140 °C) and mechanically mixed until all the aggregate was evenly coated with asphalt cement. The mixture was then placed back in an oven heated to 140 °C for at least 5-minutes but not more than 10-minutes to reheat to compaction temperature.

7. The mixture at compaction temperature was transferred to a gyratory mold (heated to 140 °C) and compacted to predetermined number of gyrations in a Pine gyratory compactor.

After compaction, the specimens were allowed to cool to room temperature before handling, after which they were subjected to the same laboratory investigation outlined in section 4.0.

5.2 Moisture Conditioning of Specimens

TDC have been observed to occur within a few years of construction, which is sooner than generally accepted instances of long term aging of the asphalt binder. Therefore, it was suspected that open gradations associated segregation increased the

moisture susceptibility of mix, and the subsequent environmental action decreased the tensile strength. Therefore, moisture susceptibility tests were conducted in accordance with ASTM standard test procedure D-4867M (1994 Annual Book of ASTM Standards). In this test, the tensile strength of the specimens is measured after moisture conditioning. The tensile strength of specimens in a control group not subjected to moisture conditioning is used as a baseline. Hence, significant loss of tensile strength relative to unconditioned specimens indicates that the mixture is susceptible to moisture damage. Michigan is located in a wet freeze region; therefore the freeze/thaw option of this test was included.

For each mixture type tested, a total of fourteen 100-mm specimens were manufactured according to the procedure outlined in section 5.1. These specimens were divided into two subsets consisting of seven specimens each; the first subset was composed of non-segregated specimens while the second subset was composed of segregated specimens. Three specimens (a triplicate) of each subset were subjected to the moisture conditioning procedure while the other three were tested without conditioning. The theoretical maximum density was obtained from the last subset by ASTM standard test procedure D-2041 (1994 Annual Book of ASTM Standards).

6.0   TESTING SUMMARY

The testing procedure outlined above indicates the final evolution of the testing program, which had been expanded over time to include new tests and procedures. This implies that each pavement tested may have been subjected to a different testing regime. A summary of the tests conducted on each site is therefore

presented below. Table 3.4 shows a matrix summarizing the field investigation

activities, and Table 3.5 shows the laboratory investigation activities.

6.1   *I-194, Test Section 2, Test Sites 1 and 2 (11941-11 and 11941-12)*

I-194 south of Battle Creek is a 4 lane (2 lanes in each direction) divided highway

with 12-ft lanes and asphalt shoulders. The general terrain consists of very gently rolling

hills. The pavement is a rubblized concrete slab with asphalt overlay. The primary

Table 3.4 Summary of field investigations

| Route | Designation number | Number of each activity conducted | | | | Pavement type |
		Distress survey	FWD	Nuclear density	Cores	
US-27	20273-11	N/A	40	0	12	Flexible
US-41	20411-11	N/A	42	0	14	
US-41	20411-12	N/A	42	0	14	
M-20	30202-11	5	30	0	11	
M-20	30202-12	5	29	0	9	
M-42	30422-11	N/A	52	52	27	
M-50	30502-11	N/A	41	0	13	
M-50	30502-21	1	48	48	38	
M-52	30521-11	N/A	44	48	25	
M-52	30521-21	N/A	41	41	10	
M-55	30552-11	4	33	0	15	
M-55	30552-12	4	37	0	14	
Marsh Road		N/A	58	0	8	
I-194	10941-11	N/A	43	0	15	Rubblized
I-194	10941-12	N/A	43	0	15	
I-75	10753-11	N/A	42	0	14	
I-75	10753-12	N/A	43	0	15	
M-15	30153-11	N/A	43	0	16	

Table 3.5 Summary of laboratory investigations

on	Number of cores prepared	Number of specimens prepared	Number of tests conducted				Pavement type
			Core specific gravity	Specimen specific gravity	ITCLT	ITST	
	12	7	6	7	7	7	Flexible
	14	14	14	6	12	12	
2	14	14	14	2	12	12	
	9	9	9	12	9	9	
2	12	9	12	14	9	9	
	27	N/A[1]	27	N/A	N/A	N/A	
	13	21	12	11	N/A	10	
	38	N/A	16	33	N/A	N/A	
	19	N/A	19	N/A	N/A	N/A	
	9	N/A	9	N/A	N/A	N/A	
	15	15	15	6	12	11	
2	13	13	13	5	12	11	
	8	18	N/A	18	18	18	
	15	15	10	18	9	8	Rubblized
2	14	9	11	18	8	8	
	11	4	11	8	3	4	
2	12	4	12	8	4	4	
	12	12	12	12	11	10	

1. N/A indicates that specific tests were not conducted for the test site in question

distress on the section is longitudinal cracking occurring randomly within the inner wheelpath of the outer lane. Full lane width transverse cracking is also visible. Finally, low severity strip segregation was noted near the outer lane centerline.

PRCE personnel identified the pavement as potentially exhibiting TDC, and field investigation was conducted on November 7, 2001. Two test sites were established according to the standard layout in the north-bound outer lane on a mild upward grade. The FWD testing proceeded normally. Upon coring, however, it was discovered that the joints had been milled out and replaced with aggregate. It also appeared that the rubblized concrete had deteriorated. Samples of both the aggregate joint filler and the deteriorated rubblized concrete were obtained for further examination in the laboratory. Detailed distress and segregation maps were not developed for this pavement, nor were nuclear density tests conducted. Ultimately, 86 FWD tests were conducted and 30 cores were obtained from this section, with 43 FWD tests and 15 cores from each test site.

The laboratory testing proceeded as outlined in section 3.5. The cores were cleaned, the physical dimensions were recorded and the loose material was removed from the bottom of the cores. The cores were subsequently subjected to specific gravity tests, sawed into test specimens and specific gravity tested again. The specimens were then tested in ITCLT and ITST modes. None of the specimens were incinerated and subjected to gradation analysis.

6.2 I-75, Test Section 1, Test Sites 1 and 2 (10753-11 and 10753-12)

I-75 just north of the US-131 interchange is a four lane divided highway with 12-lanes and a 9-ft asphalt outside shoulder. The general terrain is low rolling hills. The test section itself is located in a low area characterized by coniferous woodland and swamp. The pavement type is rubblized concrete slab with asphalt overlay. PRCE personnel identified the pavement as potentially exhibiting TDC. The most prominent feature was a continuous strip of "drip and chip" sealant along the inside edge of the outer wheelpath. A tight network of interconnected longitudinal and transverse cracks is also visible throughout the pavement section. Most of these cracks had been routed and sealed at the time of the field investigation. Although no segregation was evident on this site, a maximum of 3/8-in rut was measured in the inner wheelpath.

The field investigation was conducted on September 24, 2001. MDOT FWD and coring personnel were on hand to conduct the tests. The test section was established, and two sites using the standard test layout were placed. A total of 85 FWD tests were conducted and 29 cores obtained. 42 FWD tests and 14 cores were obtained from test site 1 and 43 FWD test and 15 cores were obtained from test site 2.

Difficulties in backcalculation of these sites resulted in a follow-up survey. On March 17, 2002, a hand auger was used to determine the soil profile to a depth of four feet in the native soil approximately 50-ft from the pavement edge. Additionally, two soil samples were obtained. Additional observations as to the condition of the pavement and

the surrounding areas were made. The most significant observation was that the water table is approximately 4-ft below the pavement surface.

The laboratory testing proceeded as outlined in section 3.5. The cores were cleaned, the physical dimensions were recorded and the loose material was removed from the bottom of the cores. The cores were subsequently subjected to specific gravity tests, sawed into test specimens and specific gravity tested again. The specimens were then tested in ITCLT and ITST modes. None of the specimens were incinerated and subjected to gradation analysis.

6.3 US-27, Test Section 1, Test Site 1 (20273-11)

US-27 south of Mt. Pleasant is a four lane divided highway. MDOT inventory data originally indicated that this pavement was a rubblized pavement (rubblized concrete slab with an asphalt overlay). This pavement had exhibited no distress, but was selected for field investigation as a control group for another project conducted by the PRCE. On June 4, 2002, the test section with only one test site was established, and 40 FWD tests conducted. Subsequent coring revealed however that the pavement was not rubblized. The removal of the rubblized material could be explained by the close proximity of an overpass approximately 300-ft to the south of the test section where the concrete materials may have been removed to maintain bridge clearance. All prescribed cores were drilled from this one site and were subjected to various tests, more as trial specimens than actual data collection. The FWD results were recorded and analyzed however, and are used as a control group for these tests on flexible pavements.

6.4 US-41, Test Section 1, Test Sites 1 and 2 (20411-11 and 20411-12)

US-41 north of Baraga is a two lane (one lane in each direction) flexible pavement running along the shore of Lake Superior. The topography is hilly coniferous forest perched on bluffs overlooking the lake. The pavement structure features a flexible surface layer placed on top of a concrete slab with an aggregate separator layer in between. On the construction plans, the separator layer varies from 2 to 4-ft thick. This pavement was identified by MDOT personnel as a candidate TDC project, and therefore field investigation was conducted on August 22, 2001. The only notable distresses on the pavement were longitudinal cracking near the inner wheelpath in an area of light to medium segregation.

The standard testing layout was placed on the pavement, and subsequent coring indicated that the cracking was indeed TDC. Segregation was noted on the section and the longitudinal TDC was observed to occur in the segregated areas. Boreholes of the underlying base material indicated that the separator layer was approximately 4-ft thick and was laid using two different materials. The first, deeper layer was approximately 3-ft thick and was composed of sand. The second, upper layer was approximately 1-ft thick and was composed of gravel. A total of 84 FWD tests were conducted and 28 cores obtained, with 42 FWD tests conducted and 14 cores obtained from each site.

The laboratory testing proceeded as outlined in section 3.5. The cores were cleaned, the physical dimensions were recorded and the loose material was removed from

the bottom of the cores. The cores were relatively thin (3.5-in approx.) and indicated that the pavement was laid in two lifts. Inventory data further indicated both courses were constructed of the same mix. Therefore, after trimming, no additional specific gravity tests were necessary, as the cores in their entirety were a convenient size for testing. The specimens were then tested in ITCLT and ITST modes. To examine the degree of segregation present, the cores were subjected to incineration and both the asphalt content and aggregate gradation were measured.

6.5 M-15, Test Section 1, Test Site 1 and 2 (30153-11 and 30202-12)

This rubblized project was investigated on November 14, 2001. The section was located on M-15 southbound approximately ½ mile north of the village of Otisville. The pavement itself consisted of two lanes (one lane in each direction) with 3-ft asphalt shoulders. The pavement is located on relatively flat terrain with low embankments beyond the drainage ditches on either side of the road. This section consisted of only one test site. The standard layout for FWD tests and coring was used for this test section. The predominant distress was longitudinal cracking. Two relatively straight, medium to high severity cracks appear on the center of lane side of each wheel path. Low to Medium severity segregation was also noted on the pavement surface. Finally, occasional short transverse cracks were noted throughout the pavement surface. Forty four FWD tests were conducted on the site and 16 cores obtained.

The laboratory testing proceeded as outlined in section 3.5. The cores were cleaned, the physical dimensions were recorded and the loose material was removed from the bottom of the cores. The specimens were then tested in ITCLT and ITST modes.

6.6   M-20, Test Section 1, Test Sites 1 and 2 (30202-11 and 30202-12)

M-20 in Mt. Pleasant is a 5 lane (2 lanes in each direction, 1 turning lane) road with 12-ft lanes and a 9-ft shoulder. The road is constructed in a flat area of alternating forest and grassland. In early June, 2001, longitudinal cracks were observed in the earliest stages of initiation on the inside edge of the outer wheelpath. Based on the observed distress, field investigation was conducted on June 6, 2001.

Once preliminary coring indicated that the cracks were top-down, the test layout was set. The test site used differed from what was used on other sites because the standard layout was still being designed. The layout used on M-20 is shown below on Figure 3.10. The only distress on the pavement was cracking and rutting, and no segregation was observed. The maximum rut measured was 0.25-in, and the cracking had appeared only faintly. A total of 59 FWD tests were conducted and 20 cores extracted with 30 FWD tests and 11 cores obtained from site 1 and the remainder from site 2.

Due to the apparent young age of the cracks, M-20 was identified as a candidate site for crack propagation measurements. Approximately each month after testing, crack surveys were conducted on both sites. In these surveys, it was assumed that the cracks

appear at a constant transverse distance across the pavement, and therefore only the growth in the longitudinal cracks was measured.

Laboratory investigation including specific gravity tests, ITCLT and ITST were conducted according to the process described in section 3.5. Additionally, select cores were later incinerated to measure the asphalt content and aggregate gradation.

6.7   *M-20, Test Section 2, Test Sites 1 and 2 (30202-21 and 30202-22)*

M-20 east of Oil City is a 4 lane (2 lanes in each direction) road with 12-ft lanes and a 9-ft shoulder much like sites 30202-11 and 30202-12. The pavement structure consists of a rubblized concrete slab with asphalt overlay, however, and the road is constructed in a flat, wooded area. This pavement was identified as potentially exhibiting TDC in a periodic survey of all the rubblized projects in Michigan. The cracks were observed in their early stages, and therefore this pavement was selected for crack
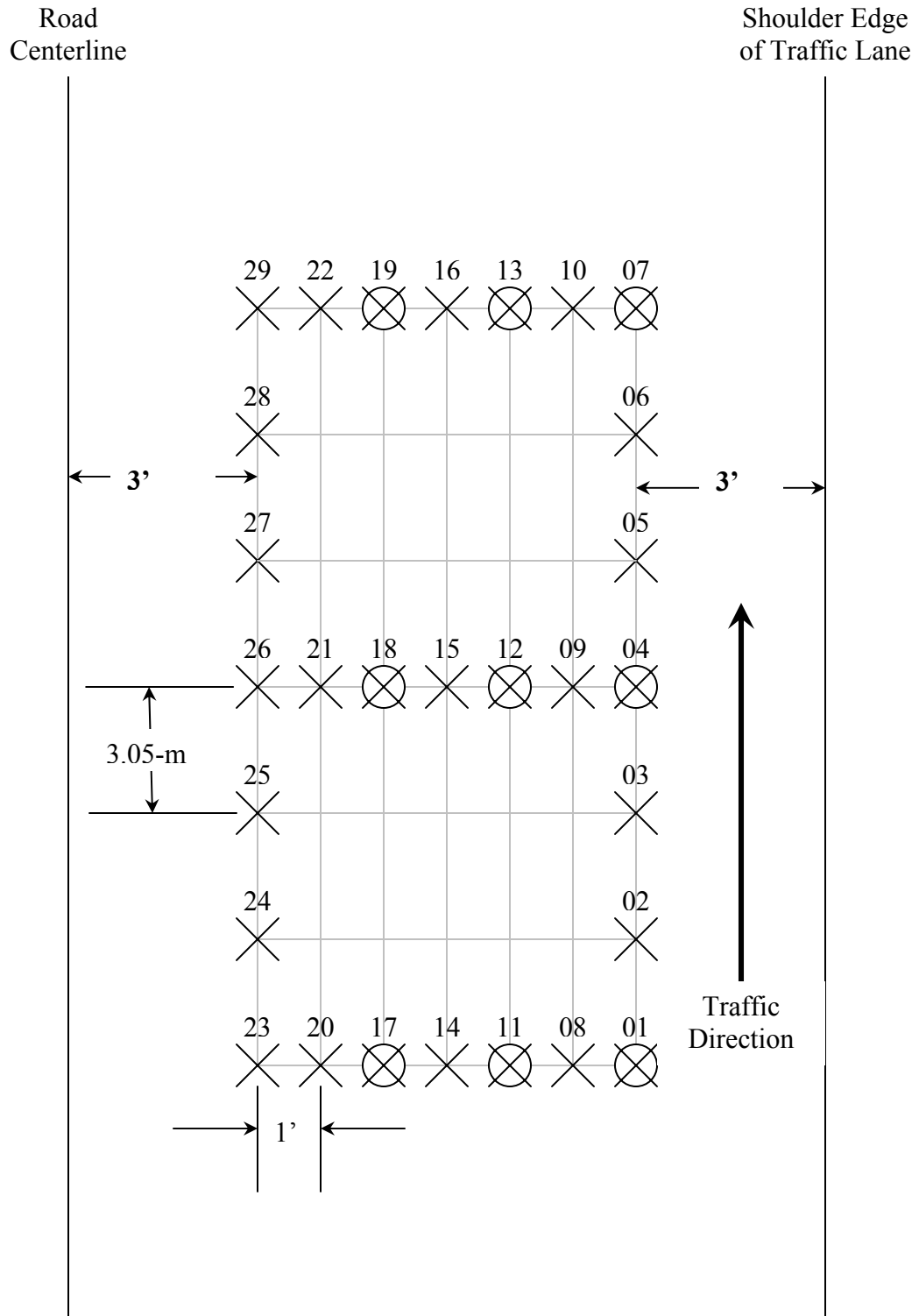
Figure 3.10 Modified test site layout of M-20, test section 1, test sites 1 and 2 (30202-11 and 12)

mapping only. No field investigation other than crack measurement has been conducted, and therefore the cracks have not been confirmed as TDC.

6.8   M-42, Test Section 1, Test Site 1 (30422-11)

M-42 between Mesick and Manton is a flexible two-lane rural road with 11-ft lanes and 3-ft asphalt shoulder. The general terrain of the area consists of rolling hills, but the test section is located along a stretch of flat agricultural land. The road is placed apparently at grade, with small earthen berms on either side of the pavement the only change in grade from the surrounding land to the road surface. The original survey of the pavement (conducted during the summer of 2002) indicated short, random longitudinal cracking appearing outside the wheelpaths. Upon returning to the site on November 7, 2002 for field investigation, a more detailed examination of the cracks revealed that they formed a network within the wheelpaths closely resembling fatigue cracks. Subsequent coring revealed however that the cracks were indeed TDC.

During the field investigation, only one site was placed on the test section due to a coring restraint imposed by MDOT. Fifty four FWD tests were conducted and twenty six 4-in diameter cores were extracted. In addition to these activities, 54 nuclear density readings were taken at points coinciding with the locations of the FWD tests. Finally, a single borehole drilled using a hand-auger to a depth of four feet at the asphalt edge on the shoulder indicated that the base consists of a 1-ft layer of clayey sand on silty sand.

6.9 M-50, Test Section 1, Test Site 1 (30502-11)

M-50 west of Charlotte is a two-lane flexible pavement that was previously investigated under a segregation project at Michigan State University conducted by Chang (2000). The roadway is a flexible pavement experiencing heavy segregation. A site survey by PRCE personnel indicated that longitudinal cracks present on the site warranted further investigation, and on November 21, 2001 a single site was established and tested. The road is located in a hilly agricultural area. The site itself is located on a hill with the down slope in the direction of traffic.

A single longitudinal crack was noted in the inner wheelpath in the segregated area. Additionally, transverse cracking was noted throughout the site. The coring on the site confirmed that the cracks are TDC. Additionally, the cross-sections of the cores indicate that the pavement may have been previously overlaid in an attempt to repair a previously observed cracking problem. The original cracks were also TDC, as indicated by cracks that occur only in the leveling course. For this site, 13 cores were extracted and 41 FWD tests were conducted. No nuclear density tests were conducted, but a single borehole was drilled to a depth of 1-ft to investigate the condition of the base.

6.10 M-50, Test Section 2, Test Site 1 (30502-21)

M-50 west of Charlotte is a two-lane flexible pavement that was identified in November, 2001 during the field investigation of M-50, section 1. Similar to section 1,

the roadway is a flexible pavement but is experiencing medium to heavy segregation strip segregation close to the outer wheel path. The pavement is located in flat farmland on an embankment elevated approximately 2-ft above the surrounding terrain. Standing water was noted in the fields on either side of the pavement. The pavement was investigated on May 29, 2002 when a single site was established and tested.

The predominant distress on the pavement consisted of longitudinal cracks in the segregated area. Short transverse cracks were also noted at regular intervals at the center of the lane. In addition to regular FWD testing and coring, nuclear density measurements were conducted in visually identified segregated and non-segregated areas. Ultimately, 48 FWD tests were conducted and 38 cores extracted. A total of 61 nuclear density measurements were conducted.

6.11 M-52, Test Section 1, Test Site 1 (30521-11)

M-52 south of Perry is a flexible two-lane rural road with 11-ft lanes and 3-ft asphalt shoulder. The general terrain of the area consists of relatively flat agricultural land alternating with wooded areas. The road is placed on a fill area, which according to historical data was the location of a gravel road. The construction of the original asphalt road entailed simply overlaying the existing gravel road. The original survey of the pavement (conducted during the fall of 2002) indicated a developed network of longitudinal and transverse cracks. The gradation of surface course appears to be a fine mix, and no segregation was apparent.

During the field investigation, only one site was placed on the test section due to a coring restraint imposed by MDOT. 44 FWD tests were conducted and 25 4-in diameter cores were extracted. In addition to these activities, 48 nuclear density readings were taken at points coinciding with the locations of the FWD tests. Finally, a single borehole drilled using a hand-auger to a depth of three feet indicated that the base consisted of a mix of clay, sand and gravel indicative of road gravel. The coring was halted at a depth of 3 where a stiff layer was encountered. The composition of the stiff layer could not be established, but it is likely the original surface of the gravel road.

6.12 M-52, Test Section 2, Test Site 1 (30521-21)

This section of road is situated several miles to the north of 30521-21 in an area of similar terrain. The pavement lane and shoulder width are the same as before. The only significant difference between the two sites is that the surface course is made of a much coarser mix and both segregation and raveling are apparent at the lane centerline. A single overbanded longitudinal crack is plainly visible throughout the section slightly to the outside of the lane centerline, but upon closer inspection, other faint longitudinal cracks are visible at the outside edge of the inner wheelpath.

During the field investigation, only one site was placed on the test section due to a coring restraint imposed by MDOT. 41 FWD tests were conducted and 10 4-in diameter cores were extracted. In addition to these activities, 41 nuclear density readings were taken at points coinciding with the locations of the FWD tests. Finally, a single borehole drilled using a hand-auger to a depth of four feet.

6.13 M-55, Test Section 1, Test Sites 1 and 2 (30552-11 and 30552-12)

M-55 west of Prudenville is a 4 lane (2 lanes in each direction) road with concrete curb and gutter. The surrounding is generally flat, and sloping to the shores of Houghton Lake. Inventory data indicates that the natural soil is sand, which was confirmed by hand-auguring a borehole. MDOT personnel originally suggested that M-55 could possibly be experiencing TDC, and a subsequent survey by PRCE indicated that TDC were very likely at the site. On August 20, 2001, the field investigation was conducted on the east bound lane outer lane. The test section was selected at Iroquois Avenue just west of Prudenville.

Longitudinal cracking was noted on the site, but in places did not follow the typical TDC pattern of forming at the centerline edges of the wheelpaths. Here, the cracks propagated specifically through medium segregated areas. Transverse cracking was also noted. TDC was confirmed by coring, and temperature profile data was also collected for the pavement. Additionally, the crack length on M-55 was also used in the crack propagation model, and therefore, monthly surveys were conducted to map the extent of the cracking.

Due to the curb and gutter, the FWD could not obtain the first row of tests. Therefore, sites 1 and 2 were modified as shown in Figures 3.11 and 3.12, respectively. Ultimately, 33 and 37 FWD tests were conducted on sites 1 and 2, respectively, and 15 and 14 cores were drilled from sites 1 and 2, respectively.

The laboratory testing proceeded as outlined in section 3.5. The cores were

cleaned, the physical dimensions were recorded and the loose material was removed from

the bottom of the cores. As before with test sites on US-41 (20411-11 and 12), the cores

were relatively thin (3.0-in approx.) and indicated that the pavement was laid in two lifts.

Inventory data further indicated both courses were constructed of the same mix (4B).

Therefore, after trimming, no additional specific gravity tests were necessary, as the cores

in their entirety were a convenient size for testing. The specimens were then tested in
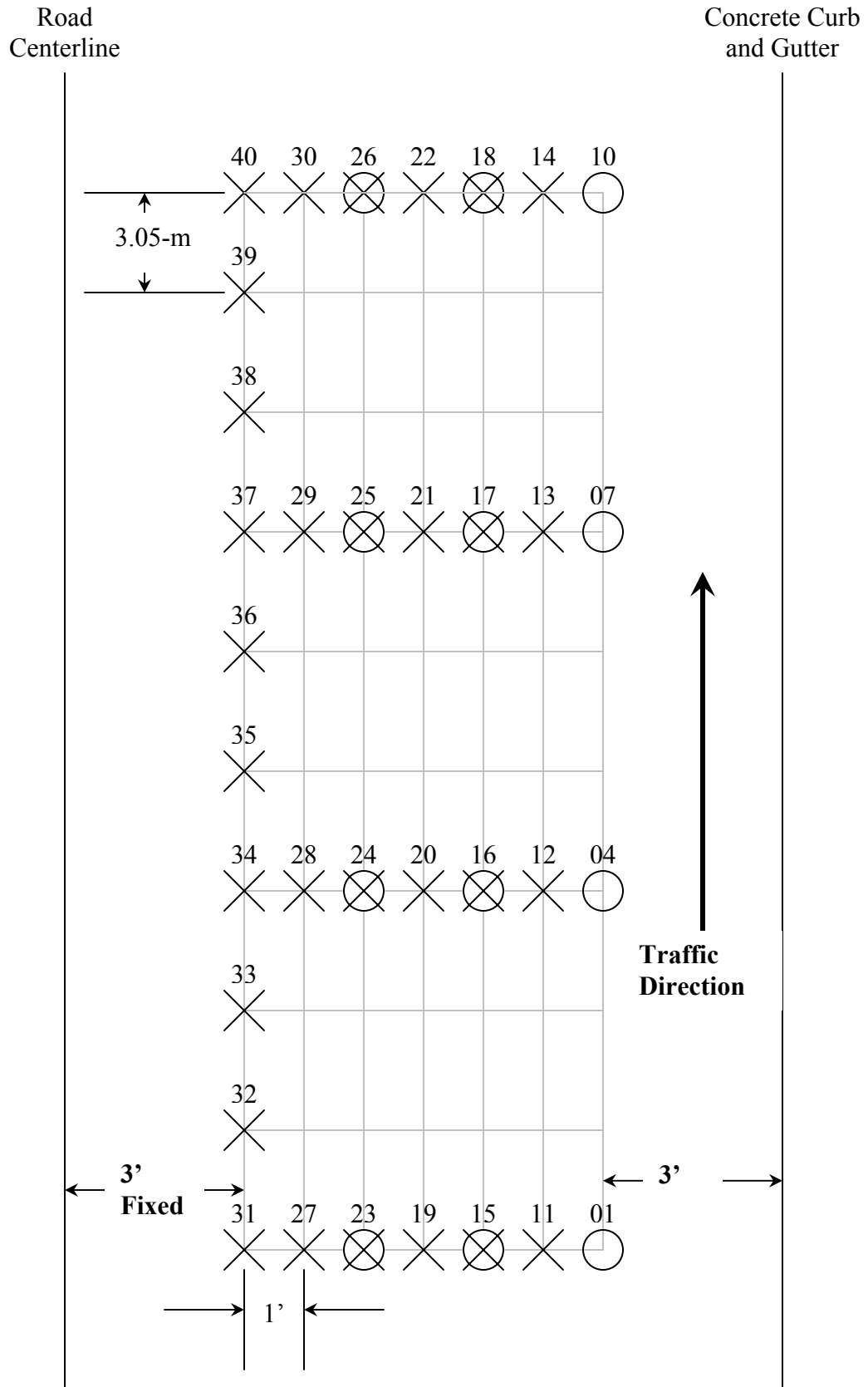
Figure 3.11 Modified test site layout of M-55, test section 1, test site 1 (30552-11)

Road
Centerline

Concrete Curb
and Gutter

3.05-m

36   26   22   18   14   10

35   09

34   08

33   25   21   17   13   07

32   06

31   05

30   24   20   16   12   04

Traffic
Direction

29   03

28   02

4'

3'
Fixed

27   23   19   15   11   01

1'
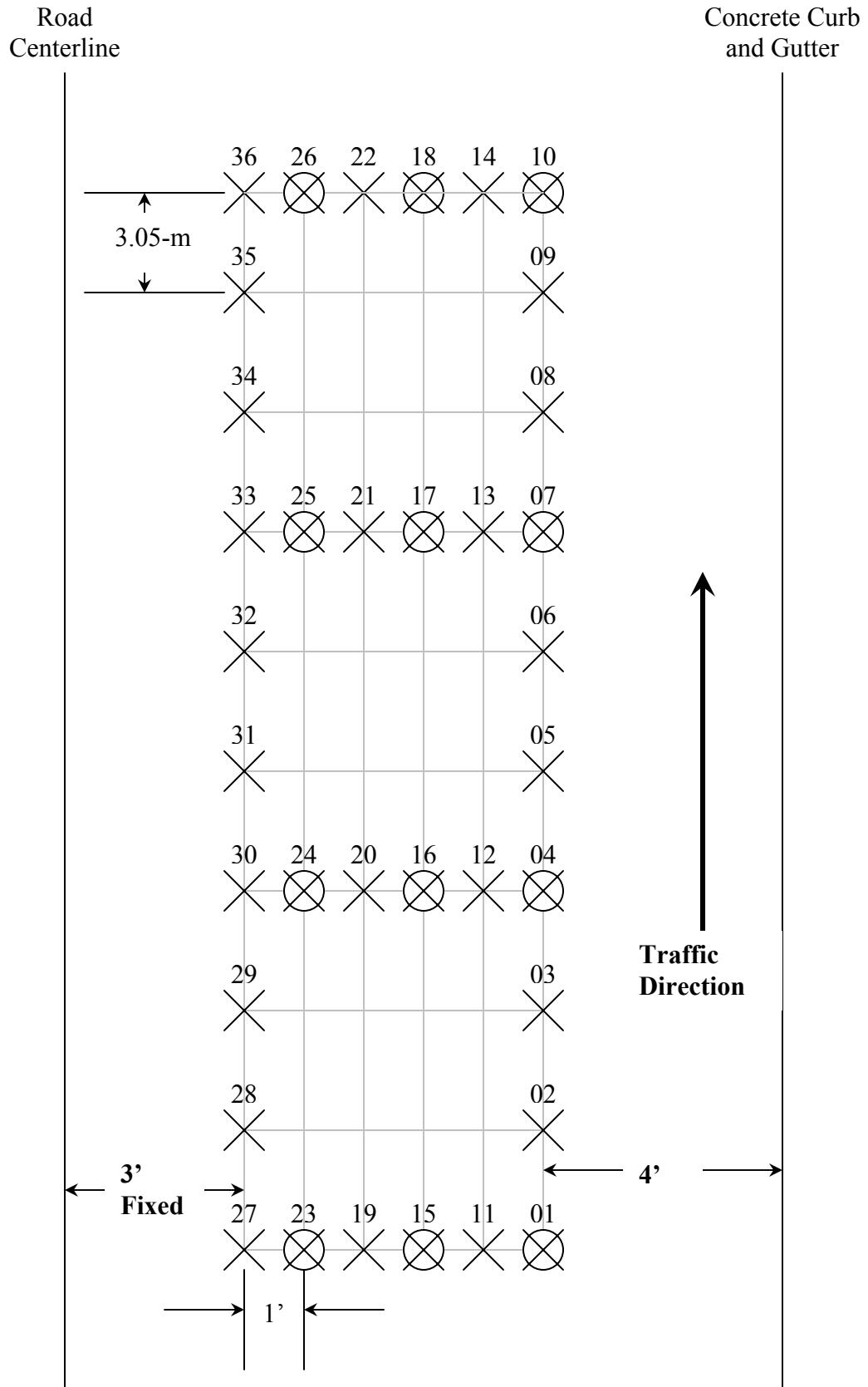
Figure 3.12 Modified test site layout of M-55, test section 1, test site 2 (30552-12)

54

ITCLT and ITST modes. To examine the degree of segregation present, the cores were subjected to incineration and both the asphalt content and aggregate gradation were measured.

6.14 Marsh Road

Marsh road in Okemos is a four lane county road (two lanes in each direction). The topography consists of primarily flat land with occasional low hills. The test section was located on the side of one of these hills. The pavement is a flexible pavement that had been repeatedly overlaid. This pavement was identified by PRCE personnel as a candidate TDC project, and therefore field investigation was conducted over two days; site 1 was tested on October 11, 2000 and site 2 was tested on October 27, 2000. The predominant distresses on the pavement were longitudinal cracking near the center of the lane. Several parallel longitudinal cracks were observed in an area of medium to heavy segregation. Transverse cracking has also appeared on the pavement. Therefore, the cracking was rated as phase II TDC.

This site was test prior to the development of the standard testing layout, and therefore followed a different testing pattern. The test layout consisted of two parallel lines arranged in the longitudinal direction along the edges of the wheelpaths. Two schematics showing the testing layout on Marsh Road Sites 1 and 2 are shown below in Figures 3.13 and 3.14. A total of 58 FWD tests were conducted and 8 cores obtained, with 30 FWD tests conducted at site 1 and 28 tests conducted at site 2. 4 cores were obtained from each site.

Road
Centerline

Yellow Line

20   60

1'

19   59

18   58

17   57

16   56

15   55

14   54

**Traffic
Direction**

13   53

12   52

3.5'

← **3.5'** →

11   51

1'
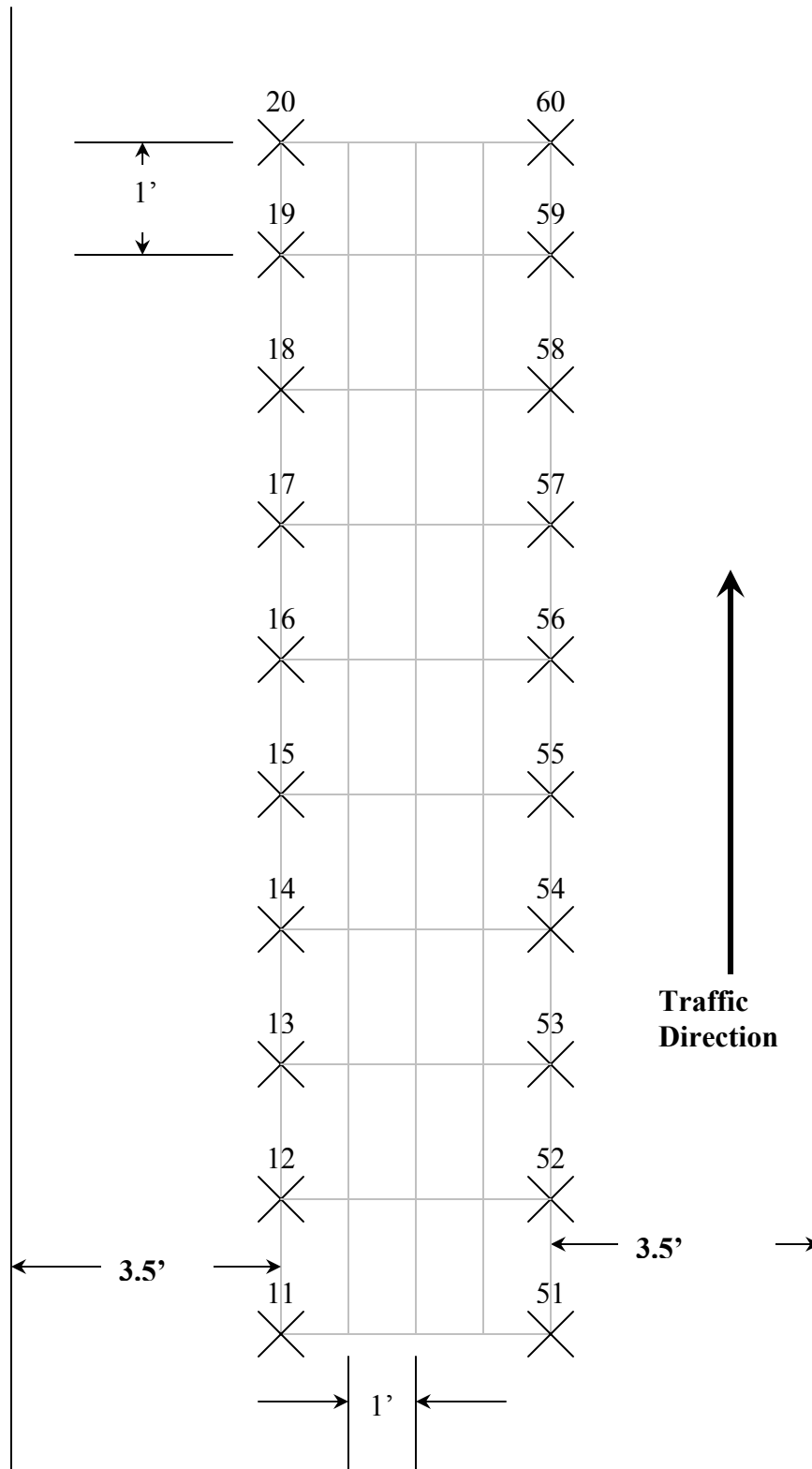
Figure 3.13 Test site layout of Marsh Road, test site 1

Road
Centerline

Yellow Line

30   87   84   85   70   86

1'

29   69

28   68

27   67

26   66

Traffic
Direction

25   65

24   64

23   63

22   62

2.5'

3.5'

21   80   81   82   61   83

1'
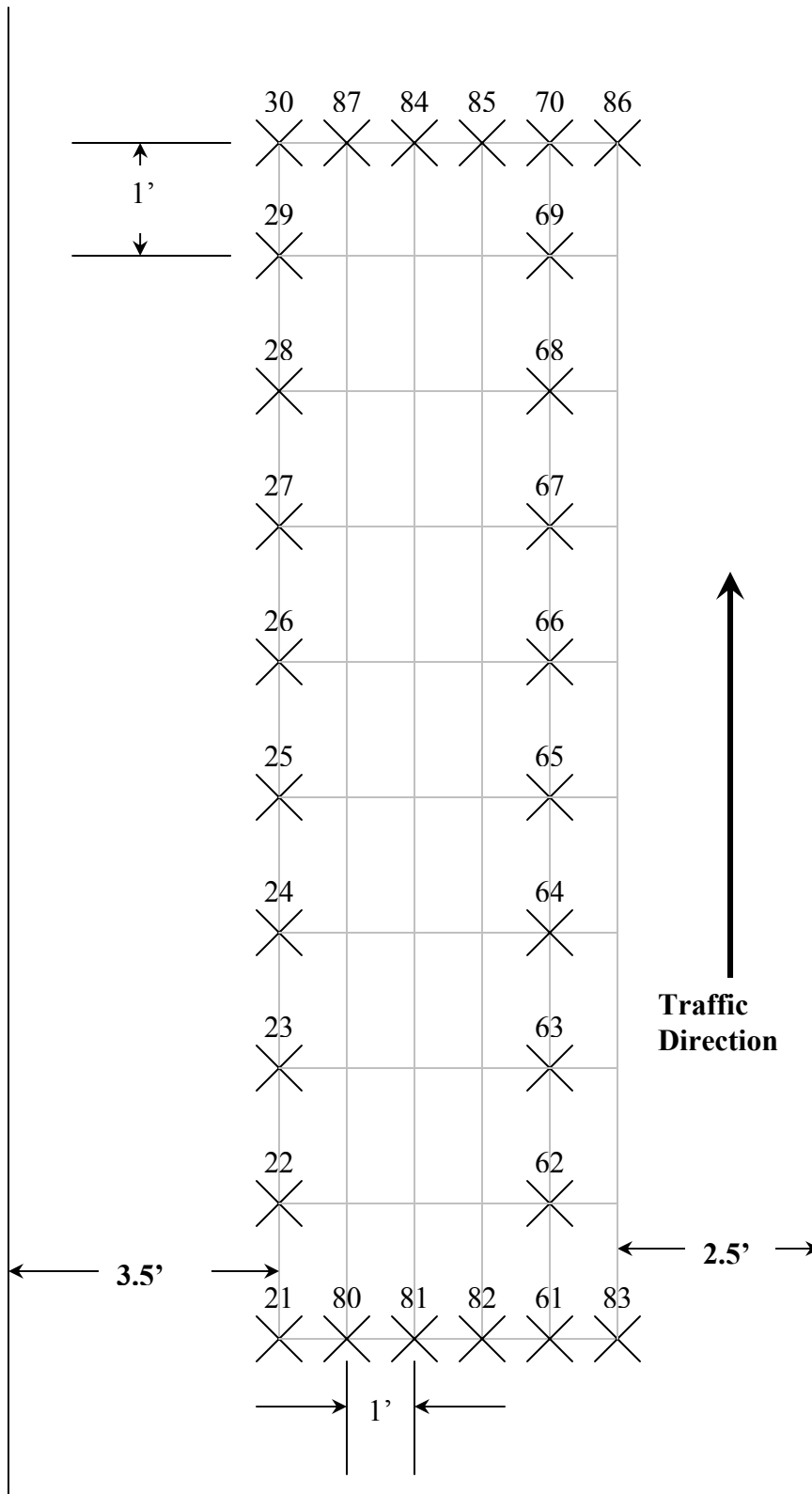
Figure 3.14 Test site layout of Marsh Road, test site 2

As with the field investigation, this pavement was the first subjected to laboratory investigation and the laboratory procedure had yet to be established. The investigation procedures for this pavement was the model on which the test procedures were based however. The cores were cleaned, the physical dimensions were recorded and the loose material was removed from the bottom of the cores. The cores were cut into test specimens after conducting specific gravity tests on the cores. Specific gravity tests were then repeated on the test specimens. The specimens were then tested in ITCLT and ITST modes. Although medium to heavy segregation was observed in the pavement, the test specimens were not incinerated.

CHAPTER 4
DATA ANALYSIS

1.0   GENERAL

As stated in chapter 1, the objectives of this study include:

4. Identify the causes of TDC and the factors affecting top-down cracking potential.

5. Compare top-down and bottom-up cracking potentials.

6. Develop a model to describe the rate of TDC propagation.

To accomplish these objectives, lab and field investigations were conducted and various

types of data were collected as stated in chapter 3. These data include:

1. Distress data that were used to develop TDC propagation models.

2. NDT data that were used to backcalculate resilient modulus of the pavement

    layers.

3. Field and lab measured density data that were used to confirm the presence of

    segregation.

4. Indirect tensile cyclic load test data that were used to determine the moduli of the

    asphalt courses.

5. Indirect tensile strength test data to determine the relative fatigue performance of

    the asphalt concrete courses.

6. Mechanistic analysis to determine load induced surface tensile stresses.

This chapter details the analyses used to determine the factors affecting TDC

potential. During the analysis, each factor was studied in reference to its variation along

and across the pavement. Further, the value of each parameter was compared to that

obtained from two control test sites that have exhibited no distress. Finally, in the

analyses of the data, the strength and resilient moduli values of the segregated specimens were compared directly to those of the non-segregated specimens.

2.0 DISTRESS DATA

Unfortunately, the historical pavement surface distress data of MDOT and other state highway agencies treat surface cracks in the same fashion regardless if the cracks are bottom-up or top-down. The reason is that no crack identification procedure has been developed whereby cracks can be identified as TDC. Such a procedure was developed during this study and is presented in this chapter. Nevertheless, the historical MDOT distress data cannot be used to determine the rate of TDC propagation. To alleviate the problem, periodical manual distress surveys were conducted.

> Various distress surveys were conducted on all test sections. During the surveys, segregated areas were noted and mapped along with their degrees of segregation and, on several test sections, crack measurements were made as to determine the crack propagation rates. Finally, to increase the time frame of the distress data, the detailed distress data collected by Chang (2000) were included in this study.

2.1 Distress

On all the projects visited, the distresses present, including segregation, were cataloged. Additionally, in a parallel study investigating the causes of TDC in rubblized pavements conducted by Svasdisant (2003), bi-annual surveys of every rubblized project in Michigan were conducted. The observed distresses for each flexible pavement investigated in this project are listed in Table 4.1. The observed distresses of the rubblized pavement survey conducted by Svasdisant are provided in Table 4.2. It should be noted that the pavements listed in Table 4.2 are only those that are strongly suspected to be experiencing TDC, since the TDC have not be confirmed by coring.

2.3 Crack Measurement

During the surveys of test sites, digital images were obtained, all cracks were mapped, and, for each crack, the coordinates of the crack tips were measured relative to the test site grid. These coordinates were then used to calculate the cumulative lengths of all transverse and longitudinal cracks. Table 4.3 provides a list of the time history of the cumulative lengths of the longitudinal and the transverse cracks. Figures 4.1 through 4.3 depict the growth in the cumulative lengths of the longitudinal and transverse cracks. Finally, Figures 4.4 to 4.13 show actual photographs of the test sites.

It is important to note that most TDC tend to initiate as longitudinal cracks and, over time, they develop according to the following three phases (Svasdisant et al, 2001):

1. Phase 1: Short, longitudinal cracks outside of the wheelpath.

2. Phase 2: The original longitudinal cracks grow longer and sister cracks form.

3. Phase 3: Both the original longitudinal cracks and sister cracks have developed into extensive longitudinal cracks connected by short transverse cracks.

Each pavement can be categorized into one of the above three phases of crack development. For example, the TDC on M-20 are typical of phase 1 cracking (see Figure 4.5), the TDC on Marsh Road show phase 2 cracking (see Figure 4.13), and the TDC on M-37 have evolved to phase 3 cracking (see Figure 4.6). It is important to note that the

Table 4.1 Distresses observed on flexible pavements

Distress type	No of projects	JTC	TTDC	RTC	LTDC	S	R	Rut
LTDC	2				2			
LTDC/TTDC	1		1		1			
LTDC/S	3				2	2		
LTDC/TTDC/S	3		3		3	3		
LTDC/TTDC/RTC	1		1	1	1			
LTDC/TTDC/S/JTC	4	5	5		5	5		
LTDC/TTDC/S/R	2		2		2	2	2	
LTDC/TTDC/S/RTC	1		1	1	1	1		
No Distress	1							
Total	**18**	**5**	**13**	**2**	**17**	**13**	**2**	**0**

LTDC = Longitudinal top-down cracks, TTDC = Transverse top-down cracks, S = segregation, JTC = Joint transverse crack, R = Raveling, RTC = Regular transverse crack

Table 4.2 The number of projects exhibiting the indicated distress observed during the May 2002 distress survey

Distress type	No of projects	JTC	TTDC	RTC	LTDC	RLC	ALC	S	R	P	PH	RJ	Rut	B	BC	B-up	D
LTDC/TTDC/S/JTC/R/RTC/RLC/P/PH	1	1	1	1	1	1		1	1	1	1						
LTDC/TTDC/S/JTC/R/P/PH/Rut	1	1	1		1			1	1	1	1		1				
LTDC/TTDC/S/JTC/R/P/Rut/Break up	1	1	1		1			1	1	1			1			1	
LTDC/TTDC/S/JTC/R/P/Bleeding	1	1	1		1			1	1	1				1			
LTDC/TTDC/S/JTC/R/P	1	1	1		1			1	1	1							
LTDC/TTDC/S/JTC/R/RJ	1	1	1		1			1	1			1					
LTDC/TTDC/S/JTC/R/Rut	1	1	1		1			1	1				1				
LTDC/TTDC/S/JTC/RLC/Rut	1	1	1		1	1		1					1				
LTDC/TTDC/S/JTC/Rut/Bleeding	1	1	1		1			1					1	1			
LTDC/TTDC/S/JTC/Rut	2	2	2		2			2					2				
LTDC/TTDC/S/JTC	3	3	3		3			3									
LTDC/TTDC/S/R/P/Rut	1		1		1			1	1	1			1				
LTDC/TTDC/S/R/RLC/P/Block crack	1		1		1	1		1	1	1					1		
LTDC/TTDC/S/R/RLC/Rut	1		1		1	1		1	1				1				
LTDC/TTDC/S/R/Rut	1		1		1			1	1				1				
LTDC/TTDC/S/R	2		2		2			2	2								
LTDC/TTDC/S/RTC	1		1	1	1			1									
LTDC/TTDC/S/RLC	1		1		1	1		1									
LTDC/TTDC/S/Rut	1		1		1			1					1				
LTDC/TTDC/S	3		3		3			3									
LTDC/JTC/S/R/RTC	1	1		1	1			1	1								
LTDC/JTC/S/R/RLC/Rut	1	1			1	1		1	1				1				

7

Table 4.2 (cont'd) The number of projects exhibiting the indicated distress observed during the May 2002 distress survey

Distress type	No of projects	JTC	TTDC	RTC	LTDC	RLC	ALC	S	R	P	PH	RJ	Rut	B	BC	B-up	D
LTDC/JTC/S/RTC/RLC/Rut	1	1		1	1	1		1					1				
LTDC/JTC/S/RTC	1	1		1	1			1									
LTDC/JTC/S	2	2			2			2									
LTDC/S/R/RTC/RLC	1			1	1	1		1	1								
LTDC/S/R/RLC/P/PH/RJ	1				1	1		1	1	1	1	1					
LTDC/S/R	1				1			1	1								
LTDC/S/RLC/RJ/Break up	1				1	1		1				1				1	
LTDC/S/RLC/RJ	1				1	1		1				1					
LTDC/S/RLC/P	1				1	1		1		1							
LTDC/S/Rut	1				1			1					1				
LTDC/S	4				4			4									
LTDC/RTC/P	1			1	1					1							
LTDC/RLC/RJ	1				1	1						1					
LTDC/Rut	1				1								1				
LTDC	2				2												
TTDC/JTC/S/RLC/RJ	1	1	1			1		1				1					
TTDC/JTC/ALC/Rut	1	1	1				1						1				
JTC/RTC	1	1		1													
JTC/RLC/Rut	1	1				1							1				

Table 4.2 (cont'd) Number of projects exhibiting the indicated distress observed during the May 2002 distress survey

Distress type	No of projects	JTC	TTDC	RTC	LTDC	RLC	ALC	S	R	P	PH	RJ	Rut	B	BC	B-up	D
JTC/RLC	1	1				1											
JTC	1	1															
S/R/RLC/P/PH	1					1		1	1	1	1						
S/P	1							1		1							
S/PH	1							1			1						
S/RJ	1							1				1					
S/RLC	1					1		1									
S/Depression	1							1									1
S	3							3									
RTC/RLC	2			2		2											
RTC	1			1													
RLC/RJ	1					1						1					
RLC	1					1											
RJ/Rut	2											2	2				
RJ	2											2					
Rut	1												1				
Bleeding	1													1			
No distress	10																
Total	**84**	**26**	**28**	**11**	**48**	**22**	**1**	**53**	**19**	**12**	**5**	**12**	**20**	**3**	**1**	**2**	**1**

LTDC = Longitudinal top-down cracks, TTDC = Transverse top-down cracks, S = segregation, JTC Joint transverse crack,
R = Raveling, RTC = Regular transverse crack, RLC = Regular longitudinal crack, P = Patch, PH = Pothole, RJ = Rough joint,
D = Depression, B = Bleeding, ALC = Alligator cracks, BC = Block cracking, and B-up = Break up

Table 4.3 Summary of crack measurements

Route	Test site	Survey date	Cracklength (ft)	
			Transverse	Longitudinal
M-20	30202-11	8/21/2001	0.0	9.3
		9/30/2001	0.0	11.0
		12/7/2001	0.0	13.8
		2/9/2002	0.0	42.6
		3/17/2002	0.0	58.1
		6/29/2002	0.0	41.7
		8/30/2002	0.0	44.3
		10/7/2002	0.0	41.6
M-20	30202-12	8/21/2001	0.0	31.0
		9/30/2001	0.0	40.4
		12/7/2001	0.0	48.9
		2/9/2002	0.0	57.1
		3/17/2002	0.0	58.7
		6/29/2002	0.0	60.0
		8/30/2002	0.0	60.0
		10/7/2002	0.0	58.8
M-55	30552-11	3/17/2002	0.0	61.3
		6/29/2002	0.0	118.7
		8/30/2002	0.0	98.1
		10/11/2002	0.0	99.3
M-55	30552-12	3/17/2002	0.0	116.1
		6/29/2002	0.0	95.9
		8/30/2002	13.8	108.9
		10/11/2002	13.8	115.1
M-20	30204-21	6/29/2002	11.1	31.2
		8/28/2002	18.2	38.2
		10/7/2002	25.0	42.8
M-20	30204-22	6/29/2002	1.3	2.2
		8/28/2002	4.0	4.6
		10/7/2002	7.7	4.6
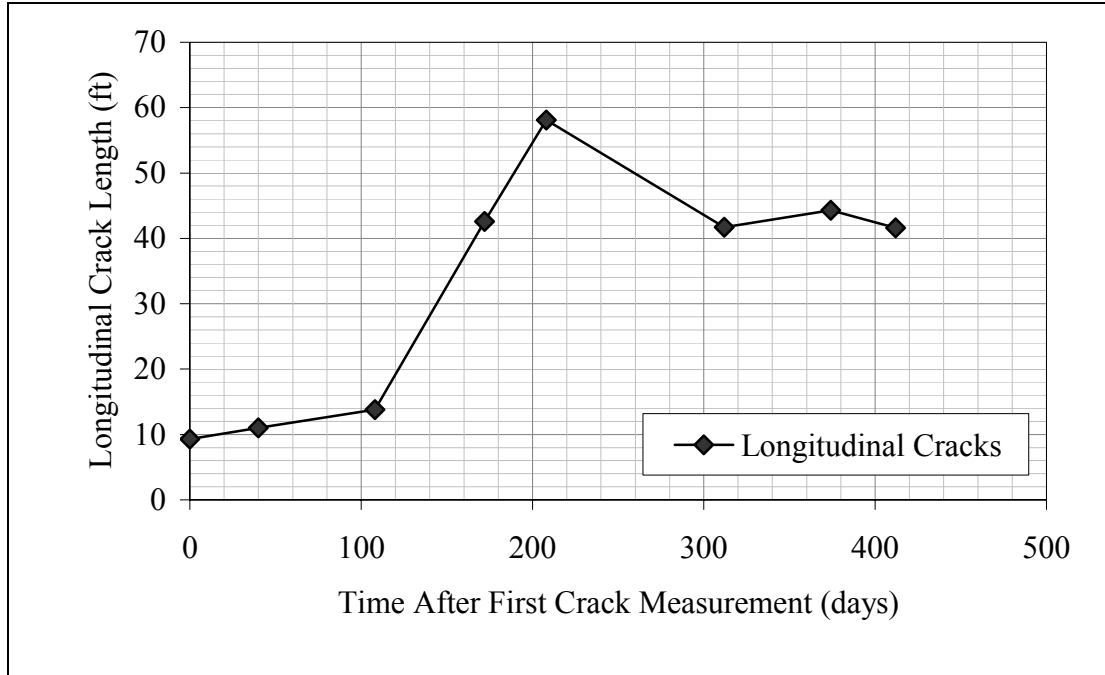
(a) Longitudinal TDC on test site 1 (30202-11)
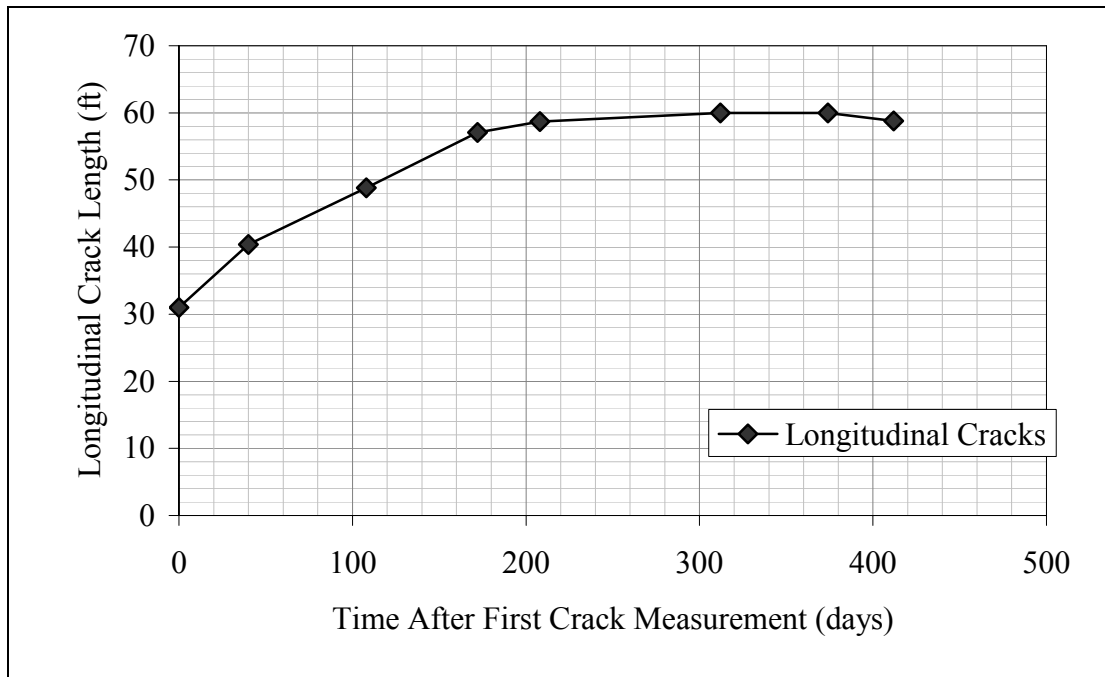
(b) Longitudinal TDC on test site 2 (30202-12)

Figure 4.1 Growth of cracking on M-20, test section 1
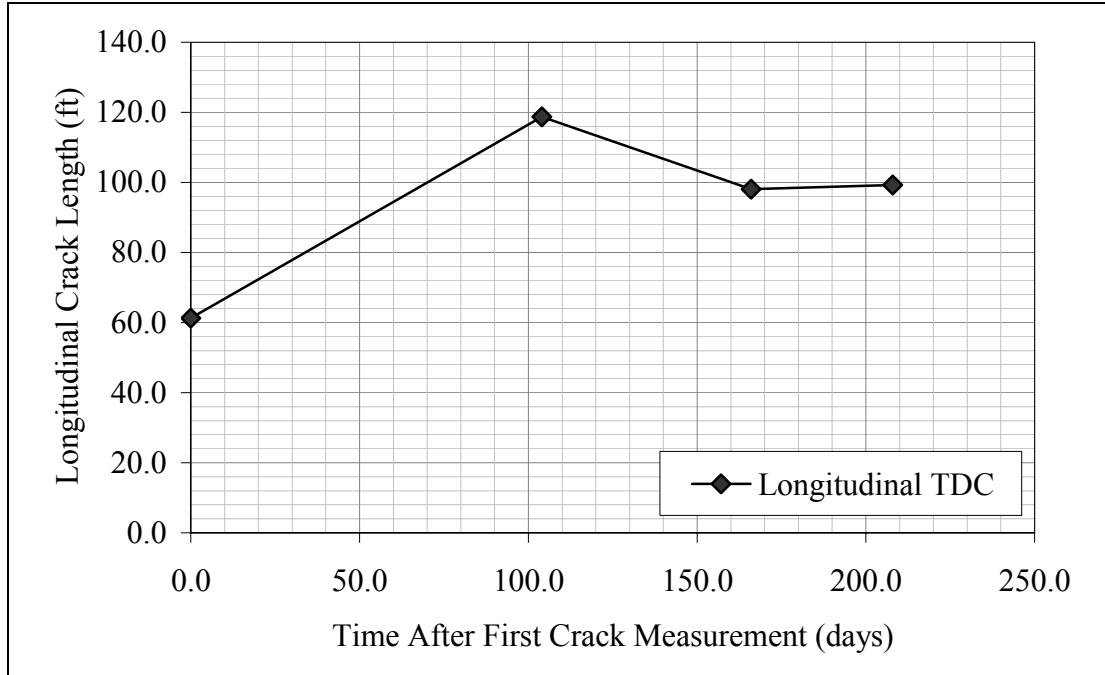
(a) TDC growth on test site 1 (30552-11)
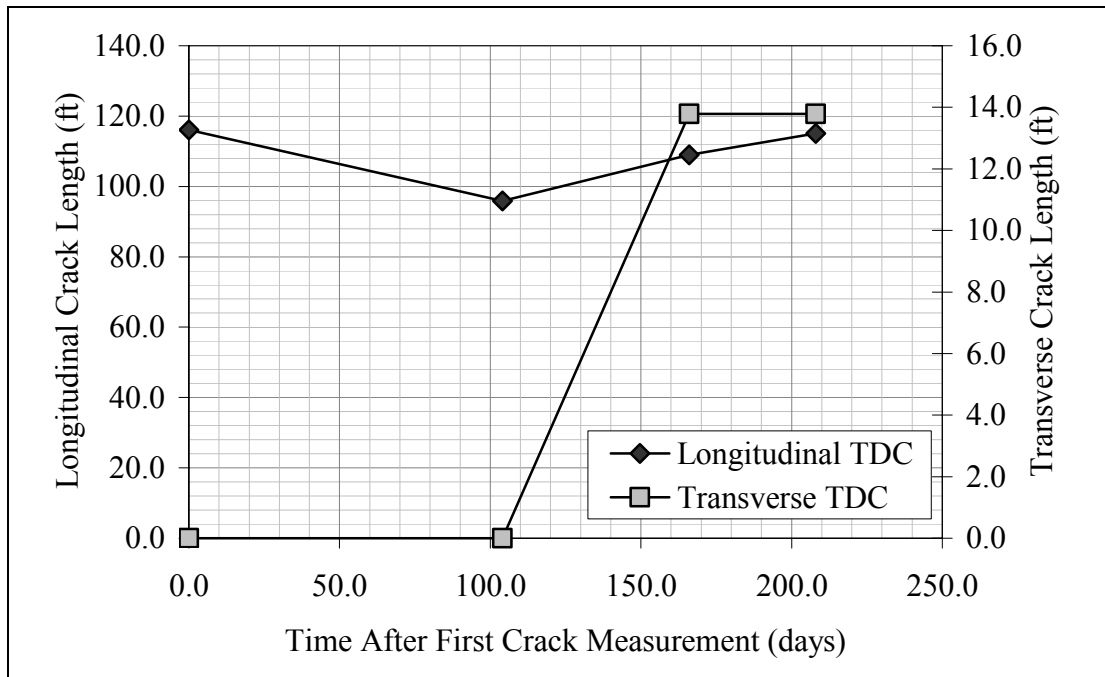
(b) TDC growth on test site 2 (30552-12)

Figure 4.2 Growth of cracking on M-55, test section 1
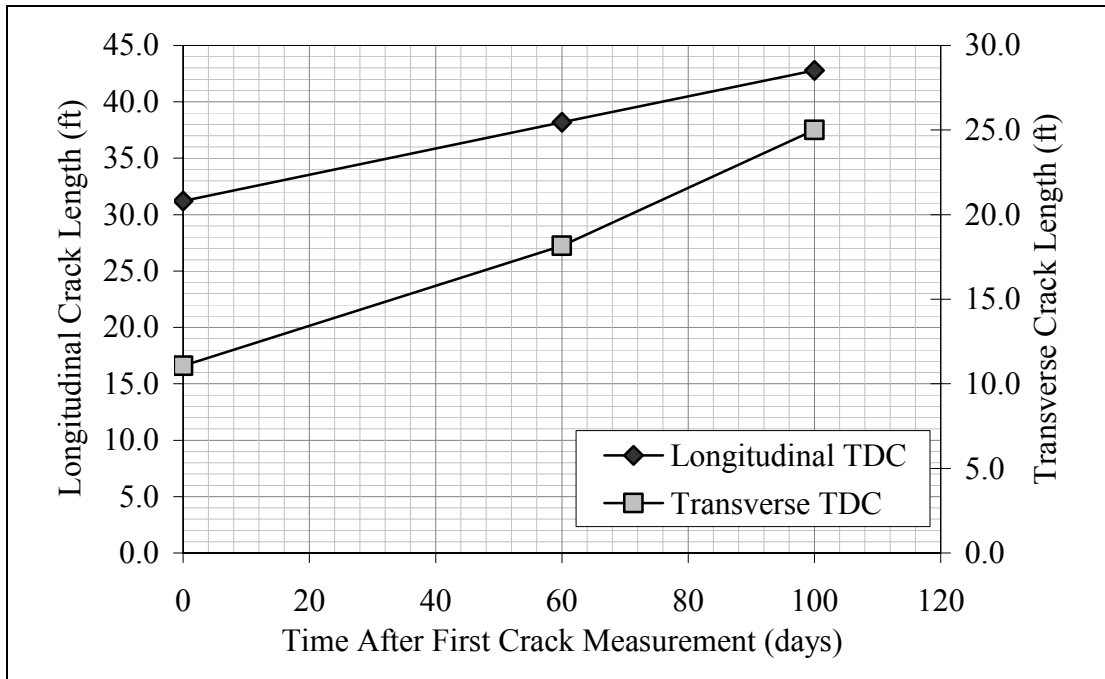
(a) TDC growth on test site 1 (30204-21)
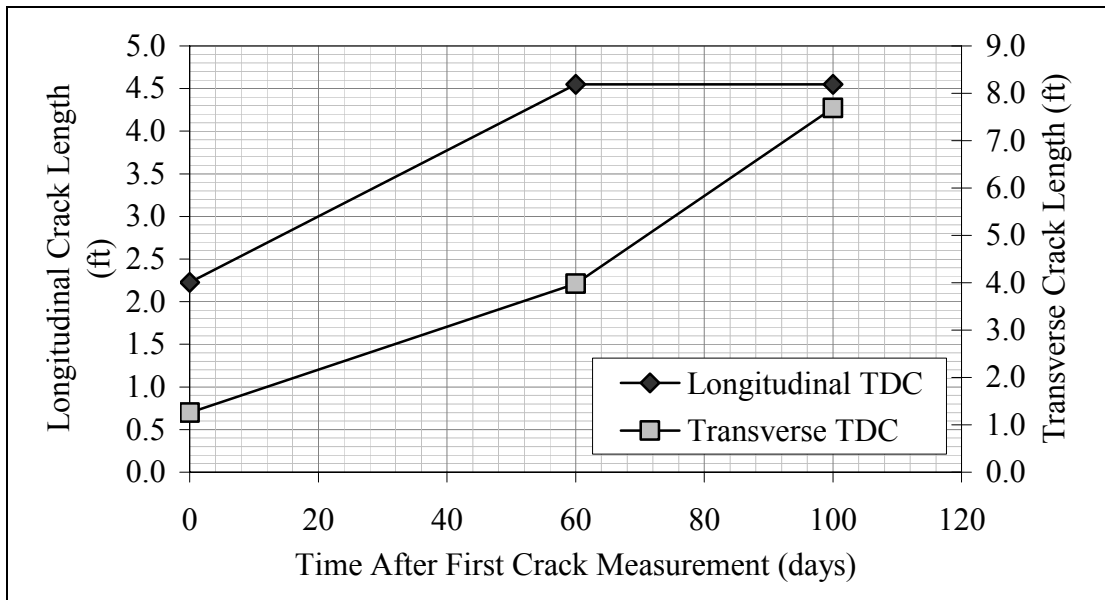
(b) TDC growth on test site 2 (30204-22)

Figure 4.3 Growth of cracking on M-20, test section 2

Figure 4.4 TDC and raveling in heavily segregated areas on US-23, May 2002, 2 years after construction (rubblized pavement)

Figure 4.5 TDC initiation at the edge of the wheel path on M-20 (flexible pavement, no segregation is visible)

Figure 4.6 Advanced level of TDC on M-37 (rubblized pavement)

Figure 4.7 TDC on M-42 (flexible pavement, no segregation visible)

Figure 4.8 TDC in segregated areas on M-50 test section 1 (flexible pavement)

Figure 4.9 TDC in segregated areas on M-50 test section 2 (flexible pavement)

Figure 4.10 TDC on M-50 test section 1 (flexible pavement, no segregation visible)

Figure 4.11 TDC in segregated area on M-50 test section 2 (flexible pavement)

Figure 4.12 TDC in segregated areas at the edge of the wheel path on M-55 (flexible pavement)

Figure 4.13 TDC in heavily segregated areas on Marsh Road (flexible pavement)

three phases of TDC propagation can be used to develop crack propagation models. That

is prediction models can be developed to address the required time for TDC in a

pavement section to develop from one phase to another.

2.4   Segregation

During the site investigation phase of this study, for each test site, segregated

areas were noted. On three test sites (M-50 test section 1, test site 1 and for M-55 test

section 1, test sites 1 and 2) detailed segregation maps were developed. To expand the

data base, crack measurement data obtained by Chang (2000) in segregated pavements

were included. In this study, the cracks that were measured by Chang were confirmed as

TDC by coring. Tables 4.4 through 4.6 show the crack and segregation data collected by

Chang and utilized in this study.

2.5   Other Distresses

During the distress surveys, other types of distress were also observed and

recorded. These include segregation, rut, raveling, and, for rubblized pavements,

reflective cracks. These distresses are summarized in Tables 4.1 and 4.2.

3.0   TDC PROPAGATION MODEL

It can be seen from Tables 4.1 and 4.2 that for 53 out of 84 pavement projects, the

TDC are associated with segregation. Hence, the initiation and propagation of TDC is

related to the degree to which the pavement is segregated. In this study, as well as in

Chang (2000), the cumulative crack length in areas with certain degree of segregation

19

Table 4.4 Segregation sites from Chang (2000)

Route	Site number	Construction date	Length of segregated areas (ft)				
			Light	Light-medium	Medium	Medium-heavy	Heavy
State Police Parking Lot	1	July, 1995	0	0	36	0	96
US-23	16	July, 1992	0	0	88	0	0
M-50	14	May, 1997	57	0	21	0	2
M-50	30502-12	May, 1997	60	0	4	0	4
I-75	20-1	Sept, 1997	0	0	0	0	12
I-75	20-2	Sept, 1997	0	0	0	0	5
I-75	20-3	Sept, 1997	0	0	0	0	7
I-75	20-4	Sept, 1997	0	8	9	11	8

Table 4.5 Length of cracks in segregated areas

Site	Survey date	Surface age (Months)	Crack Length (ft)					
			Light	Light-medium	Medium	Medium-heavy	Heavy	Non-Seg
1	Feb, 1998	31	0	0	0	0	0	0
	May, 1998	33	0	0	0	0	0	0
	Oct, 1998	39	0	0	0	0	0	0
	April, 1999	45	0	0	0	0	0	0
	June, 1999	47	0	0	0	0	0	0
	March, 2000	0.001	0	0	0	0	28	0
16	July, 1998	72	0	0	75.5	0	0	24.5
	April, 1999	81	0	0	75.5	0	0	31
	June, 1999	83	0	0	80	0	0	41
	March, 2000	91	0	0	80	0	0	48
14	Feb, 1998	10	0	0	0	0	0	0
	May, 1998	12	0	0	0	0	0	0
	Oct, 1998	17	0	0	0	0	0	0
	April, 1999	23	7	0	12	0	0	0
	June, 1999	25	7	0	12	0	0	0
	March, 2000	34	8	0	12	0	0	0
30502-12	Feb, 1998	10	10	0	0	0	3	2.5
	May, 1998	12	13	0	0	0	3	2.5
	Oct, 1998	17	13	0	0	0	3	2.5
	April, 1999	23	16	0	0	0	4	8.5
	June, 1999	25	16	0	0	0	4	15.5
	March, 2000	34	25	0	0	0	4	29
20-1	Oct, 1998	13	0	0	0	0	0	0
	April, 1999	19	0	0	0	0	0	0
	June, 1999	21	0	0	0	0	0	0
	March, 2000	30	0	0	0	0	11	0
20-2	Oct, 1998	13	0	0	0	0	0	0
	April, 1999	19	0	0	0	0	0	0
	June, 1999	21	0	0	0	0	0	0
	March, 2000	30	0	0	0	0	2	8
20-3	Oct, 1998	13	0	0	0	0	0	0
	April, 1999	19	0	0	0	0	6	4
	June, 1999	21	0	0	0	0	6	4
	March, 2000	30	0	0	0	0	7	4
20-4	Oct, 1998	13	0	0	0	0	0	0
	April, 1999	19	0	4	5	8	7	0
	June, 1999	21	0	4	5	8	7	0
	March, 2000	30	0	7	7	11	7	0

Table 4.6 Percent crack measurements on segregation projects (from Chang, 2000)

Site	Survey date	Surface Age (Months)	Crack Length in Segregated Areas (%)					
			Light	Light-medium	Medium	Medium-heavy	Heavy	Non-Seg
1	Feb, 1998	31	0	0	0	0	0	0
	May, 1998	33	0	0	0	0	0	0
	Oct, 1998	39	0	0	0	0	0	0
	April, 1999	45	0	0	0	0	0	0
	June, 1999	47	0	0	0	0	0	0
	March, 2000	0	0	0	0	0	0	0
16	July, 1998	72	0	0	85.8	0	0	0
	April, 1999	81	0	0	85.8	0	0	0
	June, 1999	83	0	0	90.9	0	0	0
	March, 2000	91	0	0	90.9	0	0	0
14	Feb, 1998	10	0	0	0	0	0	0
	May, 1998	12	0	0	0	0	0	0
	Oct, 1998	17	0	0	0	0	0	0
	April, 1999	23	12.3	0	57.1	0	0	0
	June, 1999	25	12.3	0	57.1	0	0	0
	March, 2000	34	14	0	57.1	0	0	0
3050 2-12	Feb, 1998	10	16.7	0	0	0	75	0
	May, 1998	12	21.7	0	0	0	75	0
	Oct, 1998	17	21.7	0	0	0	75	0
	April, 1999	23	26.7	0	0	0	100	0
	June, 1999	25	26.7	0	0	0	0	0
	March, 2000	34	41.7	0	0	0	0	0
20-1	Oct, 1998	13	0	0	0	0	0	0
	April, 1999	19	0	0	0	0	0	0
	June, 1999	21	0	0	0	0	0	0
	March, 2000	30	0	0	0	0	91.7	0
20-2	Oct, 1998	13	0	0	0	0	0	0
	April, 1999	19	0	0	0	0	0	0
	June, 1999	21	0	0	0	0	0	0
	March, 2000	30	0	0	0	0	100	0
20-3	Oct, 1998	13	0	0	0	0	0	0
	April, 1999	19	0	0	0	0	85.7	0
	June, 1999	21	0	0	0	0	85.7	0
	March, 2000	30	0	0	0	0	100	0
20-4	Oct, 1998	13	0	0	0	0	0	0
	April, 1999	19	0	50	55.6	72.7	87.5	0
	June, 1999	21	0	50	55.6	72.7	87.5	0
	March, 2000	30	0	87.5	77.8	100	87.5	0

was measured for each test site. The length of each crack was later calculated as a

percent of the cumulative length of the segregated areas using the following equation:

$$\text{Percent Cracking} = PC = \left(\frac{C_{DS}}{L_{DS}}\right) \times 100\% \qquad 4.1$$

Where: C_{DS} = cumulative crack length in segregated areas (ft); and

              L_{DS} = length of segregated areas (ft).

Based on the PC data, the following three-tiered approach was taken to develop crack

propagation models:

1. Each segregated area was assigned a degree of segregation based on the severity

    of the segregation, as described in chapter 3, section 4.1.

2. Each measurement of percent cracking was then graphed against time for each

    degree of segregation. The time scale is based on the surface age of the pavement,

    either the time since original construction, or the time since the most recent

    overlay.

3. For each degree of segregation, the best fit logarithmic growth equation (see

    equation 4.2) was obtained.

$$PC = b + (a)\ln(t) \qquad 4.2$$

    Where: PC = percent cracking;

                  a, b = regression coefficients; and

                  t = time (months).

    Examples of the data for crack length in each degree of segregation are shown in

Figure 4.14. Once the best fit logarithmic growth equation had been obtained for each

degree of segregation, the regression coefficients "a" and "b" were plotted against a
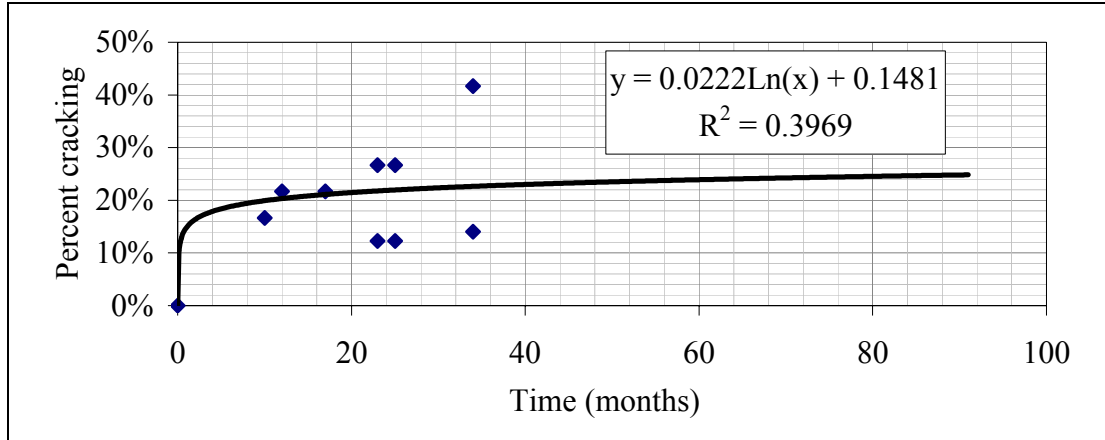
(a) Light segregation
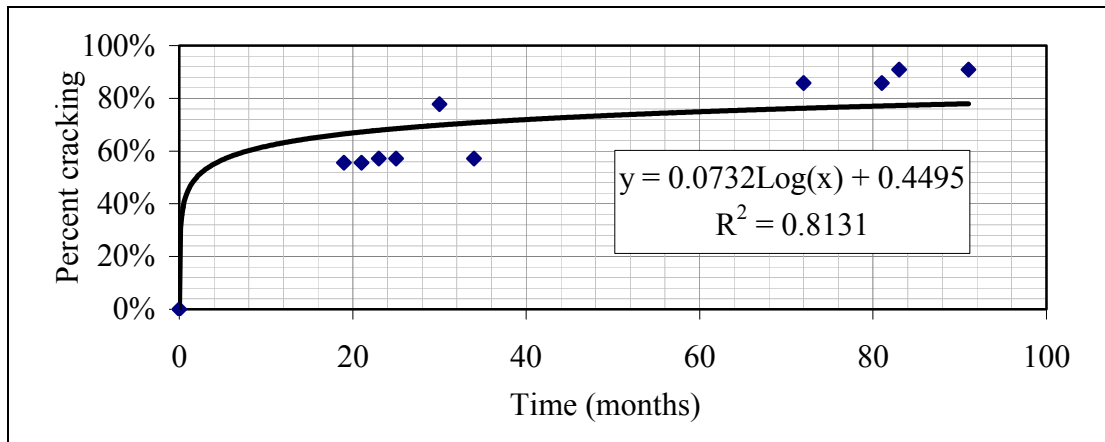
(c) Medium segregation
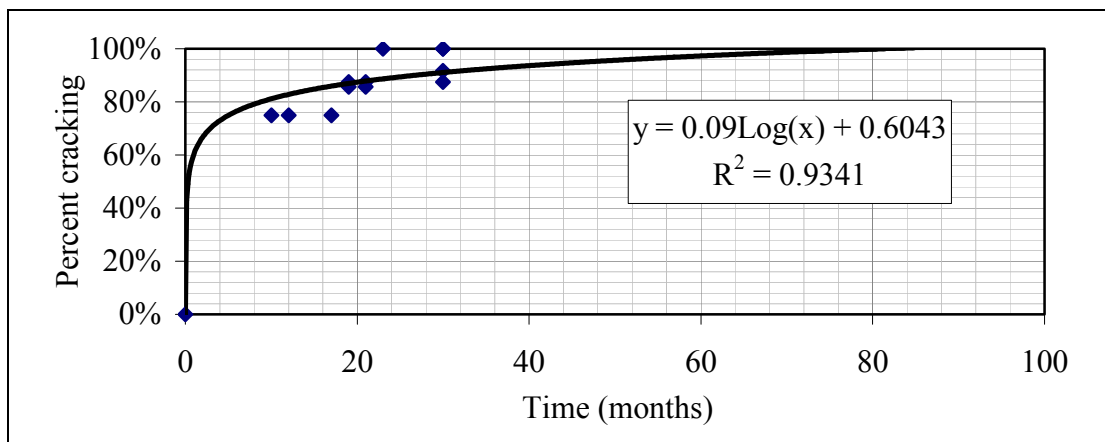
(c) Heavy segregation

Figure 4.14 Growth of cracking for three degrees of segregation

numerical degree of segregation. On the scale of numerical degree of segregation, heavy

degree of segregation was assigned a value of 10 whereas no segregation 0. The

numerical values for light and medium degrees of segregation were then obtained from

the graph where the regression coefficients fell on straight lines as shown in Figure 4.15a.

The linear equations describing the two straight lines were then obtained and substituted

into Equation 4.2. This yielded the following prediction equation for all degrees of

segregation:

$$PC = 0.0602DS + 0.0093DS\ln(t) \qquad\qquad 4.3$$

Where:　　　　DS = numerical degree of segregation (no segregation = 0.0, light = 2.5,

　　　　　　　medium = 7.5 and heavy = 10); and

　　　　　　　t = time (months).

To test the accuracy of the prediction model, the percent cracking predicted

equation 4.3 were graphed against the measured percent cracking. The comparison is

shown on Figure 4.15b. The straight line in the figure depicts the locus of equality. As

can be seen the predicted percent cracking matches well with the measured ones. It

should be noted that the reliability of the prediction model is questionable for times

immediately after construction when no crack measurement data is available. However,

the data indicates that significant cracking will occur shortly after construction, especially

in medium and heavy degrees of segregation.

4.0　CLASSIFICATION AND IDENTIFICATION OF TOP-DOWN CRACKS
This section was developed in cooperation with Tunwin Svasdisant who studied

the underperformance of rubblized pavements. Part of the problem associated with TDC
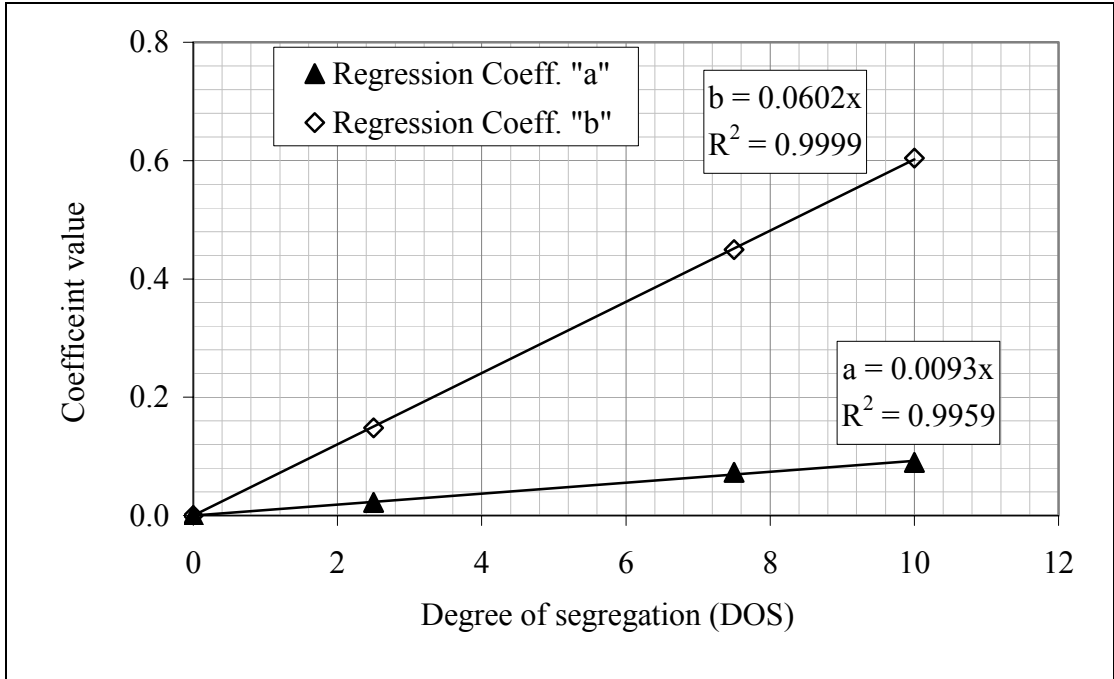
(a) Calibration of regression coefficients
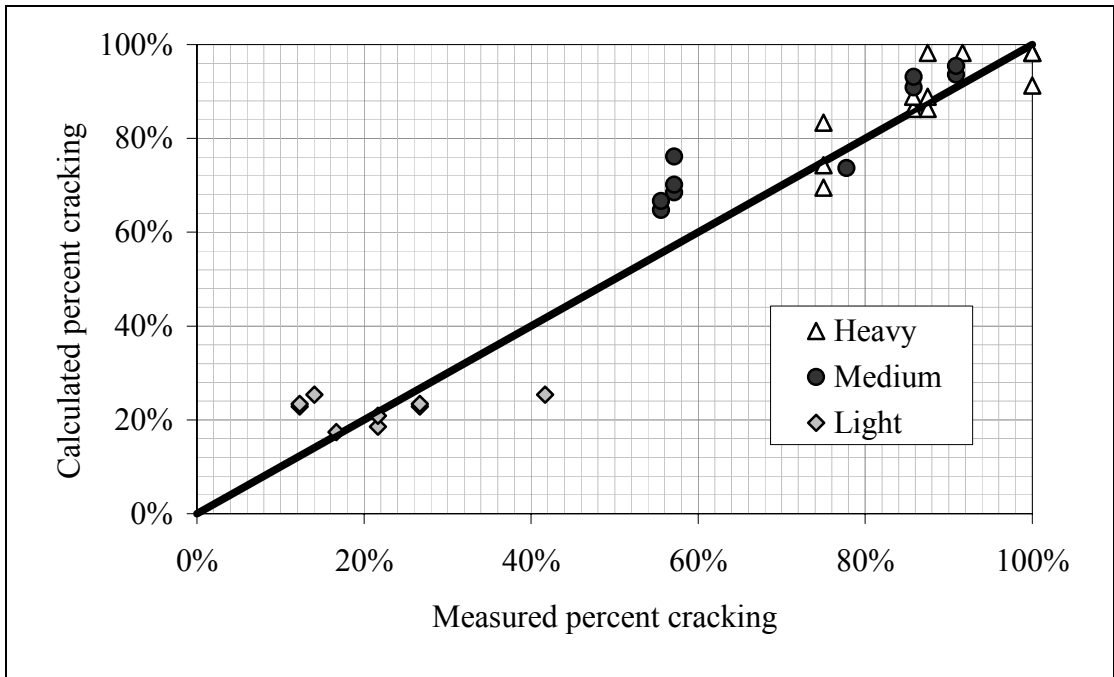
(b) Verification of prediction model

Figure 4.15 Calibration and verification of crack propagation model

is that PMS databases make no distinction between TDC and other cracks. Since most databases do not include data regarding crack locations, it is not possible to decipher the distress data and to separate regular cracks from TDC.

The main reason for the lack of TDC data is that no identification procedure has been developed whereby the TDC can be correctly documented either by manual or videotape survey. The lack of such data creates various problems including:

1. Inappropriate selection of rehabilitation alternatives; the rehabilitation options for TDC are different than those for regular cracks.

2. It is not possible to assess the impact of TDC on pavement conditions or on its remaining service life.

3. TDC propagation models cannot be verified.

Recognizing the dimension of the problem, one of the objectives of this study is to develop TDC identification procedure based on crack appearance, location and the mechanics of crack propagation. Such procedure was developed and is presented below.

4.1 TDC Descriptions and Classification

TDC were observed in the field as:

➢ Individual longitudinal or transverse cracks.

➢ Groups of parallel longitudinal cracks.

➢ Networks of longitudinal cracks.

Based on field observations and depending on the type and causes of the first observed crack, TDC can be classified into three categories as presented in the next sections.

4.1.1 Longitudinal Top-Down Cracks (LTDC) Category

The main cause of LTDC in this category is the induced tensile stress at the pavement surface. Such tensile stress could be a combination of the tensile stress due to tire-pavement interaction and thermal stress. The magnitude of the tensile stress could be increased due to differential stiffness between the AC courses and the AC layers and, for rubblized pavement only, the geometry of the interface between the fractured concrete and the rubblized material layers. The LTDC develop in three stages (Svasdisant et al, 2001) as follows:

1. In the first stage, a single short longitudinal crack develops in the vicinity of the edge of the wheel path. Over time, the crack propagates parallel to the wheel path as shown in Figures 4.16 and 4.17.

2. In the second stage, sister cracks develop and propagate parallel to the wheel path as shown in Figure 4.18 or in some pavements, transverse TDC may develop connecting to the existing longitudinal TDC as shown in Figure 4.19.

3. In the third stage, two or more longitudinal TDC connect via transverse TDC as shown in Figure 4.20.

Figure 4.21 depicts the three stages of TDC and some pavement cores showing partial propagation of TDC. Since the 5 cores were extracted from pavements with various AC thicknesses, it can be concluded that the initiation and propagation of TDC is independent of the pavement thickness

Figure 4.16 Longitudinal TDC at the edge of the wheel path on US-23, control section 01052 job number 32335 BMP
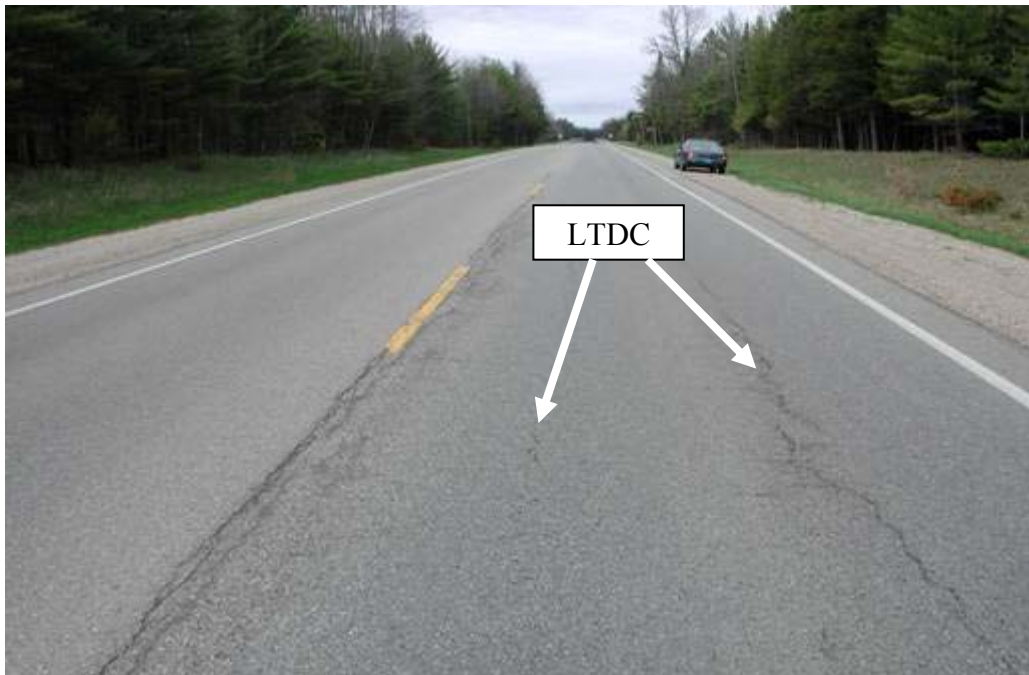
LTDC

Figure 4.17 Longitudinal TDC at the edge of the wheel path on US-131, control section 83032 job number 34060 BMP 13.0 EMP 18.7, May 2002
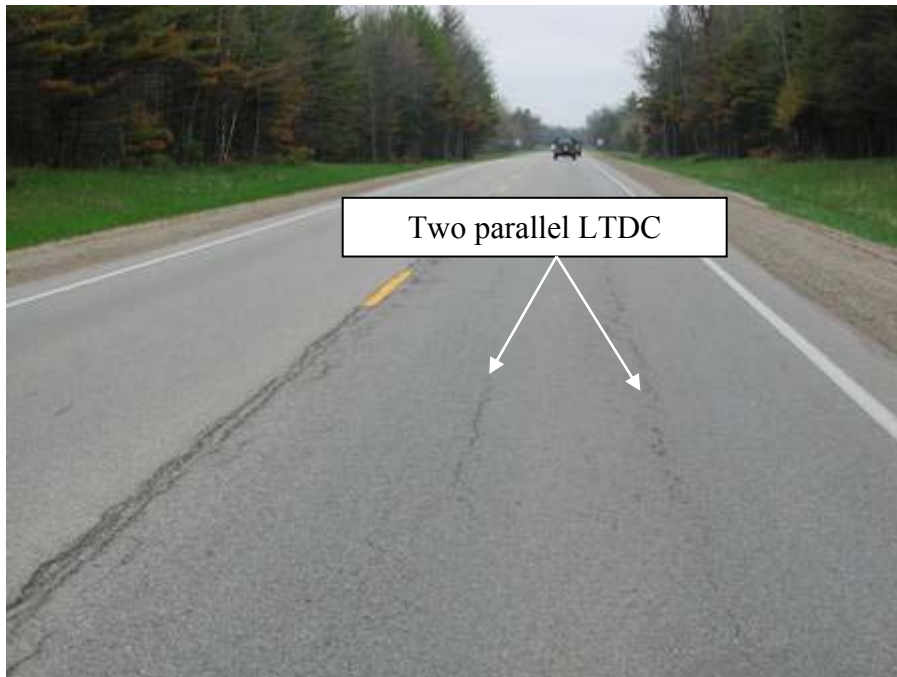
Figure 4.18 Parallel longitudinal TDC at the edge of the inner and outer wheel paths on US-131 (same location as Figure 5.2), control section 83032 job number 34060 BMP 13.0 EMP 18.7, May 2003
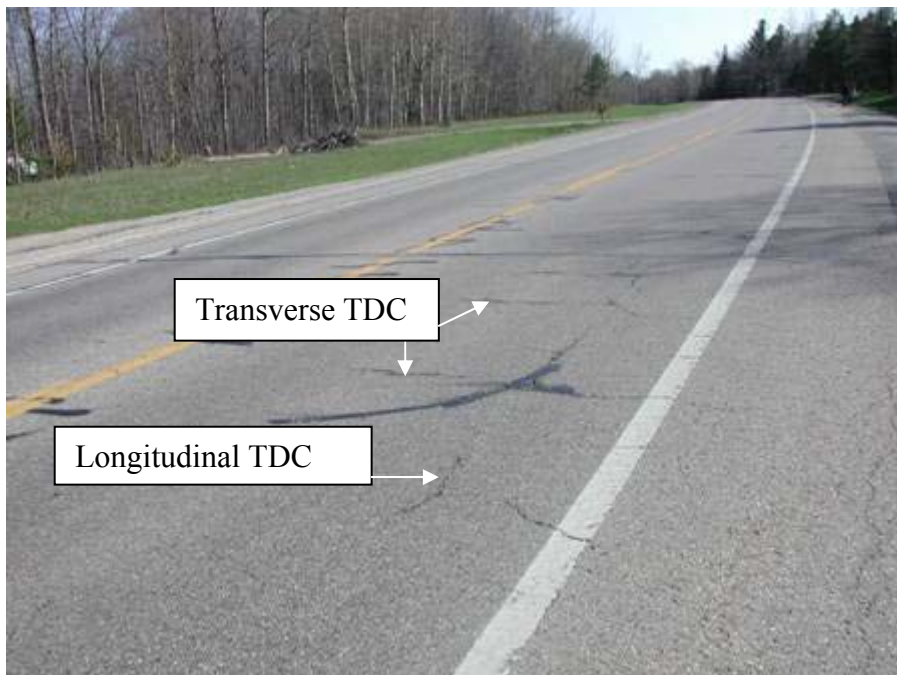
Figure 4.19 Transverse TDC associated with longitudinal TDC on M-27, control section 16302 job number 26672 BMP 9.3 EMP 11.4, May 2003

Figure 4.20 The third stage of TDC development, LTDC and TTDC forming a networks on East Michigan Avenue, control section 39555 job number 39212, May 2002
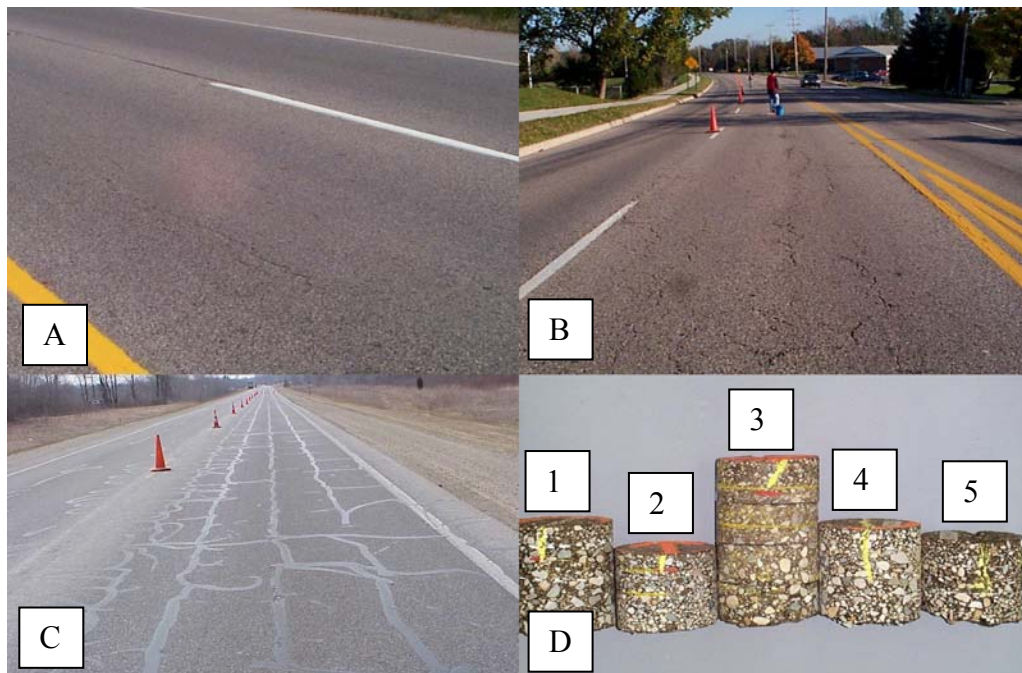
Figure 4.21 The three stages (A, B and C) of TDC development and pavement cores showing the extent of cracking

4.1.2 Transverse Top-Down Cracks (TTDC) Category

The likely cause of TTDC is thermal stresses due to cold temperatures and low tensile strength AC mixes. Most of the TTDC appear as short transverse cracks located at the center of the lane as shown in Figures 4.22 and 4.23. Over time, the cracks propagate across the lane and other transverse cracks develop. The TTDC may or may not be connected with LTDC depending on the state of the tensile stress at the pavement surface in the vicinity of the wheel path. Finally, the main reason that most TTDC initiate in the middle of the lane is because the crack in the wheel path is delayed due to the tires kneading action.

4.1.3 Crack in Segregated Areas Category

The cause of TDC in this category is particle segregation in the AC mat. Particle segregation may cause up to 60 percent reduction in the tensile strength of the AC mix in the segregated areas (Brown et al, Khedaywi and White). Further, because of the high air voids in segregated areas, the AC mix is more susceptible to oxidation and moisture damage resulting in substantial decreases in the tensile strength of the mix. Depending on the shape of the segregated area, the crack could be longitudinal or transverse, although most observed TDC in this category are longitudinal. The TDC propagate within the segregated area at a relatively fast rate, which decreases as the cracks begin to penetrate non-segregated areas.

Another type of distress that associated with segregation and TDC in segregated areas is raveling. Figure 4.24 shows raveling of the outer lane of a

32

Figure 4.22 Transverse TDC located at the center of the lane (compare the size to half of a 4-in core)

Figure 4.23 Transverse TDC located at the middle of the lane

Figure 4.24 Longitudinal TDC and raveling in segregated areas of TDC propagation with depth

two-lane highway. The pavement is two years old and the passing lane (the inner lane) shows no sign of distress and/or raveling.

4.2 TDC Identification

As stated earlier, no procedure has been developed to identify TDC and to differentiate them from regular longitudinal and/or transverse cracks. Such a procedure was developed and is based on field observations and the understanding of TDC initiation and propagation mechanism. This section presents and discusses the procedure.

4.2.1 Longitudinal Cracks

An observed longitudinal crack is highly likely TDC if it satisfies one or more of the following criteria:

1. Longitudinal cracks located at the edges of the wheel paths. These LTDC are most likely initiated by the induced tensile stresses due to tire-pavement interaction and temperature and are likely accelerated by the low tensile strength of the AC mix at the pavement surface.

2. A group of parallel longitudinal cracks separated by 1 to 3 ft. and located at the edges of, or within, the wheel paths.

3. Longitudinal cracks located between two lanes. These longitudinal TDC are caused by the opening of the paving joint.

4. Longitudinal cracks that are located in segregated areas or in areas where the AC mix is dry (low asphalt content and hence, low tensile strength).

35

For comparison purposes, the following are the locations of other types of longitudinal cracks.

1. Low to medium severity fatigue cracks, which are longitudinal cracks located at the center of the wheel paths.

2. Stripping cracks, which are longitudinal cracks located in non-segregated areas at the center of the lane. These cracks initiate at the bottom of the AC layer and propagate upward.

3. Longitudinal reflective cracks from longitudinal joints, which are typically located between two lanes, at the edge of the lane (between the traffic lane and the pavement shoulder) or between an old pavement lane and a pavement widening strip.

4.2.2 Transverse Cracks

An observed transverse crack is highly likely TDC if it satisfies one or more of the following criteria.

1. Short transverse cracks that initiate at the center of the lane. These TTDC are caused by low temperatures and low tensile strength.

2. Transverse cracks (across or almost across the lane) that appear at a constant interval throughout the pavement section. These cracks can be identified by their low profile at the crack edges, which causes roughness. The cracks initiate at the pavement surface and propagate downward because the thermal stress at the pavement surface is much higher than that at the bottom of the AC layer.

3. All short transverse cracks connecting LTDC. These short cracks could be located anywhere along the pavement.

4. Transverse cracks in segregated areas.

For rubblized and composite pavements only, straight transverse cracks that appear at a constant interval equal to the joint spacing of the original concrete slab are joint reflective cracks. The cracks start at the bottom of the AC and propagate upward. Reflective cracks typically have higher profiles at the center of the cracks.

4.2.3 Network of Longitudinal and Transverse Cracks

An observed network of longitudinal and transverse cracks is TDC if the cracks in the network satisfy one or more of the following criteria:

1. The network of cracks is located in and around the wheel paths and the distance between two longitudinal cracks is less than 3 ft.

2. A network of meandering cracks that extends throughout the pavement surface. This type of network is indicative of block cracking. The cracks are TDC caused by hardening of the AC binder.

Finally, a localized network of cracks is not TDC if it is located around the center of the wheel paths. These cracks are fatigue cracks.

5.0 AC DENSITY

Density of the AC mat was measured as to confirm the presence of the visually identified segregation areas, and to determine if any trends in the AC mix density could be attributed to TDC. As stated in Chapter 3, the density investigation in this study

included nuclear density (field measurements) and specific gravity (laboratory measurements). The data of both measurements are presented and discussed in the next two subsections.

5.1 Nuclear Density Data

Nuclear density tests were conducted to observe density differences between visually identified segregated and non-segregated (control) areas that are indicative of segregation. Chang et al (2002) showed that nuclear density is a good indicator of segregation and they established criteria for light, medium and heavy degrees of segregation that were embedded in the MBITSEG202 computer program. The program was developed by the Pavement Research Center of Excellence (PRCE) for the Michigan Department of Transportation (MDOT) as a quality control tool used during construction. The program produces three possible outputs as follows:

1. "None" indicates that significant nuclear density differences are not present. During construction, this result implies that the paving procedure needs to be monitored, since segregation is suspected. In this study, this result implies that the nuclear density differences show no segregation or light degree of segregation.

2. "Strong" indicates that significant nuclear density differences are present. During construction, this result directs the paving procedure to be adjusted to eliminate observed segregation. In this study, this result implies that at least a medium degree of segregation is present.

3. "Very Strong" indicates that severe nuclear density differences are present. For the construction operation, this means that the segregation is severe and

segregated areas should be removed. The paving procedure will, of course, have to be corrected to prevent the problem. In this study, this result implies that heavy degree of segregation is present.

Nevertheless, the MBITSEG202 computer program was used in this study to examine the nuclear density data obtained from the four test sites listed in Table 4.7. Results of the analyses indicate that:

1. No segregation or light degree of segregation is possible on two test sites (30422-11 and 30502-11).

2. Medium degree of segregation was found on test site 30502-21.

3. Test site 30521-21 is heavily segregated.

The above results confirmed the visual observations of segregation that were made during the field investigation.

5.2   Specific Gravity Tests

The dependency of the asphalt properties, including modulus and strength, on the density of the mixture has been well established. Since a variety of tests were conducted in this study, variations in the test results may be explained by density variations in the mixture.

Cores extracted from the pavement were returned to the laboratory, and the average core density was measured using the ASTM standard test procedure D-2726. The

Table 4.7 Summary of nuclear density tests

Test Site	Number of tests in each area			Density in control areas (pcf)		Density in segregated areas (pcf)	
	Total	Control	TDC	Average	Standard deviation	Average	Standard deviation
30422-11	12	6	6	146.0	1.2	147.5	1.0
30502-21	19	8	11	146.3	0.8	142.7	4.2
30521-11	12	6	6	142.9	1.2	139.4	2.0
30521-21	12	6	6	150.4	3.0	148.1	3.5

average core density was then compared from one core location to another to investigate variation in the average AC layer density.

Table 4.8 shows variations in the bulk specific gravity for the pavement cores. The specific gravities of cores obtained from test sites range from 2.286 on M-52 test section 1, test site 1 to 2.521 on US-41, test section 1 test site 1. The standard deviation ranges from a minimum of 0.008 on M-55 test section 1, test sites 1 and 2 , to 0.035 on I-75, test section 1, test site 2. Initially, the variation of these bulk specific gravity values may appear very small, but has a significant impact on air voids. The variation in the percent air voids for each test site is listed in Table 4.8. Said variation affects the AC modulus and strength.

6.0   PAVEMENT THICKNESS AND MATERIAL DATA
In this section, the measured AC thickness and the AC mix type of each test site included in this study are presented and discussed.

6.1   AC Mix Type
At the outset of this study, efforts were made to identify flexible pavement sections exhibiting TDC. The research team and MDOT personnel toured numerous flexible pavement sections and examined MDOT files. Ultimately, of more than 60 pavement sections that were investigated, thirteen showed TDC and were included in this study. Recognizing the needs for inclusion of more test sites, five rubblized pavement sections exhibiting TDC were also included in this study. Table 4.9 provides a list of the AC mixes used on the 13 flexible and 5 rubblized pavement projects investigated in this

Table 4.8 Average specific gravity tests of pavement cores

Test site	Number of tests	Bulk specific gravity					Possible variation of air voids (Gmm=2.500)	Pavement type
		Average	Maximum	Minimum	Maximum difference	Standard deviation		
20273-11	6	2.441	2.453	2.424	0.029	0.013	1.2	Flexible
20411-11	12	2.503	2.521	2.466	0.054	0.017	2.2	
20411-12	12	2.488	2.507	2.458	0.049	0.019	2.0	
30202-11	7	2.460	2.479	2.444	0.035	0.013	1.4	
30202-12	9	2.463	2.478	2.450	0.028	0.009	1.1	
30372-41	7	2.396	2.424	2.374	0.050	0.015	2.0	
30422-11	24	2.384	2.411	2.341	0.070	0.019	2.8	
30502-11	12	2.361	2.385	2.337	0.048	0.012	1.9	
30502-21	16	2.378	2.416	2.351	0.065	0.018	2.6	
30521-11	19	2.319	2.359	2.286	0.073	0.025	2.9	
30521-21	8	2.393	2.421	2.364	0.056	0.019	2.3	
30552-11	12	2.408	2.420	2.389	0.031	0.008	1.2	
30552-12	12	2.408	2.425	2.392	0.034	0.008	1.3	
Marsh Road	Cores not tested							
11941-21	10	2.399	2.430	2.361	0.068	0.021	2.7	Rubblized
11941-22	11	2.403	2.437	2.376	0.061	0.018	2.4	
10753-11	11	2.382	2.418	2.344	0.074	0.025	3.0	
10753-12	12	2.388	2.474	2.331	0.142	0.035	5.7	
0153-11	12	2.350	2.394	2.321	0.073	0.022	2.9	

Table 4.9 Summary of mix types on investigated pavements

Test Site	Control section	Job number	Surface mix type	Completion date	Pavement type
20273-11	37014	38205		10/13/2000	Flexible
20411-11	07013	34037	13A	6/23/1999	
20411-12	07013	34037	13A	6/23/1999	
30202-11	37022	38196	4B	8/29/1996	
30202-12	37022	38196	4B	8/29/1996	
30422-11	83041	44396A	4B	3/20/1996	
30502-11	23052	41007	4B	6/29/1997	
30502-21	23052	45984	13A	7/1/1998	
30521-11	33051	34530	4B	6/6/1994	
30521-21	76011	36580	4B	10/18/1994	
30552-11	72022	31009	4B	9/7/1995	
30552-12	72022	31009	4B	9/7/1995	
Marsh Rd			1400T	N/A[1]	
11941-21	13033	29670	4B	6/4/1993	Rubblized
11941-22	13033	29670	4B	6/4/1993	
10753-11	16092	25559	1300-20AAA	12/6/1988	
10753-12	16092	25559	1300-20AAA	12/6/1988	
30153-11	25092	45534	4C	10/1/1998	

1. No construction records exist for Marsh Road

study. The data in the table indicate that the majority of the pavement sections that exhibiting TDC were surfaced using the 4B AC mix. In a parallel study of 87 rubblized pavement projects in Michigan, thirteen projects were capped with 4B mix. A few years after construction, all thirteen projects exhibited TDC (Svasdisant 2003). Consequently, one can conclude that the 4B asphalt mix has high TDC potential and therefore, its properties were subjected to further investigation.

6.2   Core Thickness Data

At each test site, about 10 to 15 AC cores were extracted from the pavement and, for each core; four measurements of the AC thickness were made at the end of two orthogonal diameters. Hence, for each test site, a total of 40 to 60 AC thickness measurements were made. The average of all measurements was then calculated and used as input to the backcalculation routine.

Table 4.10 provides a list of the average, minimum, maximum and standard deviation of the measured thicknesses of pavement cores obtained from 13 flexible and 5 rubblized pavement projects. As can be seen, for some test sites, the AC thickness varies substantially (more than 1.0-in) from one point to another. Said variation would affect the accuracy of the backcalculated layer moduli. That is, if the average core thickness per test site is used in the backcalculation, one should expect variation in the backcalculated layer moduli. However, the average backcalculated moduli per test site was found to be similar to the average modulus backcalculated using the deflection data from those FWD tests conducted at the core locations where the AC thickness is accurately known.

Table 4.10 Variation in core thickness for each test site

Test site	Number of cores	Core thickness (in)				Pavement type
		Average	Maximum	Minimum	Standard deviation	
20273-11	12	9.0	9.2	8.8	0.2	Flexible
20411-11	14	3.3	3.8	2.9	0.4	
20411-12	14	2.8	3.1	2.3	0.2	
30202-11	11	4.7	5.1	4.2	0.3	
30202-12	12	4.5	4.8	4.3	0.1	
30422-11	27	3.7	5.5	2.8	0.8	
30502-11	13	6.1	7.0	5.6	0.5	
30502-21	38	6.9	7.3	5.8	0.3	
30521-11	19	5.9	6.6	5.2	0.4	
30521-21	9	9.1	9.7	7.9	0.6	
30552-11	15	3.0	3.8	2.7	0.3	
30552-12	13	3.1	3.3	2.9	0.1	
Marsh	8	10.6	11.7	10.0	0.6	
11941-11	15	7.9	8.1	7.3	0.2	Rubblized
11941-12	14	7.4	7.8	7.0	0.2	
10753-11	14	4.5	4.8	4.1	0.2	
10753-12	15	4.0	4.6	3.5	0.4	
30153-11	16	5.3	5.7	4.6	0.3	

The core thickness data were also examined from a different perspective, cores located in the wheel paths versus those outside the wheel paths. Table 4.11 provides a list of the average core thicknesses for both locations. As can be seen, for the majority of the test sites, the average core thickness, extracted from the wheel paths, is slightly less than that outside the wheel paths. This was expected because the pavement in the wheel paths has been subjected to secondary compaction due to traffic.

7.0   DEFLECTION DATA

Each pavement included in this study was tested using the MDOT KUAB falling weight deflectometer (FWD). On each test site, a minimum of 29 deflection tests were obtained in an effort to characterize the engineering characteristics of the pavement in both the longitudinal and transverse directions. A detailed description of the FWD test procedure and test site layout is presented in chapter 3. The objectives of the FWD tests are:

1. Analyze the variations in the pavement deflections along and across the pavement.

2. Backcalculate the layer moduli.

3. Assess the linearity of the pavement response to load.

The linearity of the MDOT FWD has been established in a report by Baladi and Svasdisant (2002). Therefore, only the variation of the deflection data and the backcalculation of layer moduli will be presented here.

Deflection is the response of the pavement to applied load. Deflection can be thought of as an index expressing the structural capacity of the pavement. Hence,

Table 4.11 Differences in pavement thickness in and outside the wheel paths

Test Site	In Wheelpath		Between Wheelpaths		% Difference	Pavement Type
	Number of cores	Average thickness (in)	Number of cores	Average core thickness (in)		
20273-11	4	8.8	8	9.0	2.3	Flexible
20411-11	4	3.3	8	3.3	0.1	
20411-12	4	2.8	8	2.9	5.0	
30202-11	3	4.7	6	4.7	-0.6	
30202-12	3	4.5	6	4.6	2.4	
30422-11	4	4.8	8	3.4	-38.9	
30502-12	4	6.7	8	5.9	-14.7	
30502-21	4	6.0	34	7.1	14.9	
30521-11	4	6.1	8	5.8	-5.3	
30521-21	3	8.8	6	9.1	3.7	
30552-11	4	3.2	8	3.1	-3.6	
30552-12	4	3.0	8	3.1	1.7	
11941-21	4	7.9	8	7.9	-0.7	Rubblized
11941-22	4	7.3	8	7.5	1.8	
10753-11	4	4.3	8	4.6	7.1	
10753-12	4	3.8	8	4.3	10.9	
30153-11	4	5.3	8	5.5	3.9	

variations in the measured deflection reflect variations in the structural capacity of the pavement.

In this study, FWD deflection data were collected from all sites subjected to field investigation, which included several rubblized pavements. The data presented here are used to show the differences in response between conventional flexible and rubblized pavements and also to identify trends in flexible pavements, if any exist, that link the structural response of the pavement to TDC potential. A detailed analysis of rubblized pavement response may be obtained from Baladi and Svasdisant (2002).

Table 4.12 provides a list of the variations in D1 through D7 deflections for flexible and rubblized pavement projects. Tables 4.13 and 4.14 list the measured pavement deflections along and across the rubblized pavement on I-75, test section 1, test sites 1 and 2, respectively. Table 4.15 provides similar information for the flexible pavement along US-27, test section 1, test site 1. The average and the coefficient of variation for D1 through D7 deflections are also listed in the three tables. Figure 4.25 depicts plots of D1 through D7 deflections at the various test locations along I-75, test section 1, test sites 1 and 2, respectively. The data in Tables 4.13 through 4.15 and in Figure 4.25 indicate that:

1. The variations in the deflections of the rubblized concrete pavement on I-75, test section 1, test sites 1 and 2 are much higher than the variation on flexible pavements.

2. For both test sites, the peak pavement deflections (D1) show the highest variation from about 6-mils to more than 10-mils. The reason is that D1 deflection is a measure of the cumulative deflections of all pavement layers and of the roadbed

Table 4.12 Coefficient of variation of the deflection data of rubblized and flexible pavements

Test site	Coefficient of variation of the measured deflections (%)							Pavement Type
	D1	D2	D3	D4	D5	D6	D7	
20273-11	2	2	2	2	2	2	3	
20411-11	3	3	4	6	6	7	7	
20411-12	2	3	4	4	5	6	11	
30202-11	6	5	5	5	6	8	10	
30202-12	4	3	3	3	4	3	3	
30422-11	13	8	7	10	8	6	4	
30502-11	8	7	6	6	8	13	21	Flexible
30502-21	7	7	7	8	8	10	12	
30521-11	4	4	3	4	5	5	3	
30521-21	7	7	7	8	8	10	12	
30552-11	6	6	6	7	6	5	4	
30552-12	9	9	9	9	9	6	4	
Marsh 1	10	8	7	5	4	4	10	
Marsh 2	9	6	5	4	4	5	6	
10692-11	9	10	11	10	10	10	15	
10692-12	9	10	11	10	10	10	15	
10753-11	14	13	12	10	8	5	6	
10753-12	16	14	12	11	10	10	13	
11941-21	8	7	7	7	7	7	4	
11941-22	11	8	7	7	6	6	5	
20102-11	7	7	7	7	7	7	6	
20102-12	8	8	8	8	7	6	3	
20233-11	12	12	11	10	8	7	15	Rubblized
20233-12	8	9	9	9	9	10	10	
20273-21	15	13	11	8	6	4	4	
20273-31	6	6	5	5	5	5	6	
20273-41	8	12	11	9	7	6	4	
20311-11	10	10	9	7	7	8	10	
30373-21	19	14	10	17	14	12	10	
30373-51	7	8	7	6	6	5	5	
30373-52	15	16	15	14	14	13	11	
30373-61	10	9	9	8	6	6	8	

Table 4.13 Rubblized pavement D1 through D7 deflections, I-75, test section 1, test site 1

FWD station	Deflection (mils)						
	D1	D2	D3	D4	D5	D6	D7
1	9.46	8.29	7.45	6.22	5.30	3.67	2.03
2	10.02	8.59	7.69	6.47	5.48	3.82	2.12
3	9.62	8.48	7.78	6.47	5.17	3.64	2.03
4	9.52	8.17	7.22	5.93	4.96	3.51	1.92
5	9.73	8.44	7.53	6.25	5.22	3.59	1.85
6	9.56	8.07	7.13	5.92	4.98	3.50	1.90
7	9.88	8.25	7.35	6.14	5.17	3.67	1.97
8	9.32	8.18	7.36	6.18	5.31	3.82	2.02
9	9.01	7.81	7.09	6.03	5.11	3.70	2.02
10	9.07	7.78	6.94	5.86	4.78	3.31	1.79
11	9.67	8.39	7.50	6.24	5.20	3.50	1.92
12	9.24	7.73	6.89	5.80	4.93	3.58	1.92
13	9.00	7.76	6.95	5.82	4.89	3.17	1.72
14	10.30	8.47	7.26	5.96	5.02	3.52	1.90
15	10.06	8.69	7.41	5.79	4.91	3.61	2.04
16	8.12	7.22	6.44	5.42	4.58	3.27	1.85
17	8.22	6.97	6.27	5.34	4.60	3.38	1.87
18	8.90	7.78	6.98	5.84	4.90	3.15	1.73
19	7.77	6.70	6.04	5.16	4.50	3.40	1.81
20	7.68	6.63	6.03	5.16	4.44	3.34	1.95

Table 4.13 (cont'd) Rubblized pavement D1 through D7 deflections, I-75, test section 1,
test site 1

FWD station	Deflection (mils)						
	D1	D2	D3	D4	D5	D6	D7
21	7.22	6.21	5.60	4.87	4.26	3.29	1.87
22	7.76	6.30	5.68	4.88	4.27	3.28	1.89
23	8.57	7.55	6.81	5.67	4.74	3.21	1.73
24	7.43	6.47	5.89	5.12	4.48	3.46	1.84
25	7.49	6.53	5.90	5.11	4.45	3.39	1.99
26	6.87	5.93	5.40	4.78	4.21	3.32	1.91
27	8.50	7.46	6.69	5.57	4.62	3.20	1.74
28	6.92	6.10	5.64	4.98	4.45	3.51	1.89
29	6.65	5.96	5.53	4.91	4.33	3.35	2.01
30	6.49	5.69	5.25	4.72	4.19	3.33	1.94
31	8.30	7.30	6.58	5.52	4.62	3.26	1.75
32	7.07	6.20	5.65	4.92	4.34	3.40	1.94
33	6.05	5.48	5.14	4.68	4.22	3.50	2.12
34	9.70	8.16	7.24	6.18	5.26	3.87	1.99
35	7.26	6.29	5.66	4.89	4.25	3.31	1.98
36	7.89	7.09	6.42	5.70	4.53	3.27	1.90
37	8.29	6.89	6.21	5.24	4.45	3.26	1.82
38	7.06	6.11	5.57	4.90	4.28	3.30	1.94
39	6.36	5.66	5.28	4.80	4.32	3.44	1.99
40	6.76	5.96	5.55	5.02	4.49	3.62	2.12
41	8.47	7.33	6.55	5.54	4.67	3.27	1.77
42	8.76	7.85	6.77	5.62	4.73	3.34	1.86
Average	8.33	7.21	6.48	5.51	4.70	3.44	1.91
CV[1] (%)	14	13	12	10	8	5	6

1. CV = Coefficient of variation = standard deviation as a percent of the average

Table 4.14 Rubblized pavement D1 through D7 deflections, I-75, test section 1, test site 2

FWD station	Deflection (mils)						
	D1	D2	D3	D4	D5	D6	D7
1	10.45	8.53	7.37	5.95	4.87	3.45	1.89
2	9.30	7.84	6.92	5.74	4.80	3.46	1.83
3	9.98	8.42	7.38	6.08	5.07	3.51	1.78
4	8.38	7.15	6.41	5.45	4.68	3.34	1.66
5	10.55	8.38	7.07	5.61	4.60	3.26	1.68
6	9.12	7.68	6.74	5.53	4.56	3.14	1.60
7	8.98	7.39	6.44	5.24	4.31	2.90	1.46
8	10.01	8.00	6.85	5.43	4.33	2.85	1.32
9	10.83	8.70	7.35	5.82	4.61	2.93	1.25
10	9.33	7.49	6.49	4.89	4.07	2.81	1.41
11	7.85	6.66	5.85	4.82	3.95	2.72	1.42
12	10.30	8.34	7.11	5.58	4.45	2.82	1.29
13	9.31	7.62	6.68	5.51	4.63	3.40	1.83
14	8.37	7.50	6.54	5.39	4.57	3.23	1.70
15	9.40	7.23	6.22	4.91	4.03	2.74	1.36
16	6.86	6.05	5.37	4.50	3.80	2.70	1.45
17	8.09	6.57	5.81	4.97	4.25	3.22	1.84
18	8.17	7.05	6.29	5.34	4.55	3.24	1.72
19	9.03	6.76	5.78	4.66	3.88	2.68	1.35
20	6.16	5.40	4.90	4.24	3.64	2.69	1.42

Table 4.14 (cont'd) Rubblized pavement D1 through D7 deflections, I-75, test section 1, test site 2

FWD station	Deflection (mils)						
	D1	D2	D3	D4	D5	D6	D7
21	7.68	5.99	5.27	4.52	3.93	3.09	1.81
22	8.03	6.93	6.29	5.50	4.85	3.26	1.76
23	8.63	6.41	5.51	4.48	3.72	2.60	1.36
24	6.79	5.80	5.12	4.37	3.77	2.80	1.50
25	6.79	5.96	5.25	4.32	3.63	2.62	1.41
26	7.22	5.82	5.19	4.50	3.95	3.14	1.87
27	7.89	6.82	6.23	5.51	4.89	3.35	1.79
28	7.52	6.08	5.20	4.26	3.59	2.58	1.40
29	7.16	6.22	5.48	4.49	3.74	2.18	1.34
30	6.47	5.72	5.18	4.58	4.08	3.24	1.92
31	8.08	7.05	6.37	5.60	4.96	3.37	1.80
32	7.53	6.22	5.32	4.41	3.76	2.79	1.54
33	7.52	6.46	5.70	4.67	3.88	2.68	1.37
34	6.57	5.69	5.14	4.47	3.91	3.13	1.89
35	6.53	5.77	5.34	4.72	4.11	3.18	1.82
36	7.26	6.38	5.78	4.94	4.24	3.20	1.80
37	8.73	7.58	6.82	5.88	5.11	3.42	1.74
38	5.93	5.27	4.84	4.28	3.77	2.97	1.67
39	6.65	5.84	5.28	4.53	3.92	2.97	1.65
40	7.65	6.31	5.51	4.58	3.90	2.89	1.57
41	7.20	6.21	5.63	4.89	4.30	3.17	1.69
42	10.54	7.66	6.54	5.28	4.47	3.26	1.80
43	8.40	6.82	5.99	4.92	4.05	2.81	1.42
Average	8.21	6.83	6.01	5.01	4.24	3.02	1.61
CV[1] (%)	16	14	12	11	10	10	13

1. CV = Coefficient of variation = standard deviation as a percent of the average

Table 4.15 Flexible pavement D1 through D7 deflections, US 27, test section 1, test site 1

| FWD station	Deflection (mils)						
	D1	D2	D3	D4	D5	D6	D7
1	7.50	6.48	5.81	4.91	4.18	2.93	1.43
2	7.39	6.36	5.68	4.79	4.07	2.86	1.44
3	7.33	6.34	5.69	4.80	4.07	2.85	1.37
4	7.58	6.48	5.80	4.85	4.11	2.86	1.36
5	7.32	6.27	5.64	4.75	4.03	2.84	1.40
6	7.52	6.40	5.74	4.85	4.12	2.91	1.40
7	7.68	6.60	5.90	4.97	4.24	2.99	1.47
8	7.51	6.45	5.78	4.91	4.15	2.95	1.44
9	7.58	6.41	5.80	4.93	4.18	2.94	1.46
10	7.43	6.34	5.71	4.84	4.12	2.90	1.46
11	7.44	6.36	5.75	4.89	4.14	2.90	1.43
12	7.44	6.34	5.66	4.75	3.99	2.80	1.36
13	7.49	6.37	5.73	4.87	4.15	2.90	1.44
14	7.24	6.22	5.59	4.75	4.03	2.87	1.44
15	7.23	6.23	5.60	4.71	4.03	2.82	1.43
16	7.32	6.20	5.55	4.64	3.93	2.75	1.35
17	7.28	6.30	5.65	4.79	4.10	2.91	1.42
18	7.12	6.12	5.51	4.69	3.98	2.78	1.44
19	7.05	6.14	5.53	4.68	3.97	2.85	1.41

Table 4.15 (cont'd) Flexible pavement D1 through D7 deflections, US 27, test section 1, test site 1

FWD station	Deflection (mils)						
	D1	D2	D3	D4	D5	D6	D7
21	7.09	6.11	5.50	4.71	3.98	2.86	1.45
22	7.13	6.09	5.50	4.66	3.97	2.81	1.44
23	7.03	6.08	5.46	4.64	3.96	2.86	1.45
24	7.17	6.12	5.47	4.62	3.93	2.79	1.39
25	7.06	6.07	5.48	4.67	4.01	2.86	1.46
26	7.22	6.20	5.60	4.72	4.04	2.86	1.48
27	7.14	6.20	5.57	4.69	4.01	2.80	1.38
28	7.15	6.19	5.58	4.75	4.05	2.93	1.45
29	7.27	6.25	5.65	4.80	4.07	2.94	1.49
30	7.17	6.22	5.60	4.75	4.06	2.89	1.45
31	7.32	6.31	5.71	4.80	4.08	2.88	1.45
32	7.43	6.41	5.80	4.93	4.15	2.93	1.45
33	7.23	6.26	5.66	4.81	4.10	2.88	1.43
34	7.06	6.10	5.47	4.67	3.97	2.79	1.39
35	7.10	6.13	5.53	4.73	4.04	2.88	1.42
36	7.31	6.29	5.69	4.83	4.13	2.91	1.44
37	7.22	6.21	5.58	4.72	4.02	2.85	1.45
38	7.15	6.18	5.56	4.75	4.02	2.88	1.49
39	7.51	6.43	5.76	4.89	4.15	2.92	1.45
40	7.27	6.19	5.55	4.62	3.92	2.74	1.39
Average	7.29	6.26	5.63	4.77	4.05	2.87	1.43
CV[1] (%)	2	2	2	2	2	2	3

1. CV = Coefficient of variation = standard deviation as a percent of the average
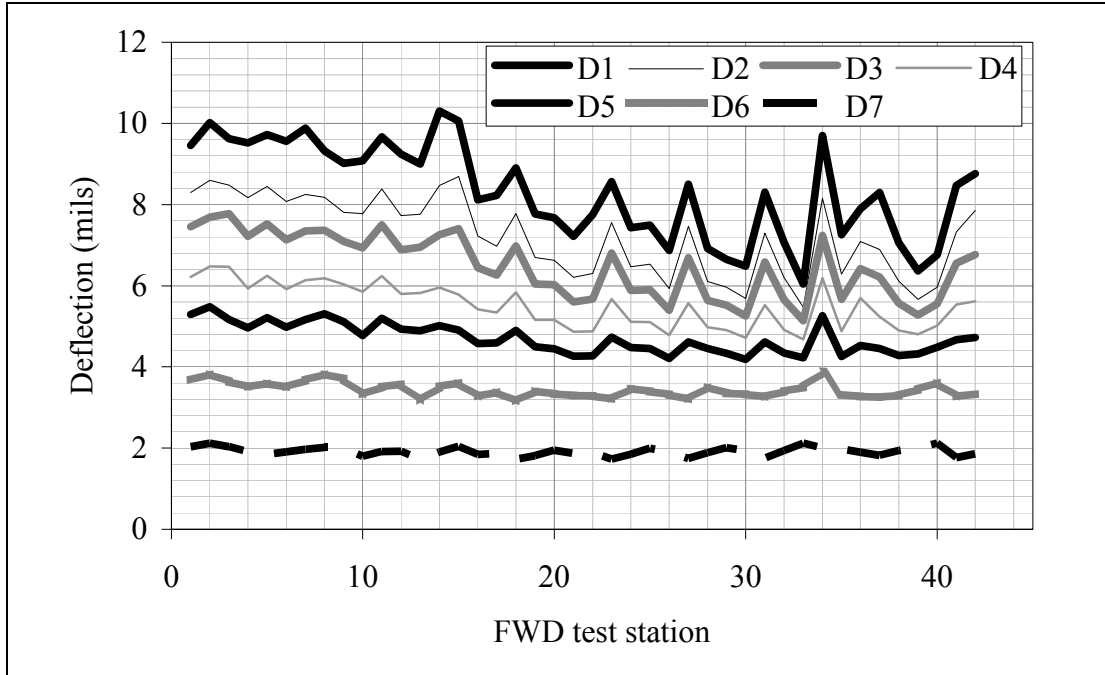
(a) Test site 1
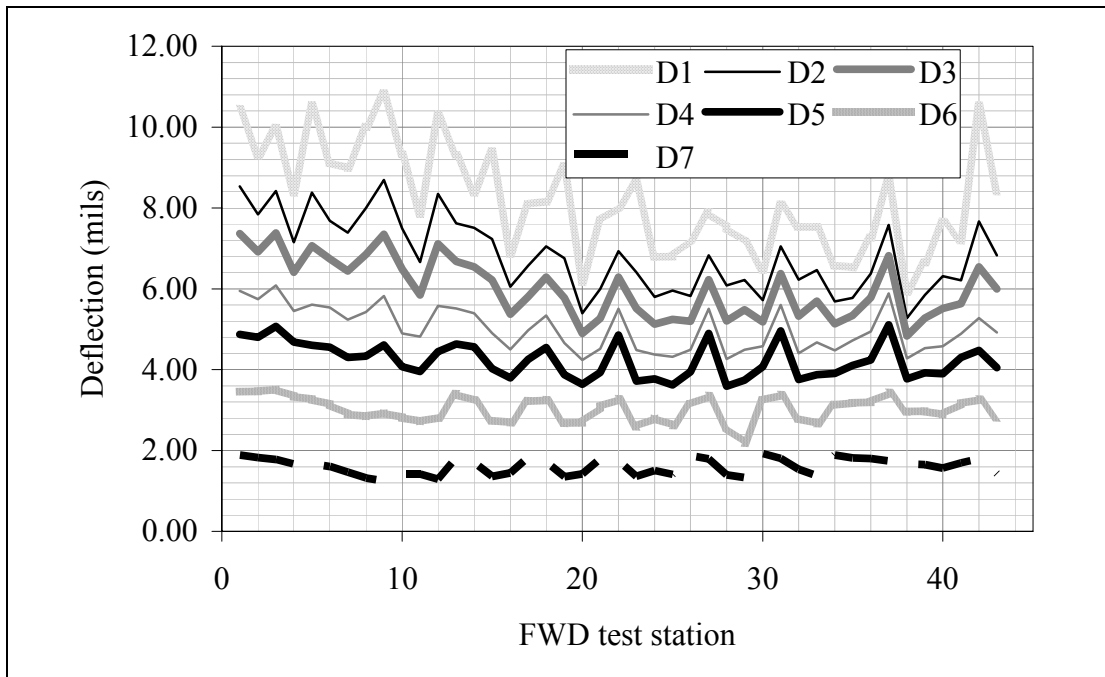
(b) Test site 2

Figure 4.25 Variations of D1 through D7 deflections, I-75 SB, test section 1

soil. Hence, variations in these layers and in the roadbed soil are reflected in the measured D1 deflection.

For comparison purposes, the coefficients of variation of the measured D1 through D7 deflections for 30 test sites are listed in Table 4.12.   As can be seen, the coefficients of variation for I-75 SB section 1 test site 2 are relatively high compared to the other rubblized test sites. On average, however, most of the rubblized pavements show more variation than the flexible ones. This indicates that the structural capacity of a rubblized pavement is more variable than that of a conventional flexible pavement. Given that the main difference between conventional flexible and rubblized pavement sections is the rubblized concrete slab, one can conclude that the high variations in deflections could be directly related to variations and/or non-uniformity of the rubblized concrete slab. These and other rubblized pavement issues are detailed in Baladi and Svasdisant (2002).

Several of the flexible pavement test sections, such as M-50 test sections 1 and 2 and M-52 test section 1, exhibit high variations in the D7 sensor. The D7 deflection reflects the energy delivered to the roadbed soil and the lower portion of the subbase, if present. The pavements with high variation in D7 deflection (M-50, test sections 1 and 2 and M-52 test section 1) were constructed at-grade with little roadbed soil improvement. Hence, these variations are indicative of variability in the roadbed soil. Other pavements, in particular M-42, show high variation in the D1 deflection sensor and low variations in the outer sensors. This implies that there is high variation in the asphalt layer and low variation in the roadbed soil. While these results are inconsistent with most of the other pavements, the high variability is not surprising. Cores of M-42 show high thickness

variability, which affect the structural response of the asphalt layer, but not necessarily the response of the roadbed soil.

Detailed analyses of the rubblized pavements investigated in this study are presented in Svasdisant and Baladi (2002), therefore only the data pertaining to conventional flexible pavements are discussed in this report. For each pavement investigated, the deflection data were normalized relative to the mean deflection of the test site. Profiles for these data are shown in Figures 4.26 to 4.33.

8.0   BACKCALCULATION PROCEDURE

In a parallel study conducted by Svasdisant (2003), various factors affecting the backcalculation of flexible and rubblized pavements layer moduli were analyzed and a backcalculation procedure for rubblized pavements was developed. It was found that the procedure substantially improves the robustness of the backcalculation of conventional flexible pavements. An overview of the procedure is presented below.

8.1   Overview of Backcalculation Procedure

As stated above, Svasdisant was successful in developing a procedure for the backcalculation of layer moduli of rubblized pavements. The procedure has been adapted for conventional flexible pavements, and consists of the following steps:

1. Obtain the following information/data:

   ➤ the thicknesses of the pavement layers and material types from the inventory data and/or from coring and drilling;

   ➤ the pavement condition at the FWD test site;

Figure 4.26 Normalized deflections on 20273-11
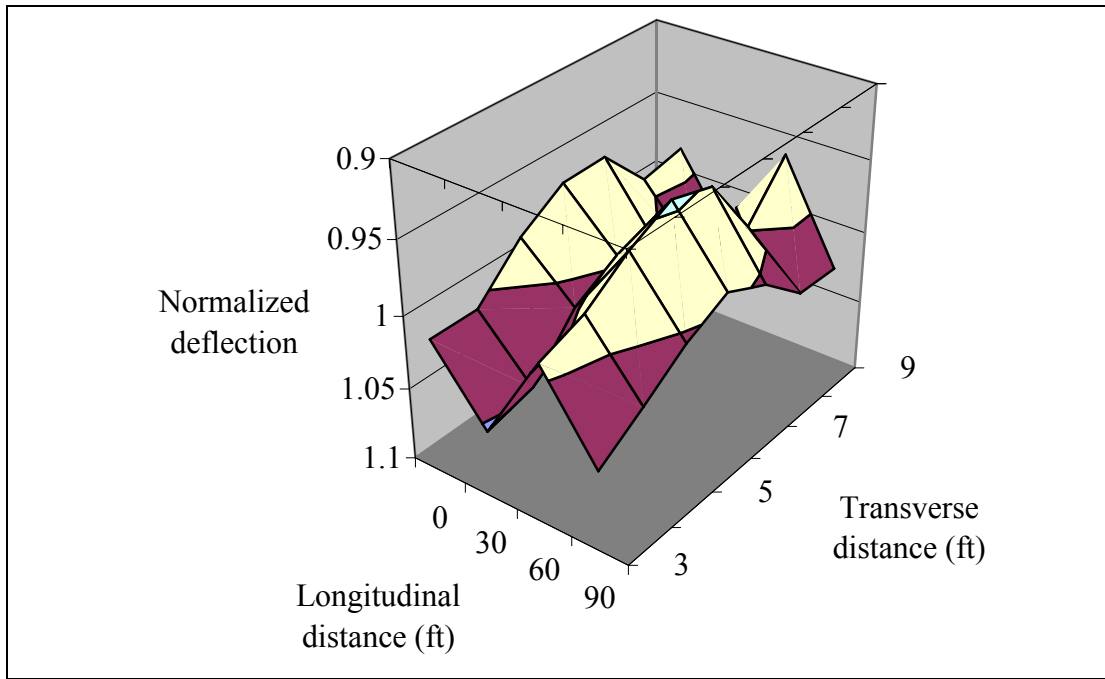
(a) Test site 1 (20411-11)
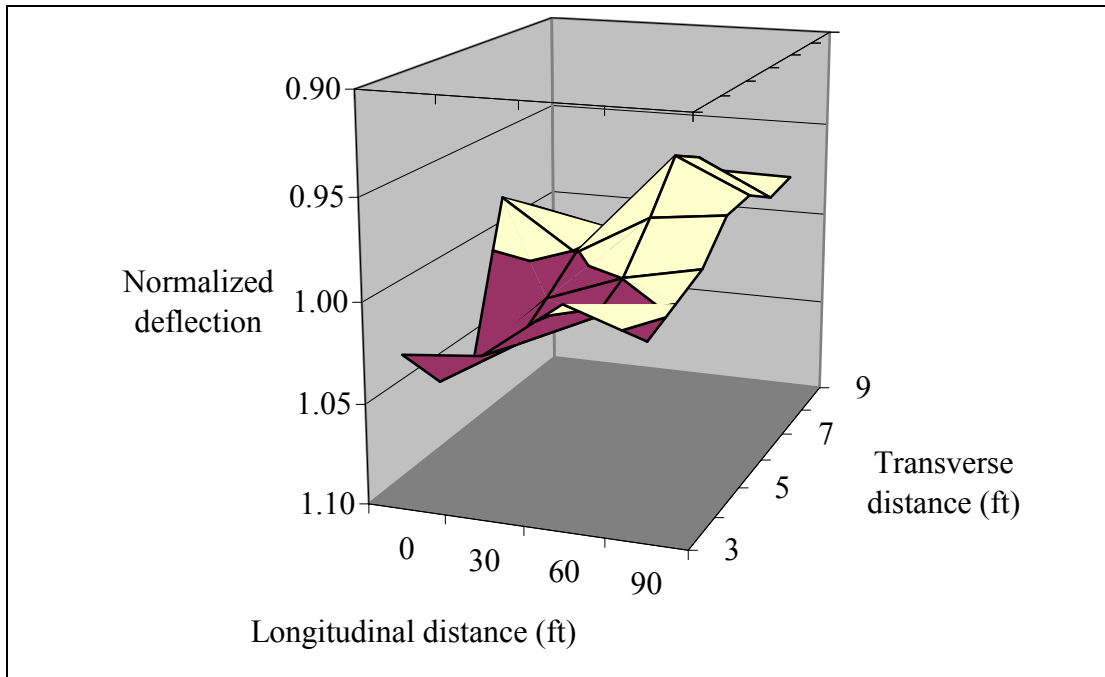
(b) Test site 2 (20411-12)

Figure 4.27 Normalized deflections on US-41, test section 1
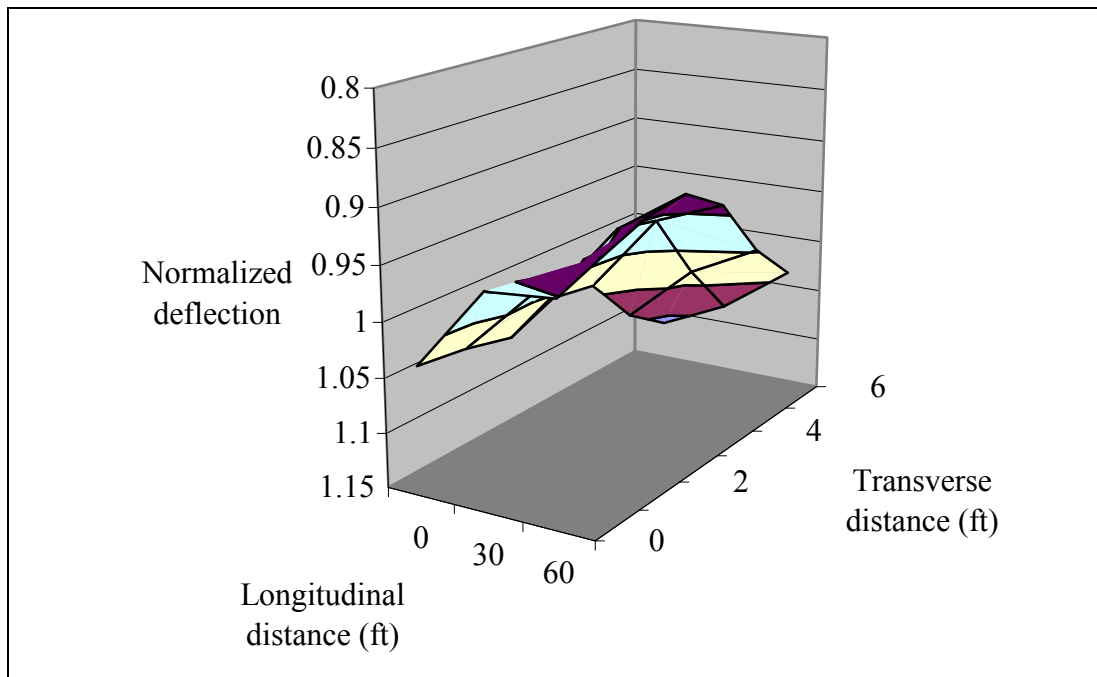
(a) Test site 1 (30202-11)
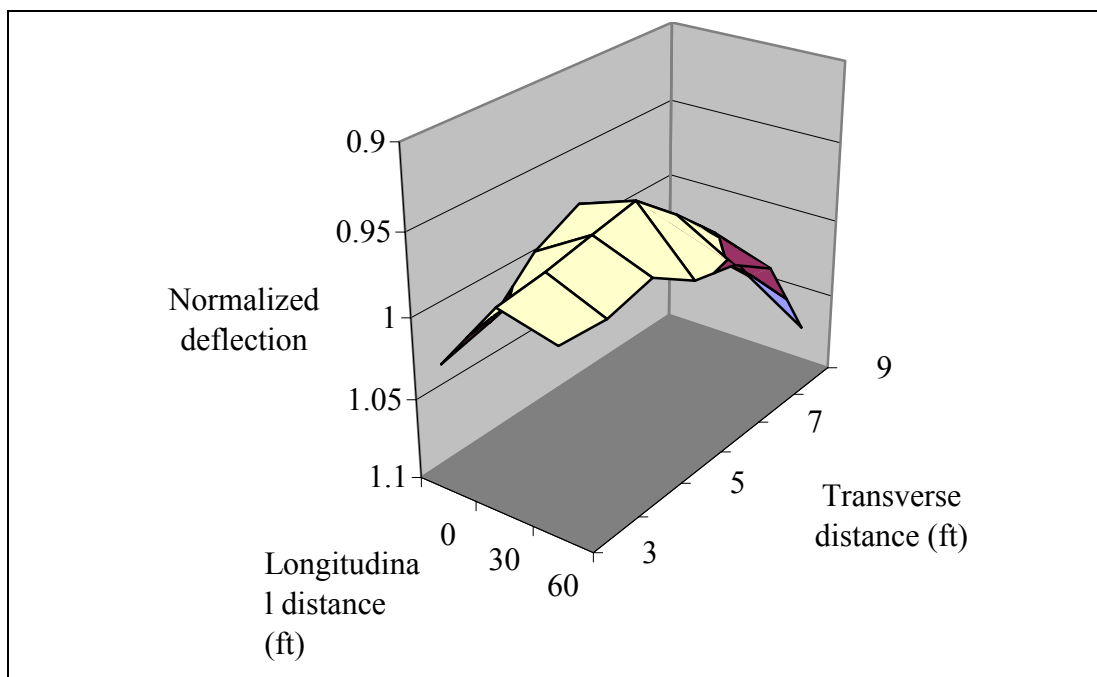
(b) Test site 2 (30202-12)

Figure 4.28 Normalized deflections on M-20, test section 1
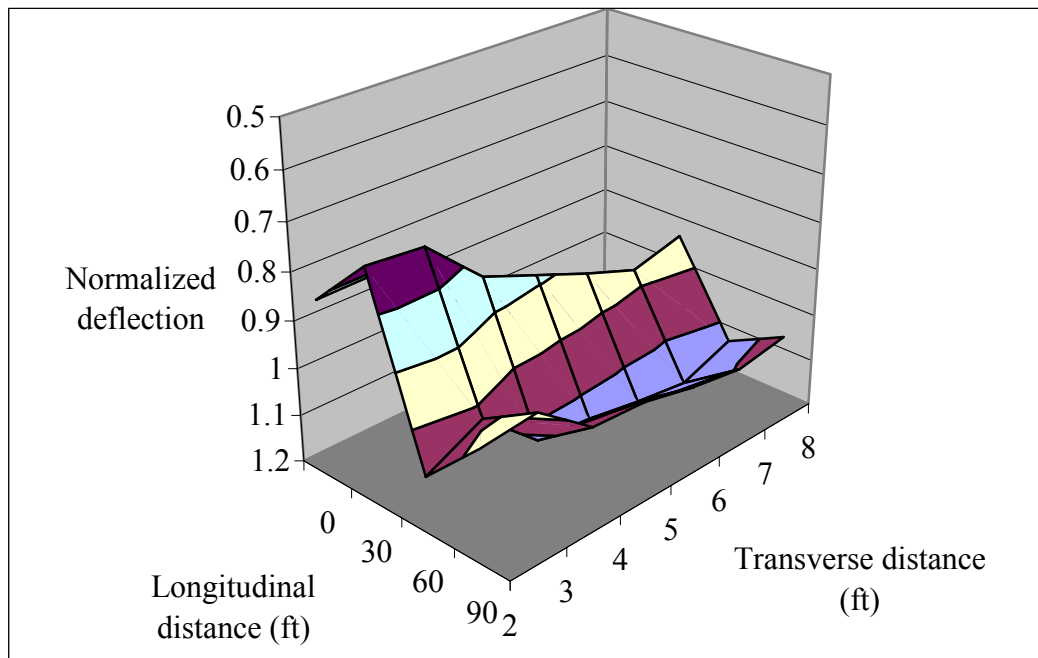
Figure 4.29 Normalized deflections on 30422-11
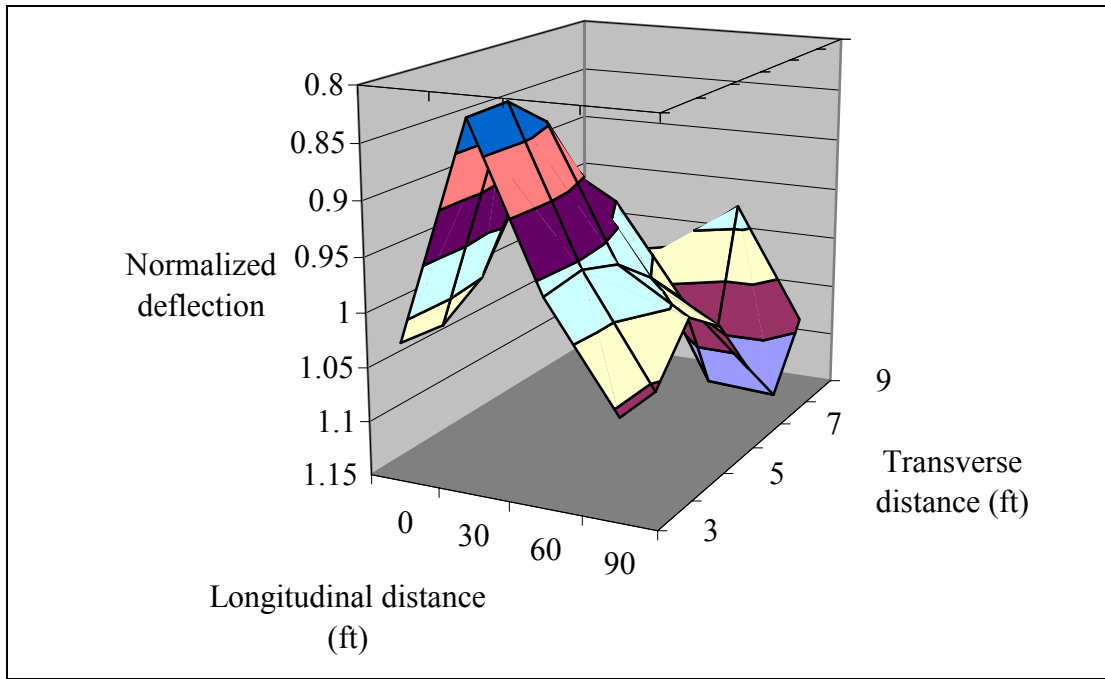
(a) Test section 1, test site 1 (30502-11)
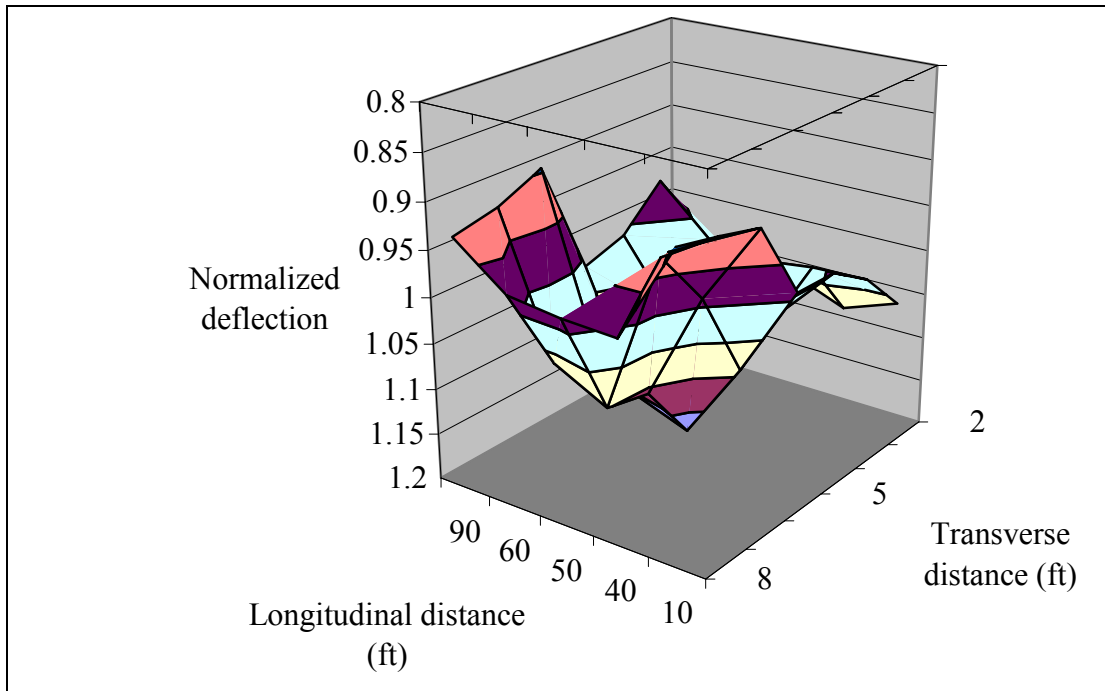
(b) Test section 2, test site 1 (30502-21)

Figure 4.30 Normalized deflections on M-50

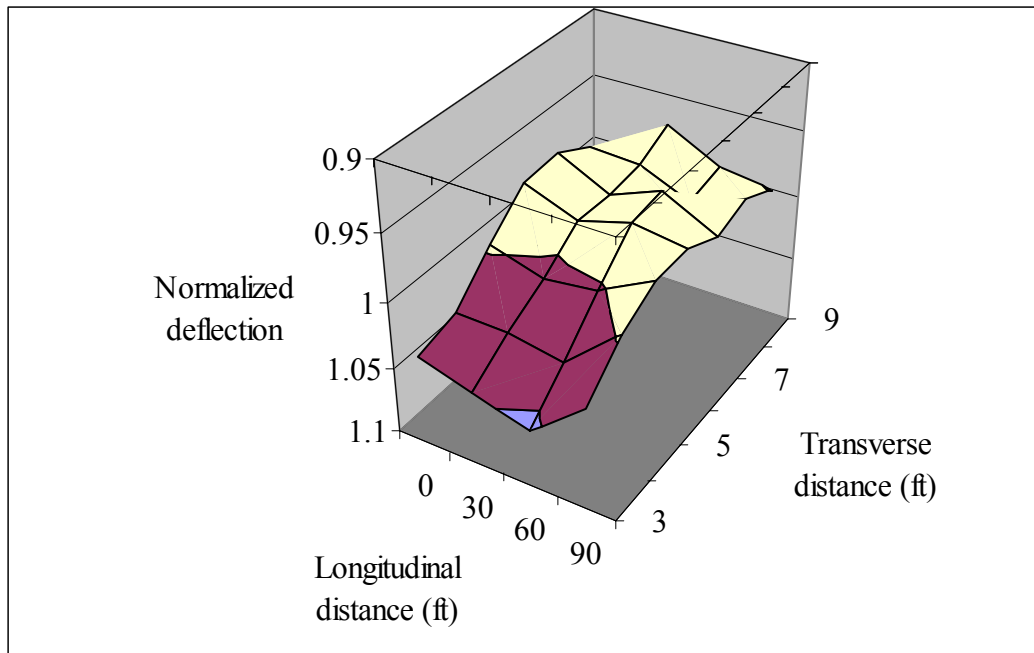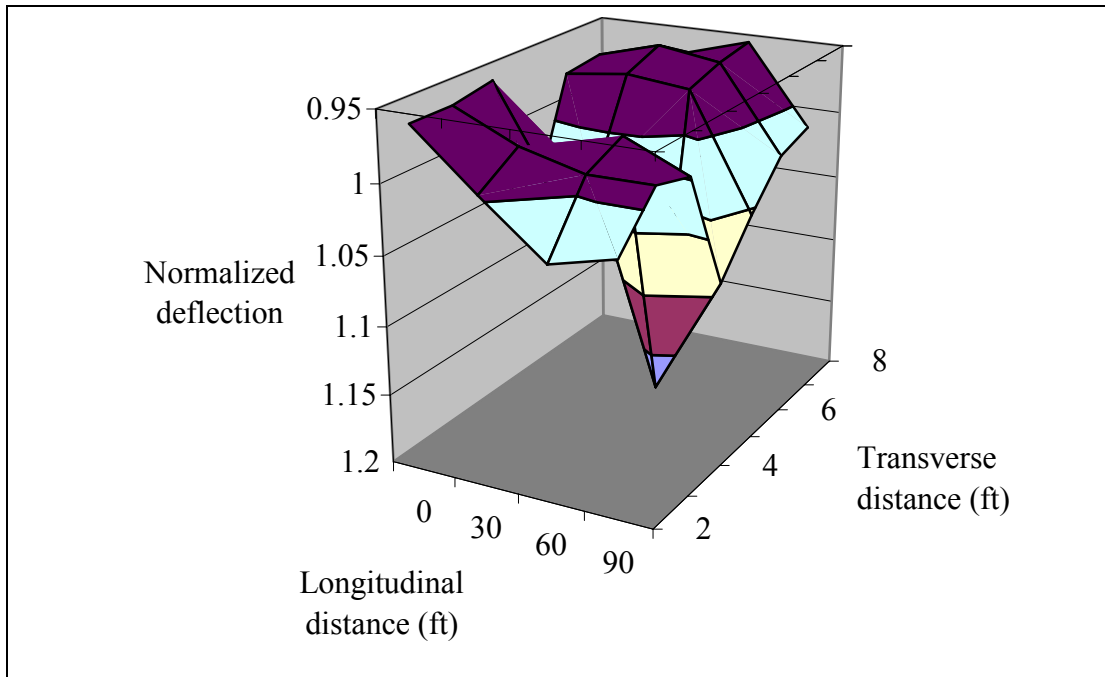(a) Test section 1, test site 1 (30521-11)
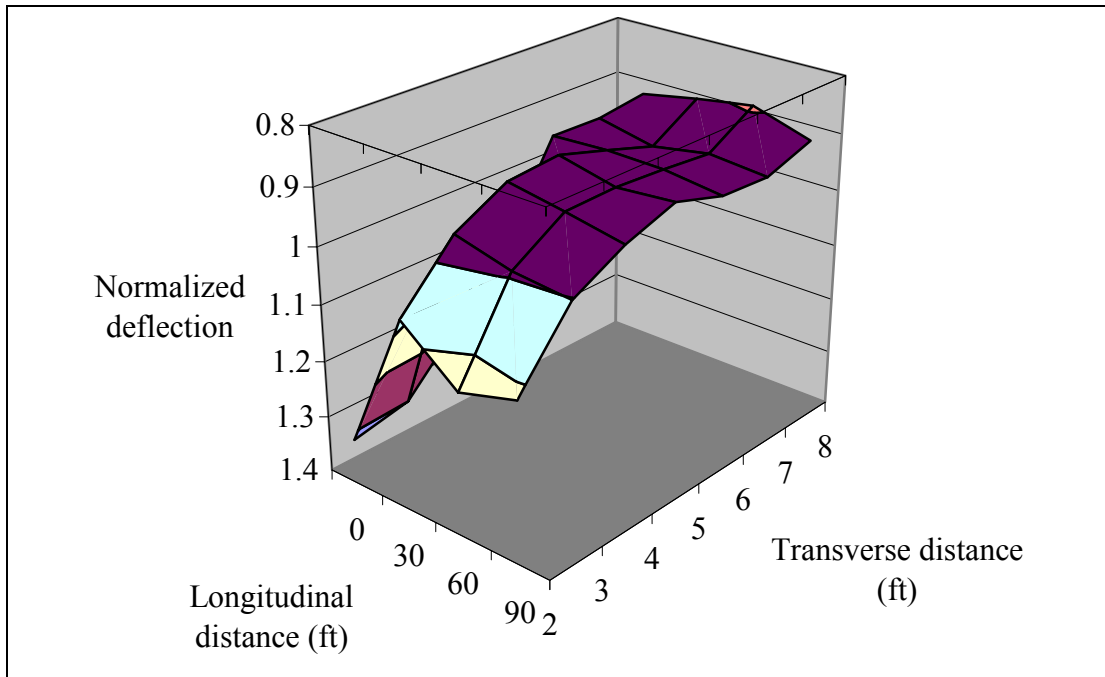
(b) Test section 2, test site 1 (30521-21)

Figure 4.31 Normalized deflections on M-52

64
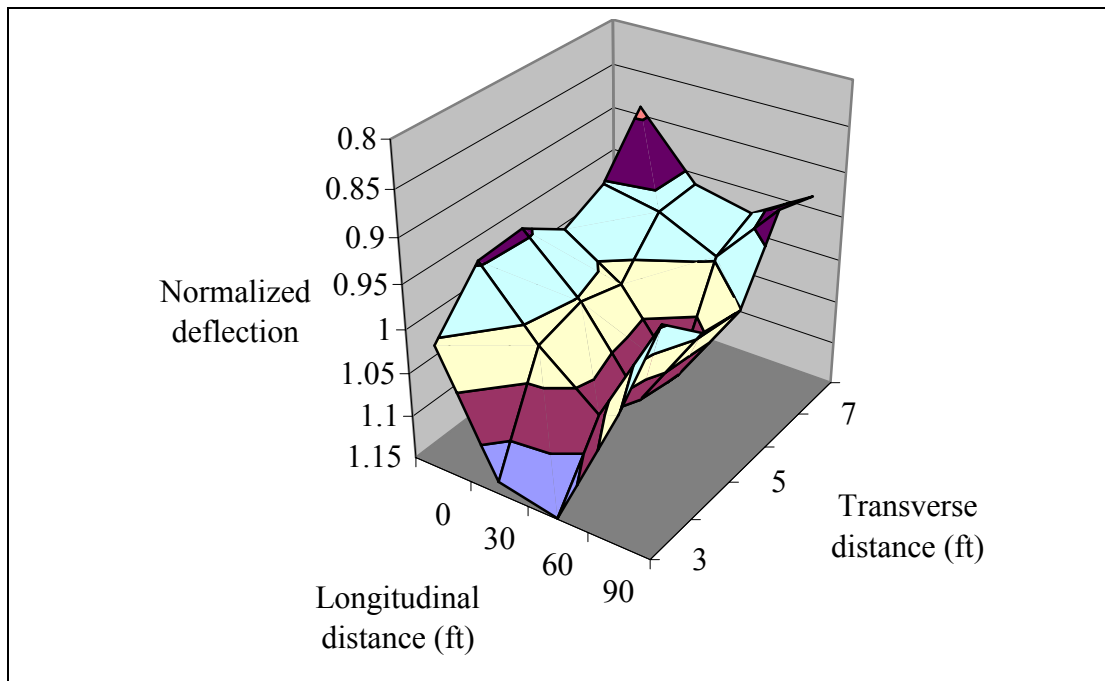
(a) Test site 1 (30551-11)
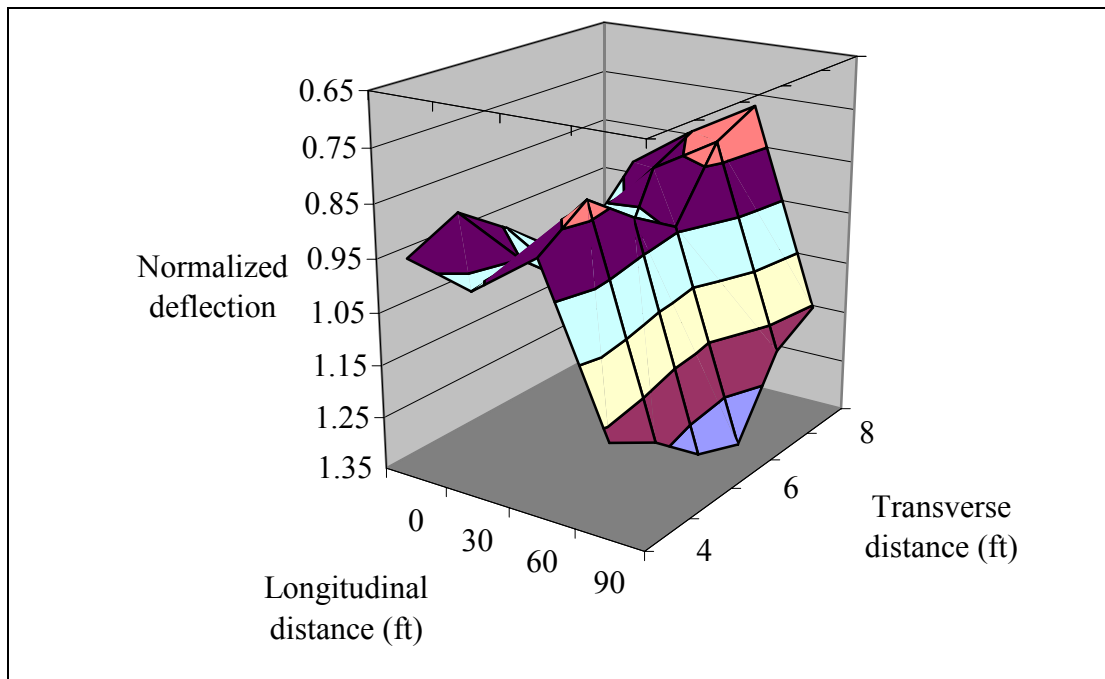
(b) Test site 2 (30551-12)

Figure 4.32 Normalized deflections on M-55, Test Section 1
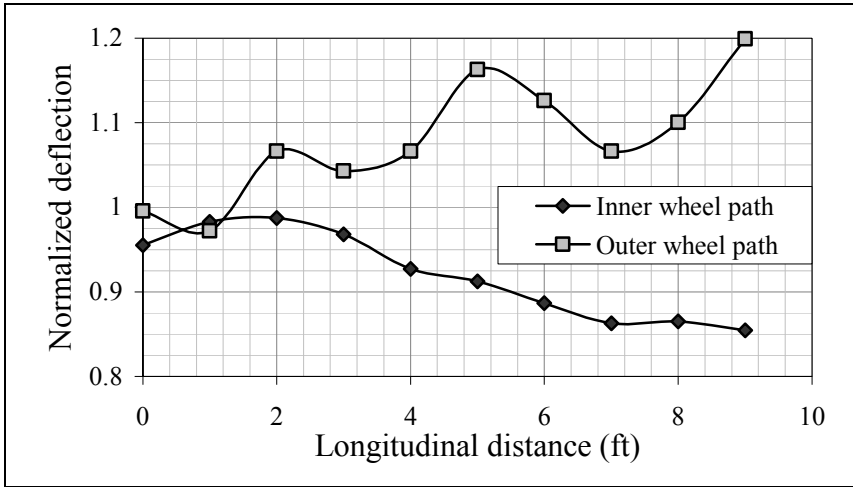
(a) Site 1
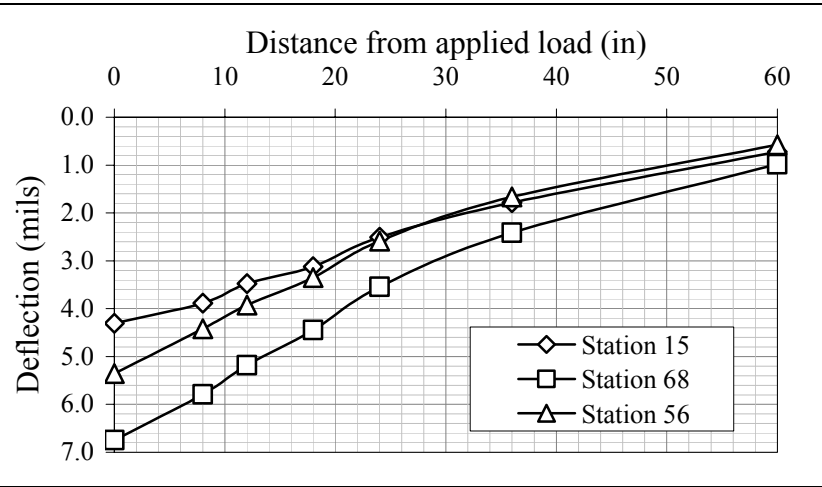
(c) Irregular deflection basins from Marsh Road
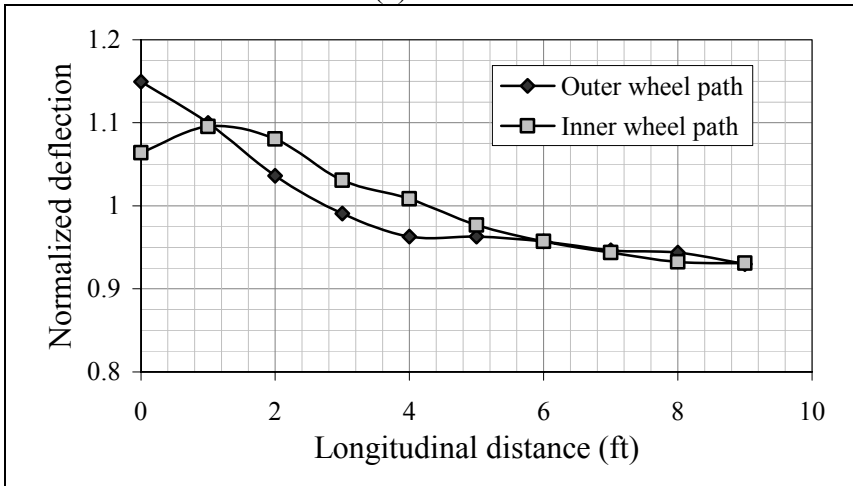
(b) Site 2

(d) Extensive TDC in Marsh Road

Figure 4.33 Normalized deflections on Marsh Road

> the measured deflection data and the distances between the deflection sensors; and

> pavement temperature and time of the day for each FWD test.

2. Examine the deflection basins for possible irregularities. Irregular deflection basins should not be included in the backcalculation. The irregular deflection basins could be the results of:

> Cracks in the vicinity of the FWD test;

> Edge effects; and

> Underground utility pipes or drainage pipes/culverts.

3. Use Boussinesq's equation to determine whether or not a stiff layer is shallow or deep and conduct trial backcalculation using 3- and 4-layer systems as to determine the approximate depth to stiff layer.

4. Set the convergence criteria in the backcalculation software.

5. Based on engineering judgment, establish acceptance criteria to accept or reject the backcalculated modulus values at certain FWD test locations.

6. Input the proper data into the backcalculation software including the deflection data, the number of pavement layers, their thicknesses, and Poisson's ratios, and the seed modulus value of each layer.

7. Conduct backcalculation of layer moduli.

8. For each FWD test location, examine the backcalculated results against the acceptance criteria.

9. Calculate the temperature corrected AC moduli (TCAC). Note that, in this study the backcalculated AC moduli were adjusted to the standard temperature of 68° F using temperature correction model.

10. For each test site, calculate the average values and the coefficients of variation (CV) of each backcalculated layer moduli.

8.2 Depth to Stiff Layer

The load induced-stresses and strains in most pavement sections dissipate to almost zero value within few feet from the pavement surface due to the arching effects in the soil. Hence, such stresses cause no measurable deflection. Theoretically, an elastic layered computer program calculates stresses and deflections at great depths from the pavement surface. In the backcalculation process, such calculations affect mainly the backcalculated modulus of the roadbed soil. To alleviate the problem and to force the layered elastic program to slow down the calculation of deflection, most backcalculation software (including the MICHBACK program) allow the users to place a stiff layer at a certain depth below the pavement surface. Such placement is problematic in that, if the estimated depth to stiff layer is incorrect, it produces errors in the backcalculated layer moduli. For example, if the depth to stiff layer is erroneously estimated at 400-in rather than the true 200-in then the errors in the backcalculated roadbed, subbase, base and AC moduli could be as high as 70, 40, 20, and 10 percent, respectively. In this study, an innovative procedure based on two independent methods was developed to accurately estimate the depth to stiff layer. The procedure is detailed in the next two subsections.

8.2.1 Equivalent Pavement Modulus

The approximate depth to stiff layer can be estimated using the equivalent (or composite) modulus of the pavement and the roadbed soil as explained in the following steps:

1. Select a minimum of three deflection basins (one at the beginning, one in the middle and one at the end of the test site) and calculate the equivalent modulus of the pavement layers and the roadbed soil at deflection sensors D2 through D7 using the following Boussinesq's equation:

$$E = \frac{P\left(1 - \upsilon^2\right)}{\pi(r)(d_r)}$$
(4.4)

   Where: E = equivalent modulus (psi);

   P = applied load = 9000 lb in this study;

   υ = Poisson's ratio (assume 0.4);

   r = radial distance from the center of the load to the deflection sensor in question (in.); and

   d_r = deflection at distance r from the center of the load (in.)

2. Plot the calculated E versus the distance "r" as shown in Figure 4.34. The resulting curve would have three possible shapes as follows:

   a) The E values at the tail of the curve increases with increasing distance r. This indicates possible shallow stiff layer. Higher rates of increasing E relative to d_r imply shallower depth to stiff layer as shown in Figure 4.34.
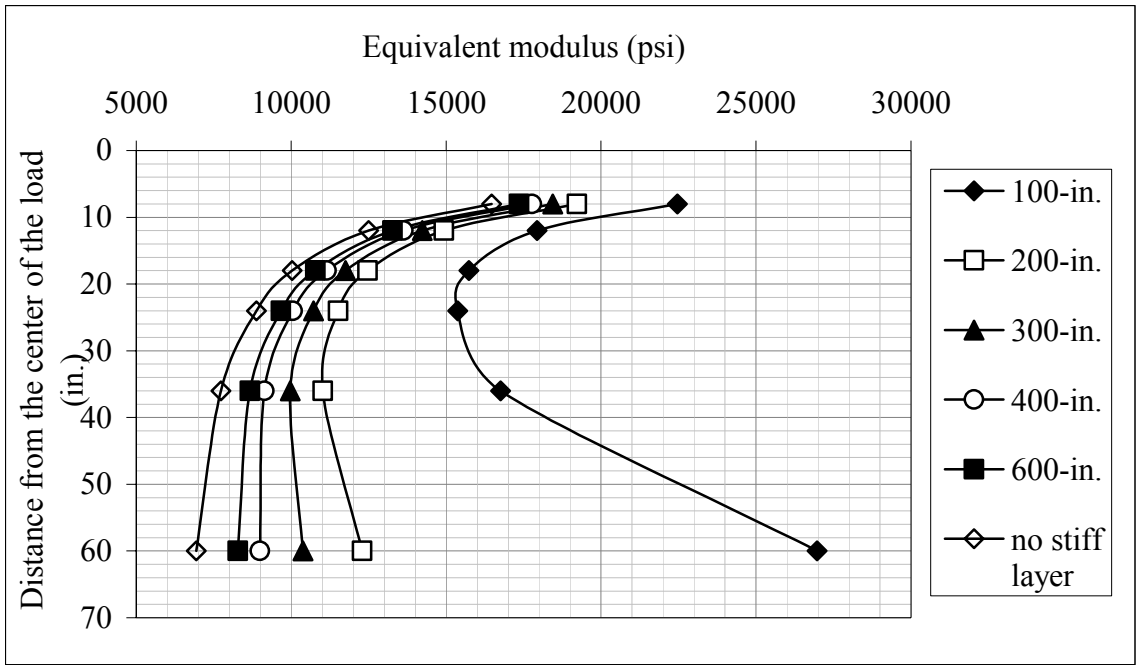
Figure 4.34 Plots of equivalent pavement modulus versus the distance from the center of load for 6 pavement sections having different depths to stiff layer

b) The E value at the tail of the curve is constant with increasing distance. This implies relatively deep (400 to 660-in) stiff layer.

c) The E value continuously decreases with distance, which implies deep or no stiff layer is needed as shown in Figure 4.34.

If the plots from the three deflection basins indicate different depths to stiff layer (e.g., one basin shows shallow stiff layer while the others show deep stiff layer), the following two scenarios are possible.

a) There may be underground facilities such as drainage culvert or utility pipe under the FWD test locations.

b) There may be cracks in the vicinity of the FWD test location, especially under the load plate or between the load plate and the deflection sensors. Regardless which scenario is true, it should be verified and deflection basins from those locations should be dropped or treated differently from the rest of the data.

Note that this method can only be used to determine whether or not a stiff layer should be incorporated in the backcalculation of layer moduli. The method by itself cannot be used to closely estimate the depth to stiff layer. This can be done using the next method.

8.2.2 Three- and four-layer system Backcalculation

For a given set of deflection data, the approximate depth to stiff layer can be estimated by backcalculating the layer moduli for three and four layer systems as outlined in the following steps:

1. Based on Boussinesq's equation results, obtain a rough estimate of the range of the depth to stiff layer (e.g., between 100 and 400-in). Divide this range to three or four equal increments. For example, 100, 200, 300 and 400-in.

2. For each incremental depth to stiff layer and for each deflection basin of one test site, perform backcalculation of layer moduli for the 3- and 4-layer systems shown in Figure 4.35. For flexible pavements, the 3-layer system consists of an AC layer (AC), combined base and subbase layer (BS) and roadbed soil (RB). The 4-layer system consists of an AC layer (AC), base layer (B), subbase layer (S) and roadbed soil (RB). This configuration is used because on many flexible pavements, a subbase is either not included in the construction, or is constructed of a similar material to the base.

3. Calculate the average backcalculated BS and RB moduli from the results of the 3-layer system and the average RB modulus from the 4-layer system.

4. Plot the average backcalculated BS and RB modulus and the average backcalculated RB modulus against the depth to stiff layer.

5. From the plots, obtain the approximate depth to stiff layer as the depth of the intersection of the two curves where the average BSRB and RB moduli are equal. Based on information obtained from soil maps and/or other sources, the true depth to stiff layer can be estimated as follows:

   ➢ The true depth to stiff layer is the depth at which the two curves representing the moduli of BS and RB intersect (the two moduli are equal). This is the likely scenario for pavement having the same type subbase and roadbed soil.
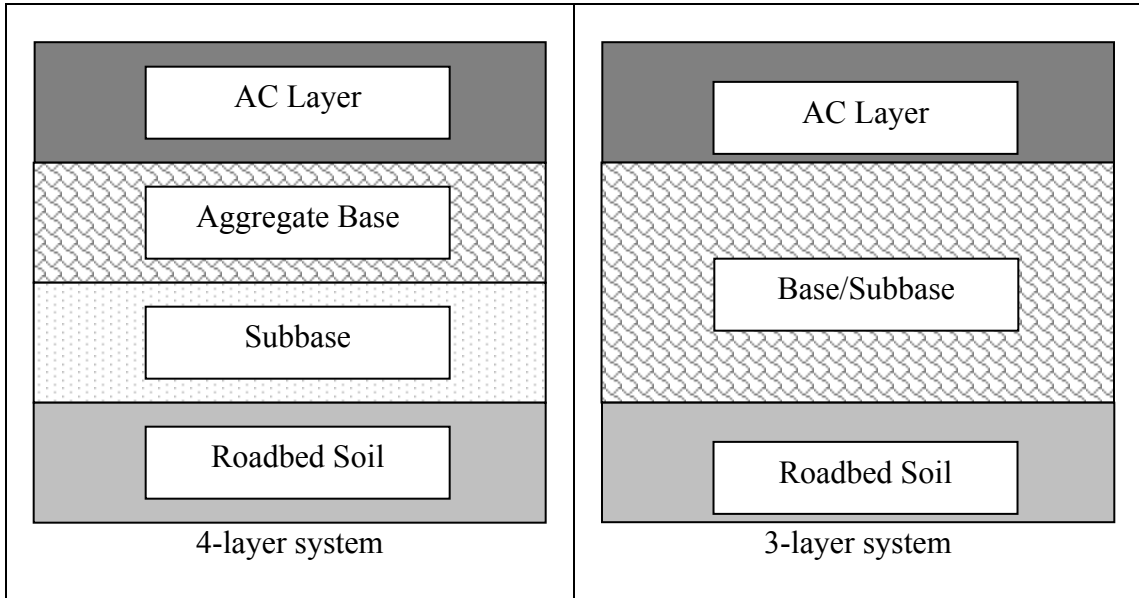
Figure 4.35 Three and four layer systems for flexible pavements used to determine the approximate stiff layer depth

> The true depth to stiff layer is Shallower than the depth at which the two curves intersect when the BS modulus is higher than RB modulus, which is the likely scenario for most pavements. The higher is the BS modulus relative to the RB modulus, the shallower is the true depth to stiff layer relative to the depth of intersection.

> The true depth to stiff layer is deeper than the depth at which the two curves intersect when the BS modulus is lower than the RB modulus. This is the likely scenario when the RB is hard and desiccated clay or hard pan. The lower is the BS modulus relative to RB modulus, the deeper is the true depth to stiff layer relative to the depth of intersection.

> The true depth to stiff layer is infinite or, in other words, no stiff layer should be incorporated into the backcalculation, if the plots of the average BSRB and RB modulus never intersect.

In some cases, the true cross-section of flexible pavement consists of AC, and thick aggregate base layers only situated on roadbed soil (no subbase layer). For such cases, the 3-layer system is the true pavement cross-section whereas the 4-layer system can be made by splitting the aggregate base into two layers (base1 and base2). Since in this case, the base in the 3-layer system is split into base1 and base2, the estimated depth to stiff layer is the depth at which the average modulus of base2 in the 4-layer system equal to the average modulus of the base in the 3-layer system.

Finally, the selected depth to stiff layer should yield reasonable values for all the backcalculated moduli, and the backcalculation should satisfy the convergence criteria, which are explained in section 8.3.

To illustrate the procedure, two sets of 15 deflection basins were generated using the CHEVRONX computer program. One set of 15 deflection basins is based on 300-in depth to stiff layer whereas no stiff layer was incorporated in the second set of 15 basins. The pavement cross-section and the layer moduli used in the forward analyses are listed in Tables 4.16 and 4.17. Figure 4.36 depicts the average backcalculated RB modulus from the 4-layer system and the average backcalculated BS modulus from the 3-layer system. As can be seen, for the set of deflection basins with 300-in deep stiff layer, the two curves intersect at the depth to stiff layer of 350 in. implying that the stiff layer is shallower than 350-in. For the second set of deflection basins where no stiff layer was incorporated, the two curves do not intersect even at a stiff layer depth of 800-in. implying that no stiff layer is required.

8.3 Convergence Criteria

In this study, several convergence criteria are specified in the MICHBACK computer program. After each iteration; the criteria are automatically checked by MICHBACK to determine whether or not the calculated and the measured deflection basin converged. These criteria are:

1. The modulus tolerance between two subsequent iterations is 0.1 %

Table 4.16 Thickness and moduli of pavement layers and roadbed soil of a pavement section having stiff layer at 300 in. used in the analyses

AC		RCS		Subbase		Roadbed		Stiff layer	
Thickness (in.)	Mod (ksi)	Thickness (in)	Mod (ksi)	Thickness (in)	Mod (ksi)	Thickness (in)	Mod (ksi)	Depth (in)	Mod (ksi)
5			50			271			
			100						
			300						
5.5			50			270.5			
			100						
			300						
6	1000	9	50	15	20	270	15	300	2000
			100						
			300						
6.5			50			269.5			
			100						
			300						
7			50			269			
			100						
			300						

Table 4.17 Thickness and moduli of pavement layers and roadbed soil of a pavement section with no stiff layer used in the analyses

AC		RCS		Base and subbase		Roadbed		Stiff layer	
Thickness (in)	Mod (ksi)	Thickness (in)	Mod (ksi)	Thickness (in.)	Mod (ksi)	Thickness (in)	Mod (ksi)	Depth (in)	Mod (ksi)
5			50						
			100						
			300						
5.5			50						
			100						
			300						
6	1000	9	50	15	20	Infinite	15	None	
			100						
			300						
6.5			50						
			100						
			300						
7			50						
			100						
			300						

(a) True depth to stiff layer 300-in
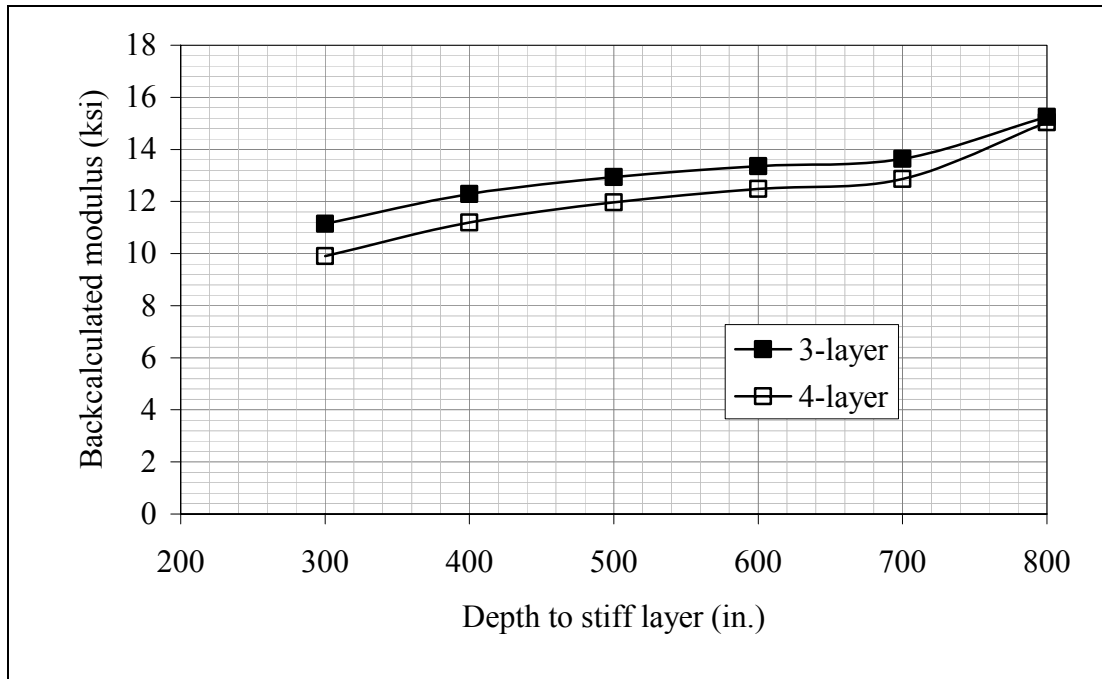
(b) No stiff layer (in the plot, 800 in. represents no stiff layer)

Figure 4.36 Backcalculated roadbed soil moduli (4-layer) and the combined moduli of the base, subbase and roadbed soil (3-layer) of the pavement for different stiff layer depths

77

2. The root mean square (RMS) error between the calculated and the measured deflection basins does not change by more than 0.1 percent between two subsequent iterations.

8.4 Acceptance Criteria

For quality control purposes, after the convergence criteria are satisfied, each value of the backcalculated layer moduli was scrutinized based on several acceptance criteria. These criteria and the reasoning behind them are listed below and summarized in Tables 4.18 and 4.19, respectively.

1. The RMS between the calculated and the measured deflection basins is equal to or less than 2 percent. This enhances the accuracy of the backcalculated modulus values.

2. The backcalculated BS and RB moduli satisfy the following equation:

$$1.1* \text{ BS modulus} \geq \text{RB modulus}$$

   This criterion is based on the principles of pavement design, decreasing layer modulus with depth. This criterion could be waved, if and only if, available and reliable information indicate that the RB modulus is higher than the BS modulus.

3. The RM modulus is equal to or greater than 20 ksi but less than or equal to 100 ksi. This criterion is based on definition of RM that was established in this study.

4. The FC modulus is greater than 100-ksi but equal to or less than 4,000-ksi. This criterion is also based on definition of FC that was established in this study.

Table 4.18 The acceptance criteria for the results of different backcalculations at each FWD test location

Acceptance criteria	Backcalculation		
	3-layer system (AC, RCS and BSRB)	4-layer system (AC, RCS, BS and RB)	4-layer system (AC, RM, FC and BSRB)
Convergence	Yes	Yes	Yes
RMS ≤ 2%	Yes	Yes	Yes
$1.1 * E_{base+subbase} \geq E_{roadbed}$		Yes	

The 3- and 4-layer systems used in the backcalculations are illustrated in Figure 4.31

Table 4.19 The reasons for each of the acceptance criteria

Acceptance criteria	Reasons
Convergence	To eliminate the unaccepted results by the backcalculation program
RMS ≤ 2%	To eliminate low accuracy backcalculation results and to assure close matches of the measured and the calculated deflection basins.
$1.1 * E_{base+subbase} \geq E_{roadbed}$	Unless otherwise indicated, the stiffer material layers are put on top to protect the lower material layer as a concept of pavement design. The 1.1 factor is provided to allow slight interaction in the backcalculation.

8.5 The Temperature Correction of the Backcalculated AC Moduli

The backcalculated AC moduli are corrected to the standard temperature of 68° F

using the temperature correction equation below (after Baladi and Harichandran, 1987).

$$TCAC = E_{AC}e^{0.03658(68 - T_o)} \qquad (4.5)$$

Where: TCAC = AC modulus corrected to standard temperature of 68° F (psi)

E_{AC}= Backcalculated AC modulus at the measured pavement surface

temperature (T_S),(psi)

T_o= Mid-depth temperature of the AC layer (°F)

$$T_o = T_S + (\sin(-6.3252t + 5.0967))\left(-0.8767\frac{h}{2} + 0.2788\left(\frac{h}{2}\right)^2 + 0.0321\left(\frac{h}{2}\right)^3\right) \qquad (4.6)$$

Where: h = AC thickness (in.); and

t = time of the day

Note that, during sunny days, the pavement surface temperature may vary from one FWD

test location to another depending on the wind speed, clouds and tree shadow. Therefore,

abrupt changes in the measured pavement surface temperature (such as 3°F or more)

between two FWD test locations were smoothed out by replacing the odd temperature by

the measured temperature at the two adjacent FWD test stations. After this, the moving 5-

test location average temperature was employed to minimize the differences between the

temperatures of two adjacent FWD stations. Note that, the time between two adjacent

FWD tests is about 2-minutes, it is physically not possible for the pavement surface

temperature to rise by more than 3°F and then drop. After calculating the 5-moving

average, the mid-depth pavement temperature was then calculated using equation 4.6 (Park, 2000).

9.0   BACKCALCULATION RESULTS

In this study, all measured deflection data were used to backcalculate the pavement layer moduli. The primary input for the backcalculation program is the thickness of each layer. Hence, data pertaining to the pavement cross-section were obtained before the backcalculation was initiated. Table 4.20 shows, for each flexible pavement layer, the type of material and the layer thickness that were obtained from the inventory data. As can be seen, for several roads, some of the cross-section data are missing (not available). The reason is that some pavement cross-sections are the result of repeated maintenance and overlay activities dating back to before such data were cataloged. For example, on M-52, the current road surface is placed over the original gravel road. On M-50, the lowermost AC courses date back almost 40 years and on US 41, an old concrete pavement was found about 36-in below the existing pavement surface. The average AC core thickness for each site is listed in Table 4.20.

Table 4.21 provides a list of the layer thicknesses used in the backcalculation. For some pavements, the data were obtained by drilling, for some others, from construction records, and still for others, from the typical design practice of providing frost protection of the roadbed soil. An example of the latter is M-55 where the thickness of the sand base layer (no subbase) was assumed 30-in as to provide frost protection for the roadbed soil.

The average values of the deflection data for flexible and rubblized pavements are listed in Tables 4.22, while the backcalculated moduli for flexible and rubblized pavements are listed in Tables 4.23 and 4.24, respectively. The backcalculated moduli were used as inputs for the mechanistic analysis of the structural response of the

81

Table 4.20 Inventory data (material type and layer thickness) and the average AC core thickness

| Test Site | Pavement Cross Section | | | | | | Roadbed Soil | Distresses in the test site |
| | AC Thickness (in) | | Base | | Subbase | | | |
	Inventory Data[1]	Core	Material	Thickness	Material	Thickness		
20273-11	N/A	9.0	Aggregate Base	N/A	N/A	N/A	Loamy Sand	None
20411-11	2.6	3.3	Aggregate Base	10	Select Subbase	24	Sandy, Mucky Loam	LC (TDC)
20411-12	2.6	2.8	Aggregate Base	10	Select Subbase	24	Sandy, Mucky Loam	LC (TDC)
30202-11	4.9	4.7	Aggregate Base	6	Subbase (CIP)	18	Loamy Sand	LC (TDC)
30202-12	4.9	4.5	Aggregate Base	6	Subbase (CIP)	18	Sand	LC (TDC)
30422-11	N/A	3.7	N/A	N/A	N/A	N/A	Sand	LC (TDC)
30502-12	N/A	6.1	Aggregate Base	N/A	N/A	N/A	Sandy Loam	Cracks
30502-21	N/A	6.9	Aggregate Base	N/A	N/A	N/A	Sandy Loam	LC (TDC)
30521-11	N/A	5.9	N/A	N/A	N/A	N/A	Loam	Cracks
30521-21	N/A	9.1	N/A	N/A	N/A	N/A	Loam	LC (TDC)
30552-11	3.1	3.0	Aggregate Base	N/A	N/A	N/A	Sand	Cracks
30552-12	3.1	3.0	Aggregate Base	N/A	N/A	N/A	Sand	Cracks
Marsh	N/A	10.6	Aggregate Base	4	N/A	N/A	Sandy Loam	Cracks

1. Data that could not be obtained or was otherwise unavailable is denoted by "N/A"

Table 4.21 The layer thicknesses used in the backcalculation of layer moduli

Test Site	Thickness used in the backcalculation of layer moduli of the asphalt pavements (in.)			
	AC (average core thickness)	Base	Subbase	Source of data
20273-11	9.0	27	0	Inventory data
20411-11	3.3	12	36	Hand borings
20411-12	2.8	12	36	Hand borings
30202-11	4.7	30	0	Hand borings
30202-12	4.5	30	0	Hand borings
30422-11	3.7	30	0	Hand borings
30502-12	6.1	30	0	Design/construction practices
30502-21	6.9	30	0	Design/construction practices
30521-11	5.9	36	0	Hand borings
30521-21	9.1	36	0	Inventory data
30552-11	3.0	15	0	Design/construction practices
30552-12	3.0	15	0	Design/construction practices
Marsh Road[1]	-	-	-	-

1. Marsh Road was not included in the backcalculation

Table 4.22 Average measured deflections and mid-depth AC temperature (MDT), flexible and rubblized pavements

Route	Test site	Radial distance of the deflection sensors (in) and the average measured pavement deflection (mils)							Pavement Type
		0	8	12	18	24	36	60	
		D1	D2	D3	D4	D5	D6	D7	
US-27	20273-11	7.29	6.26	5.63	4.77	4.05	2.87	1.43	Flexible
US-41	20411-11	14.37	10.61	8.31	5.83	4.29	2.38	1.05	
US-41	20411-11	14.83	10.54	8.04	5.56	4.03	2.14	0.80	
M-20	30202-11	9.37	7.17	5.80	4.23	3.17	1.84	0.80	
M-20	30202-12	9.56	7.15	5.65	3.95	2.86	1.58	0.65	
M-42	30422-11	16.31	13.71	11.80	9.27	7.27	4.50	2.15	
M-50	30502-11	11.51	9.30	7.84	5.92	4.48	2.50	0.91	
M-50	30502-21	12.27	9.17	7.40	5.49	4.17	2.45	1.09	
M-52	30521-11	10.58	8.64	7.29	5.56	4.22	2.42	1.08	
M-52	30521-21	6.86	5.92	5.35	4.56	3.80	2.59	1.18	
M-55	30552-11	11.91	9.00	7.03	4.97	3.81	2.51	1.43	
M-55	30552-12	12.93	9.78	7.69	5.64	4.47	3.13	1.88	
Marsh Road		6.19	5.26	4.66	4.06	3.22	2.17	0.86	
I-194	11941-11	5.03	4.44	4.09	3.66	3.29	2.70	1.82	Rubblized
I-194	11941-12	6.10	5.34	4.87	4.34	3.86	3.11	2.07	
I-75	10753-11	8.34	7.21	6.48	5.52	4.72	3.45	1.91	
I-75	10753-12	8.05	6.82	6.03	5.01	4.21	3.00	1.57	
M-15	30153-11	7.68	6.75	6.08	5.12	4.33	3.12	1.75	

Table 4.23 Average backcalculated moduli and the temperature corrected AC moduli for the flexible pavement test sites

| Route | Test site | Backcalculated modulus (ksi) | | | | | | Depth to stiff layer (in) [1] | Stiff layer modulus (ksi) [1] | Included | Accepted |
		AC	Mid-depth temperature (°C)	Temperature corrected AC	Base	Subbase[1]	Roadbed				
US-27	20273-11	851	21.8	905	29	-	17	200	2,000	40	40
US-41	20411-11	2,268	31.0	1,084	38	17	41	-	-	42	42
US-41	20411-12	3,098	34.8	1,151	44	16	56	-	-	42	42
M-20	30202-11	1,017	23.2	1,248	38	-	22	150	2,000	30	30
M-20	30202-12	952	27.6	1,559	37	-	26	150	2,000	29	29
M-42	30422-11	2,406	7.9	1,104	17	-	12	250	2,000	52	49
M-50	30502-11	670	14.4	451	22	-	16	120	485	41	28
M-50	30502-21	312	30.0	584	28	-	17	150	485	48	48
M-52	30521-11	865	14.3	584	21	-	36	-	-	44	43
M-52	30521-21	1,063	8.0	456	18	-	34	-	-	40	40
M-55	30552-11	1,728	31.0	2,546	42	-	27	-	-	33	33
M-55	30552-12	1,256	36.9	2,794	48	-	21	-	-	37	23
Marsh Road	Marsh Road was not included in the backcalculation.										

1. Non existent layers are indicated by "-"

Table 4.24 Average backcalculated moduli and the temperature corrected AC moduli for the rubblized pavement test sites

Route	Station	Backcalculated modulus (ksi)						Depth to stiff layer (in)	Stiff layer modulus (ksi)	Included	Accepted
		AC	Mid-depth temperature (°C)	Temperature corrected AC	Rubblized concrete	Fractured concrete	Roadbed				
I-194	11941-21	1506	16.2	1170	71	406	24	None	2000	30	30
I-194	11941-22	1633	20.5	1682	79	334	21	None	2000	32	31
I-75[1]	10753-11	I-75 was not included in the backcalculation.									
I-75	10753-12										
M-15	30153-11	2020	16.4	1598	62	194	20	500	2000	33	33

1. I-75 was not included in the backcalculation.

pavements. Tables 4.25 and 4.26 show the coefficients of variation of the backcalculated

moduli for each flexible and rubblized test site, respectively.

In general, the coefficient of variation is low, indicating that the backcalculation

results are consistent within individual test sites. Special cases do occur however, which

are discussed in the following sections. It is important to note that only the descriptions of

the backcalculation of flexible sections are included. Details of the backcalculation for

rubblized sites are available elsewhere (Baladi and Svasdisant, 2002).

9.1   US-27 Southbound, Section 1, site 1 (20273-11)

This pavement section is located north of Mt. Pleasant on loamy sand. The test

section is a flexible pavement located in the middle of a rubblized concrete pavement

project. The section (in the vicinity of an overpass, Isabella Road) was constructed after

removing the old concrete pavements to maintain bridge clearance. For this test section,

no specific cross section data were available from MDOT. The cross section was

established based on investigations of the surrounding rubblized pavements.

The variation in the measured peak deflections along and across the pavement is

shown on Figure 4.26. It can be seen that the variation in the deflection across the

pavement is relatively small; on average, the edge deflection is about 5% higher than the

deflection at the center of the lane. The relatively higher deflection at the outer wheel

path could be attributed to lack of edge support.

The pavement cross-section used in the backcalculation was composed of three

layers; an 8.9-in AC layer, 20-in base layer (for approximately 30-in of frost protection)

and a roadbed soil. The Boussinesq equivalent pavement modulus indicates that a

Table 4.25 Coefficients of variation of the backcalculated layer moduli of the flexible pavement test sites

| Route | Test site | Coefficients of Variation | | | | | |
		AC	Temperature corrected AC	Base	Subbase	Roadbed	RMS (%)
US-27	20273-11	5	10	7	-[1]	3	30
US-41	20411-11	11	15	7	8	7	28
US-41	20411-11	16	17	6	5	11	29
M-20	30202-11	12	11	8	-	10	37
M-20	30202-12	9	8	5	-	3	31
M-42	30422-11	29	31	10	-	3	40
M-50	30502-11	24	21	9	-	16	43
M-50	30502-21	15	15	9	-	12	35
M-52	30521-11	15	16	8	-	3	54
M-52	30521-21	22	24	13	-	11	78
M-55	30552-11	18	20	14	-	4	37
M-55	30552-12	27	30	17	-	4	34
Marsh Road	Marsh Road was not included in the backcalculation.						

1. Non-existent layers are indicated by "-"

Table 4.26 Coefficients of variation of the backcalculated layer moduli of the rubblized
pavement test sites

Route	Test site	Coefficients of variation				
		AC	Temperature corrected AC	Rubblized concrete	Fractured concrete	Roadbed
I-194	11941-21	2	2	3	5	0
I-194	11941-22	3	2	2	5	1
I-75[1]	10753-11	I-75 was not included in the backcalculation				
I-75	10753-12					
M-15	30153-11	2	2	4	7	1

shallow stiff layer exists. By splitting the base layer into separate base and subbase layers and by calculating the layer moduli for different depths to stiff layer, it was concluded that the stiff layer is located at 200-in below the pavement surface.

The backcalculated moduli of the pavement layers fall within the ranges of typical values for the respective materials, and are therefore reasonable. The RMS is consistent along and across the pavement and the average RMS is less than 0.50. This was expected because of the following reasons:

1. Uniform AC thickness as measured from the pavement cores.

2. The consistency of the deflection data.

3. The lack of pavement distress.

Additionally, the results of the backcalculation almost match those obtained for the surrounding test sites, which indicates that the backcalculated moduli are relatively accurate.

9.2 US-41 North bound, section 1 sites 1 and 2 (20411-11, 20411-12)

The flexible pavement at the test sections on US-41 is unique in that it consists of the following layers:

1. About 3-in thick AC layer.

2. A 12-in sand layer.

3. A 39-in thick uniformly graded, rounded and loosely compacted peastone.

4. A 9-in thick concrete slabs (on average, 54-in below the pavement surface).

5. Sandy, mucky loam roadbed soil.

The variations in the measured peak deflection along and across the pavement are shown in Figure 4.27. It can be seen that the deflections on sites 1 and 2 exhibit a similar trend as that observed on US-27 with the peak deflections occurring near the outer wheel path and the minimum at the center of the lane. On site 2, the deflection decreases along the pavement and tends to be the greatest on the inside edge of the outer wheelpath. Unlike rubblized pavements, the variation in the deflection is relatively small (it varies about 5% from the mean).

Analysis of the deflection data using Boussinesq's equation confirmed that a very shallow stiff layer exists (in this case, the PCC slabs). The average AC thicknesses used in the backcalculation were 3.3-in and 2.8-in, for test sites 1 and 2, respectively. On both sites, the sand base thickness was set at 12-in, and the gravel subbase thickness at 39-in. In the backcalculation, the roadbed was assumed to include the roadbed soil and the concrete slab. This assumption eliminated the need to place a stiff layer at certain depth and, as it was expected, resulted in a relatively high modulus of the roadbed soil. Therefore, the acceptance criterion relative to the modulus values of the roadbed and subbase layer was not applied due to the presence of the concrete slab.

9.3   M-20 East Bound, Section 1, Sites 1 and 2 (30202-11 and 30202-12)

This pavement section is located east of Mt. Pleasant. The pavement cross-section consists of:

1. AC thickness of 4.7 and 4.5-in on test sites 1 and 2, respectively.

2. A minimum of 30-in clean sand base and subbase layer (hand auguring indicates a minimum of 60-in of sand).

3. Sand roadbed soil.

The measured deflection profiles are shown in Figure 4.28 for sites 1 and 2. Each site shows the trend that has been observed with consistency for all flexible pavement sections; the deflection at the pavement edge is higher than at the center of the lane. In this case however, the maximum deflection is at the inside edge of the lane, as opposed to the outside edge as has been observed in other test sites. Additionally, for site 2, the deflections along the pavement decrease from the beginning to the end of the site.

The Boussinesq equivalent modulus of the pavement indicates that a shallow stiff layer exists. By splitting the base layer into separate base and subbase layers, the stiff layer was determined to occur at 150-in.

The average backcalculated moduli of the pavement layers are listed in Table 4.25 along with the average RMS. As can be seen, all values are reasonable and the average RMS is about 1.07. One note is that the average roadbed modulus on M-20 of 22 and 26 ksi is close to the 17-ksi that was backcalculated on US-27. This was not expected because according to the USGS soil maps of Isabella County, the native soils at both test sections are identical. The discrepancy could be related to the assumed thickness of 30-in on M-20, which would cause slight inflation in the backcalculated modulus.

9.4   *M-42 East-Bound, Section 1, Site 1 (30422-11)*

No construction and/or cross-section records were available for this pavement section, which is located east of Mesick. Based on coring and boring, the pavement cross-section consists of:

1. An AC layer whose thickness is highly variable.

2. A 1-in thick silty gravel that was likely placed to provide stable surface for construction traffic.

3. Deep deposit of sand roadbed soil.

The measured deflections were normalized and plotted in Figure 4.29. The deflection data shows that the measured deflection is lowest at the outer wheelpath and then increases to the inner wheelpath. In addition to this trend, an area of low deflection occurs across a transverse line approximately 30-ft from the beginning of the test site. This lower deflection is not associated with and physical features on the pavement such as culvert, drainage or utility line and/or distress. Nevertheless, the maximum deflection is approximately 17.7% higher than the average whereas the minimum is approximately 28.2% less than the average deflection.

In the backcalculation, due to the high variability of the AC thickness, two AC thicknesses were used; 3.3-in was assigned to 38 FWD test locations and 4.7-in to 14 locations. Further, the 1-in layer of silty gravel was ignored, and a base thickness of 30-in was assumed, which would provide adequate frost protection. In reality, this 30-in represents the approximate depth to which the deep sand roadbed soil would have been improved during construction. In any event, it was anticipated that the backcalculated layer moduli of the 30-in base layer and the roadbed soil would have similar values.

The Boussinesq's equivalent modulus indicates that a moderately shallow stiff layer exists. By splitting the base layer into separate base and subbase layers, the depth to stiff layer was estimated at 250-in.

Because of cold temperature during the FWD test, the backcalculated moduli of the pavement layers were high. Reasonable values were obtained after they were

corrected to the standard temperature of 68° F. As was expected, the base and roadbed

moduli values were not excessively different with the average base modulus of 17-ksi

and the average roadbed modulus of 12-ksi. The difference between the two moduli could

be explained by improvement of the upper portions of the roadbed (for stability and frost

protection) during construction and/or by the effect of the 1-in thick silty gravel layer.

Finally, the average percent RMS is less than 1.00.

9.5 M-50 East-Bound, Test Section 1, Test Site 1 (30502-11)

According to the USGS soils map of Eaton County, the roadbed soil is comprised

of sandy loam. MDOT inventory data indicates repeated milling and overlays operations

back to the 1960's. Therefore, no definitive cross section is available in the inventory

data. Although hand boring was not conducted on this test sections, the base was sampled

after coring. It appears that the sandy loam roadbed soil was simply compacted and an

AC layer was placed on top. Therefore, a base thickness of 30-in (for frost protection)

was used in the backcalculation of layer moduli.

The deflection variation on M-50 test section 1, test site 1 is provided in Figure

4.30a. The deflection on this site exhibits similar trend as that observed on M-20, the

maximum deflection occurs close to the inner wheelpath. Additionally, an area of

abnormally low deflection occurs in the vicinity of test points 3, 4, 5, and 12. Finally, the

measured D7 deflection (the outer sensor) is highly variable with coefficients of variation

of 22 and 12 (see Table 4.12).

The Boussinesq equivalent pavement modulus indicates that a relatively shallow

stiff layer should be used in the backcalculation. Multiple attempts to estimate the depth

to stiff layer were made by examining the results of various backcalculation using different depths to stiff layer; none were successful. This could be the consequence of the high variation in the D7 deflection.

In the backcalculation, a depth to the stiff layer of 120-in and modulus of 485 ksi were used. These produced reasonable results (see Table 4.23). One note is that of the 41 test locations, the results from only 28 locations were accepted. A good number of FWD tests were located over and/or in the vicinity of cracks. This tests section had experienced significant distress and cracking was prevalent throughout the test site.

9.6   M-50 East-Bound, Section 2, Site 1 (30502-21)

Test section 2 on M-50 is situated on the same type roadbed soil as test section 1. Therefore, similar difficulties in backcalculating the depth to stiff layer were expected. Except for the thickness of the AC, the pavement cross section (30-in base layer, semi-infinite roadbed) was the same as before. However, no hand borings were obtained on this site.

The deflection variation on M-50 Section 2, site 1 is illustrated in Figure 4.30b. As can be seen, the deflection varies from 12.1% less to 17.8% higher than the average deflection. The lowest deflection occurred at the beginning of the site whereas the highest at the center of the site along the center of the lane. The primary distress on the site is a longitudinal crack running along the outer wheelpath.

Similar to test section 1, a relatively shallow depth to stiff layer was found. Analyses of the deflection data by splitting the base layer into separate base and subbase

layers indicated a stiff layer depth of 185-in, which was assigned a modulus value of 485-ksi. An AC layer thickness of 6.9-in was used based on core measurement data. As opposed to the backcalculation on test section 1, all 48 test stations converged and passed the acceptance criteria. The average percent RMS for the site was less than 1.00. The temperature corrected AC and the roadbed moduli were similar to those obtained from test section 1. However, the backcalculated base layer modulus was on section 2 was about 30 percent higher than that of section 1. This could be attributed to the difference in the distress between the two sections.

9.7   M-52 North-Bound, Section 1, Site 1, (30521-11)

M-52 test section 1 is situated in northern Ingham County. The MDOT inventory data indicates that M-52 was built on a raised embankment over a gravel road. Hand borings indicate that a base of silty gravel exists to a depth of 36-in. At 36-in, a hard layer was encountered that could not be bored through using the equipment on hand. It is likely that this hard layer is the original surface of the gravel road. This is confirmed by the Boussinesq's equivalent modulus procedure, which indicated very shallow stiff layer.

The measured deflection data were normalized and plotted in Figure 4.31a. The data show moderate variation in the deflection along and across the pavement.

The thicknesses of the extracted cores were highly variable. Hence, in the backcalculation, three AC thicknesses were used as follows:

1. 5.3-in AC for 4 test stations.

2. 5.9-in AC for 37 test stations.

3. 6.5-in AC for 3 test stations.

The base layer thickness was set at 36-in as measured from the hand boring.

A three layer system was employed in the backcalculation of layer moduli; AC, base and a semi-infinite layer comprised of combination of the gravel road structure and roadbed soil. Because of this modeling technique, it was anticipated that the modulus of the semi-infinite layer would be higher than the modulus of the base layer, and therefore would fail the acceptance criteria. Consequently, the semi-infinite layer was labeled a stiff layer due to the presence, and the inclusion, of the gravel road. The backcalculation converged without difficulty at all 40 test stations and the average percent RMS was less than 1.00.

9.8   M-52 North-Bound, Section 2, Site 1, (30521-21)

M-52 test section 2 has an identical cross section to that of section 1 including the old gravel road at about 40-in below the pavement surface. Hence, the backcalculation of layer moduli were conducted using the same procedure. To avoid unnecessary repetition, only the normalized deflection data are presented herein.

Figure 4.31b depicts the normalized deflection data. As can be seen the deflection profile varies along and across the pavement. Results of the backcalculation are listed in Table 4.23.

9.9   M-55 East Bound, Section 1, sites 1 and 2 (305552-11,12)

This pavement section is located west of Prudenville, and the soil map of Roscommon County indicates that the test section is located on sand. While no hand borings of the pavement structure were obtained, sampling of the base material indicates

that the base is sand. Construction plans for the project indicate that an engineered base was placed, but its thickness was not specified. Therefore, the base thickness was assumed to be 30-in for frost protection.

The deflection variation on M-55 Section 1, sites 1 and 2 can be found in Figure 4.32. The deflection data on site 1 shows that the measured deflection is highest at the outer wheelpath. This is consistent with the cracking observed near the curb. In this case, the deterioration of the asphalt is likely due to different expansion rates between the concrete curb and gutter and the asphalt mat. The overall deflection of the site does not vary by more than $\pm$ 15%. However, on site 2, about 30 percent higher than average deflections were measured at the transverse line 90-ft into the beginning of the site. The reason for the high deflections is transverse cracks at that location.

The Boussinesq equivalent modulus procedure indicates a moderate depth to stiff layer. By splitting the base layer into separate base and subbase layers, the stiff layer was determined to occur at 270-in.

The backcalculation was conducted using an average AC thickness of 3-in and 30-in thick base layer on top of semi-infinite roadbed soil. The temperature corrected AC modulus was abnormally high. This caused re-examination of the data and the backcalculation procedure. It was found that since the AC thickness is only 3.0-in, minor variation would cause significant impact on the backcalculated modulus. Therefore, the backcalculation of layer moduli was re-conducted using, for each test site, the 12 FWD test stations where AC cores were extracted. Results of the analyses are listed in Table 4.23. As can be seen, the backcalculated and temperature corrected AC modulus is still

higher than typical values (higher than 2000-ksi), no adequate explanation can be given at this time.

9.10 Marsh Road (2 test sites)

Marsh Road in Okemos is located on sandy loam. The test sites were located almost half way between Hamilton Road and Grand River Avenue. The pavement has been milled and overlaid repeatedly, which resulted in 10.6-in AC thickness. No inventory data exists regarding the thicknesses of the pavement layers. Construction plans indicate that a 4-in base layer was placed.

At each test site, the deflection data were collected only in the outer and inner wheel paths, therefore, 3-dimensional plots could not be made. Figure 4.33a and 4.33b depicts variation in the measured and normalized peak pavement deflection along the wheel paths while Figure 4.33c shows three typical deflection basins. The data in the two figures indicate that the peak pavement deflection varies by about $\pm$ 15 percent and that the shapes of the deflection basins are irregular.

For each test site, various unsuccessful attempts to backcalculate the layer moduli were made. The reasons include the irregularity of the deflection basins and the condition of the pavement surface of Marsh Road. The pavement showed an extensive network of top-down cracking and raveling in moderate and high severity segregated areas as shown in Figure 4.33d.

10.0   INDIRECT TENSILE TESTS

Indirect tensile cycle load tests (ITCLT) and indirect tensile strength tests (ITST) are convenient and useful tests to determine the resilient moduli and strength of AC specimens. The tests require a minimum specimen thickness of 2.2-in. In no case however, an asphalt had the required thickness. For this reason, the test specimens were composed of more than a single AC course. Hence, the test is a useful indicator of relative trends in pavement strength. In this study, both tests were utilized. The findings are summarized in the following sections.

10.1 Indirect Tensile Cyclic Load Tests (ITCLT)

Most asphalt pavements are constructed using multiple lifts or courses. Each course may be composed of a different mix than the other courses. Also, different courses may be subjected to construction anomalies such as segregation or varying compaction. These factors affect the modulus of the AC course in question. ITCLT are used to study the variation in the AC modulus throughout the thickness of the AC layer and along and across the test site.

ITCLT were conducted on specimens obtained from 9 flexible and 5 rubblized pavement test sites. The results of the tests are shown in Table 4.27. The data in the table are divided into different categories based on where the test specimens were obtained from within the AC layer. As can be seen, several pavements have only one set of test results. This is because the AC layer on these pavements was so thin that the entire core was used as a test specimen. This situation occurred on US-41, test section 1, test sites 1 and 2, on M-55, test section 1, test sites 1 and 2 and on I-75, test section 1, test sites 1 and

Table 4.27 Moduli calculated from ITCLT for specimens cut from different depths in the AC layer

| Route | Test site | Top portion of core | | | Middle portion of core | | | Bottom portion of core | | | Pavement Type |
		Number of tests	Average modulus (ksi)	Standard deviation (ksi)	Number of tests	Average modulus (ksi)	Standard deviation (ksi)	Number of tests	Average modulus (ksi)	Standard deviation (ksi)	
US-27	20273-11	1	176	-	4	211	17	2	213	8	Flexible
US-41	20411-11	12	175	26	-	-	-	-	-	-	
US-41	20411-12	12	205	15	-	-	-	-	-	-	
M-20	30202-11	5	193	28	-	-	-	4	160	28	
M-20	30202-12	6	176	18	-	-	-	3	165	14	
M-50	30502-11	3	180	7	3	191	30	5	191	11	
M-55	30552-11	12	180	20	-	-	-	-	-	-	
M-55	30552-12	12	182	16	-	-	-	-	-	-	
Marsh Road		2	181	8	8	188	17	8	196	15	
I-194	11941-21	3	189	10	3	196	11	3	203	15	Rubblized
I-194	11941-22	2	220	2	3	217	13	3	203	14	
I-75	10753-11	3	209	13	-	-	-	-	-	-	
I-75	10753-12	4	196	6	-	-	-	-	-	-	
M-15	30153-11	5	228	14	-	-	-	5	214	10	

Table 4.28 Average indirect ITST data

| Route | Test site | Strength Data | | | ITST Equivalent modulus (ksi) | | Pavement Type |
		Number of tests	Average strength (psi)	Standard deviation (psi)	Average modulus	Standard deviation	
US-27	20273-11	7	82	13	36	5	Flexible
US-41	20411-11	12	165	19	90	19	
US-41	20411-12	12	183	13	95	14	
M-20	30202-11	9	93	19	42	15	
M-20	30202-12	8	82	21	28	14	
M-50	30502-11	10	122	30	88	37	
M-55	30552-11	11	114	10	60	13	
M-55	30552-12	11	116	15	59	13	
Marsh Road		15	138	26	75	21	
I-194	11941-21	6	206	40	109	38	Rubblized
I-194	11941-22	8	241	56	85	32	
I-75	10753-11	4	146	8	62	11	
I-75	10753-12	4	174	18	73	15	
M-15	30153-11	10	172	9	84	19	

2. Nevertheless, test specimens from other sites indicate that significant variation occurs throughout the depth of AC layer. Test specimens from the lower portions of the AC layer tend to have higher modulus values than the specimens tested from the upper portion of the AC layer. This is due to the fact that, in general, coarser aggregates are used in the lower AC courses. Variation across the site is not insignificant either; most sites show at least 5% variation for all portions of the AC layer, with 10% variation common. Ultimately, it shows that the behavior of the AC layer is a complex interaction of multiple courses having different moduli values, which contribute to the overall variation in pavement behavior.

10.2 Indirect Tensile Strength Test Data

Indirect tensile strength tests (ITST) were conducted using the apparatus specified in ASTM standard test procedure D-1559 and the loading strips specified in D-4123 to determine the tensile strength of the asphalt mix. In this study, tests were conducted on specimens obtained from pavement cores. The purposes of the strength tests are:

1. Determine if the mixes experiencing TDC show abnormally low tensile strengths.

2. Determine relative fatigue performance of the mixtures.

The second point is possible because tensile strength is an indicator of fatigue performance of the mixture.

10.2.1   Indirect Tensile Strength

ITST were conducted on specimens from cores drilled from 11 test sites. Table 4.28 summarizes the test data for specimens obtained from the top (surface)

portion of the pavement cores. It is important to note the indirect tensile strength of compacted asphalt is typically 200-psi. The measured strengths of the asphalt mixtures are all substantially lower than 200-psi, with the exception of those obtained from US-41, which showed 185-psi strength. This indicated that the compacted mixtures are substantially weaker than would be expected. It also indicates that the ability of the mixtures to resist fatigue cracking is severely impaired.

The mixture obtained from US-27 also shows very low strength, but no TDC was found in the field. However, this pavement is only 2 years old. It is likely, based on these results, that this pavement will develop TDC in the near future. The pavement is being monitored for the appearance of cracks.

Specimens obtained from US-41 test section 1, test sites 1 and 2 show high strengths compared to specimens obtained from other test sites. However, the TDC on US-41 is occurring in an area of medium segregation. All cores were drilled in non-segregated and non-distressed areas. Hence, no measurement of the segregated pavement strength was obtained. It is reasonable to assume that the segregated areas, in which the distress is occurring, has lower strengths than the surrounding non-segregated areas. This situation is typical for all pavements investigated in this study. The loss of strength is especially important when the non-segregated mix strength is already low, as on M-50 test sections 1 and 2 and on M-55 test section 1, test sites 1 and 2.

Finally, the mixture strength on M-20 test section 1, test site 1 is very low, despite the fact that no segregation was observed in the pavement. This may be due to several problems, two of which are addressed later in this chapter:

1. Poor compaction of the mix leads to low mixture strength.

2. The mix itself is susceptible to environmental impacts such as moisture.

10.2.2   Equivalent Modulus

The indirect tensile test apparatus is equipped to record the deformation of the specimen during loading. From the deformation, an equivalent modulus (EM) of the test specimen was calculated using the following equation:

$$E_M = \frac{P}{L\Delta_v}\left(4.08595 - 0.0417333\upsilon\right) \tag{4.7}$$

Where: E_M = Equivalent modulus (psi);

P = half the maximum load magnitude (lbs);

L = specimen thickness (in);

Δ_v = specimen deformation in the vertical direction (in); and

υ = Poisson's ratio, which was assumed = 0.3

Table 4.28 summarized the ITST data including the EM. Young's modulus values for asphalt mixes typically range from 100 to 1,000-ksi. The EM values range from 28 to 95-ksi. It is not the intention to use the EM values as replacement to Young's modulus. Rather, it can be used to provide a comparative framework of the stiffness of each mix.

The lowest stiffness values were obtained from mixes on M-20 test section 1, test sites 1 and 2 while the highest stiffness belongs to mixes obtained from US-41 test section 1, test sites 1 and 2. Coupled with the strength data, this implies that the mix on M-20 is "soft and weak" while the mix on US-41 is "strong and hard."

11.0   EXTRACTION OF AGGREGATE

The purpose of the aggregate extraction was twofold:

1. Conduct sieve analysis on the recovered aggregate to determine the gradation of the pavement.

2. Determine the asphalt content of the recovered cores.

Extraction of aggregate was conducted using a forced air ignition oven heated to $450^{o}C$. At this temperature, the asphalt cement was burned off, leaving the dry aggregate, which was sieved. Table 4.29 summarizes results of the sieve analysis.

Gradation is the ultimate indicator of segregation. If the mixture gradation varies across the site, then by definition, the mixture is segregated. Also, asphalt content is an indicator of segregation, which can be determined by weighing the specimens before and after incineration. Finally, knowing the exact mixture properties is useful in manufacturing test specimens.

11.1 Gradation Analysis

Gradation analysis on the recovered aggregate was conducted in accordance with ASTM standard test procedure D-5444. In each analysis, the gradations of cores from

visibly segregated and non-segregated areas were compared to the job-mix formula

(JMF).

Table 4.29 Sieve analysis of extracted aggregate and asphalt content

| Sieve number	Sieve opening size (mm)	Test site designation number					
		20411-11		20411-12	30552-11		30552-12
		Seg	Non-Seg	Seg	Seg	Non-Seg	Non-Seg
1	25.4	100.0%	100.0%	100.0%	100.0%	100.0%	100.0%
0.75	19.05	100.0%	100.0%	100.0%	100.0%	100.0%	100.0%
5	12.7	94.3%	96.4%	94.6%	98.0%	98.4%	99.0%
0.375	9.525	75.5%	82.8%	77.1%	86.3%	91.2%	91.1%
#4	4.76	45.6%	57.9%	50.6%	53.7%	64.5%	64.1%
#8	2.38	31.3%	43.4%	38.1%	36.6%	46.5%	46.2%
#16	1.19	22.4%	33.5%	30.3%	28.9%	36.7%	36.5%
#30	0.59	21.1%	25.6%	23.5%	23.0%	28.6%	28.1%
#50	0.3	10.5%	14.8%	15.0%	11.9%	13.7%	11.1%
#100	0.149	6.2%	6.4%	7.3%	5.6%	5.8%	4.8%
#200	0.074	2.0%	0.9%	3.5%	3.7%	3.6%	2.6%
%AC		7.1%	6.0%	5.6%	5.0%	6.5%	6.4%

Table 4.29 (cont'd) Sieve analysis of extracted aggregate and asphalt content

| Sieve number	Sieve opening size (mm)	Test site designation number					
		30202-11		30202-12		30502-21	
		Cracked	Non-cracked	Cracked	Non-cracked	Seg	Non-Seg
		100.0%	100.0%	100.0%	100.0%	100.0%	100.0%
0.75	19.05	100.0%	100.0%	100.0%	100.0%	100.0%	100.0%
5	12.7	100.0%	99.8%	99.8%	99.9%	98.6%	98.6%
0.375	9.525	94.4%	95.3%	93.3%	94.8%	78.6%	90.0%
#4	4.76	64.0%	67.2%	68.9%	70.3%	40.3%	57.6%
#8	2.38	46.1%	47.7%	48.4%	50.6%	34.5%	40.4%
#16	1.19	35.9%	36.0%	37.4%	37.2%	26.0%	30.6%
#30	0.59	27.2%	27.1%	28.4%	28.1%	18.6%	22.6%
#50	0.3	12.7%	12.1%	13.8%	13.2%	9.8%	13.9%
#100	0.149	4.6%	3.4%	5.2%	5.0%	4.2%	7.3%
#200	0.074	2.9%	1.6%	2.9%	2.8%	1.9%	4.5%
%AC		5.7%	7.1%	6.8%	6.4%	7.5%	6.8%

Gradation comparisons for US-41, test section 1, test sites 1 and 2 (20411-11, 20411-12), M-20, test section 1, test sites 1 and 2 (30202-11, 30202-12) and M-55, test section 1, test sites 1 and 2 (30552-11, 30552-12) are shown below in Figures 4.37 through 4.39, respectively. Gradation differences in specimens from US-41 and M-55 (20411-11, -12 and 30552-11, -12) indicate segregation consistent with that observed in the field. On US-41, test section 1, test site 1 (20411-11), the segregated specimens show a difference of gradation of about 12% on the number 4 and number 8 sieves. On US-41, test section 1, test site 2 (20411-12), the differences on the number 4 and number 8 sieves are less severe but still noticeable at 5.7% and 7.3%, respectively. On M-55, test section 1, test site 1 (30552-11), the differences on the number 4 and number 8 sieves were 10.8%, and 9.8%. On M-55, test section 1, test site 2 (30502-21), the differences in the number 4 and number 8 sieves were 17.2% and 5.9%. Gradation differences are not apparent on M-20 (30202-11 and 12) and segregation was not observed in the pavement.

11.2 Asphalt Content

As previously mentioned, asphalt content may be used as an indicator of segregation or to detect dry mixtures. The measured asphalt contents are shown in Table 4.29. As can be seen, the measured asphalt contents are inconclusive of segregation. On 30502-21 and 20411-11, the asphalt content of the segregated areas is actually greater than that of the non-segregated areas. Although the pavement on M-20 showed no visually identified segregation, the cores were incinerated and the recovered aggregate were sieved. Results of the sieve analysis confirmed non segregation. In this study, the asphalt contents did not provide any conclusive evidence of segregation. The data were
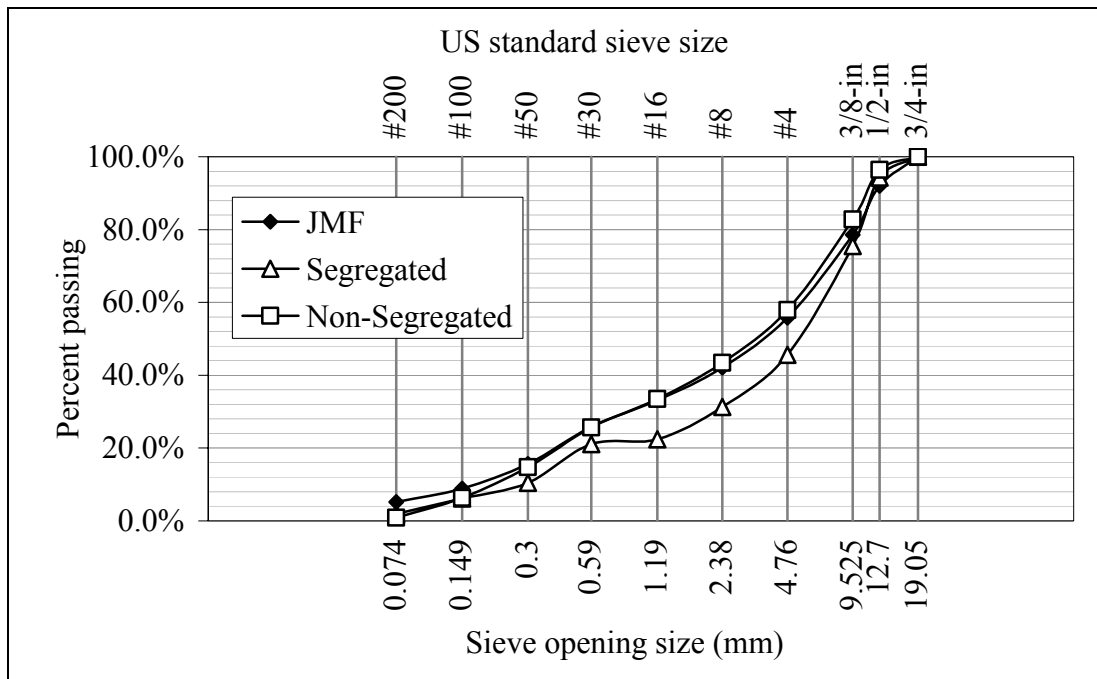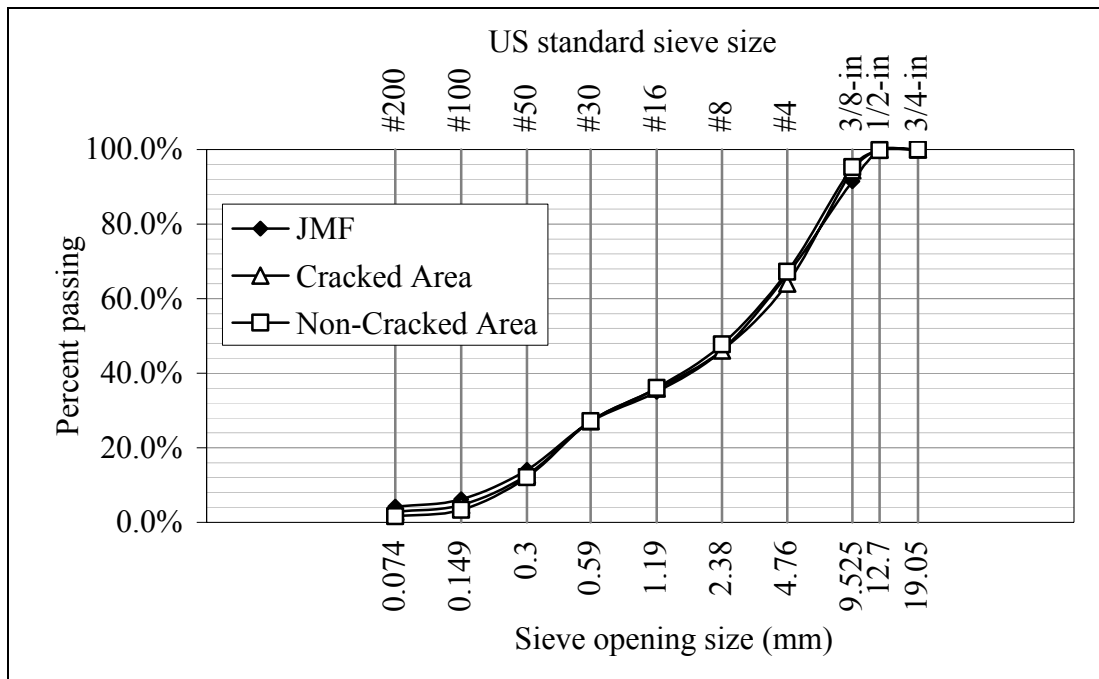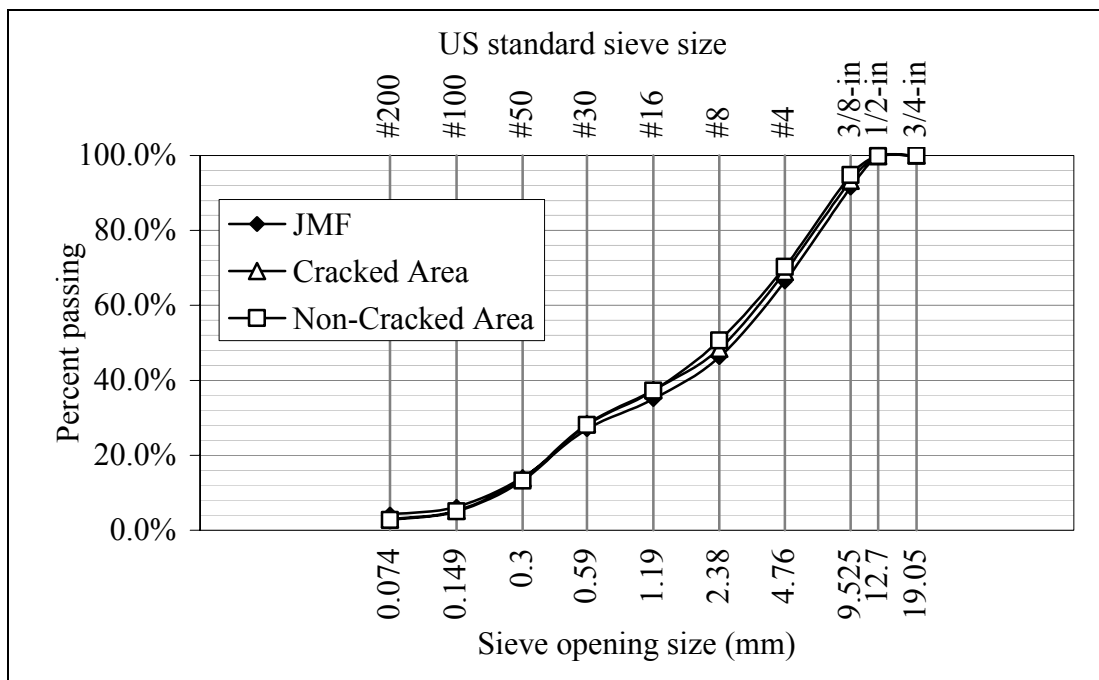
(a) Test site 1 (20411-11)
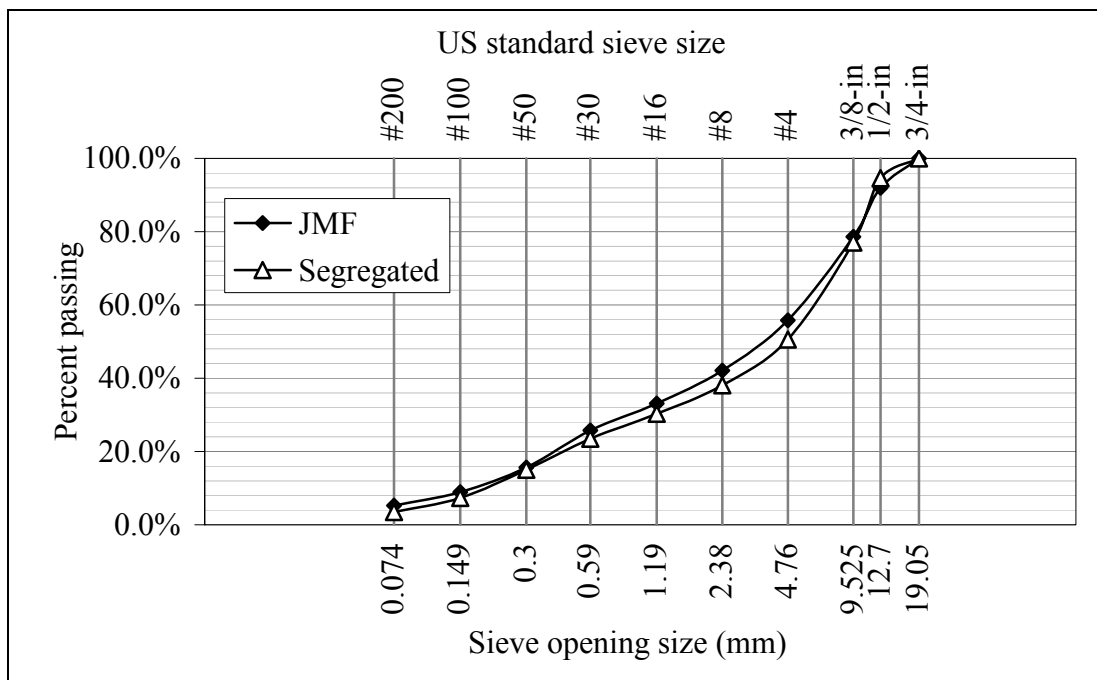
(b) Test site 2 (20411-12)

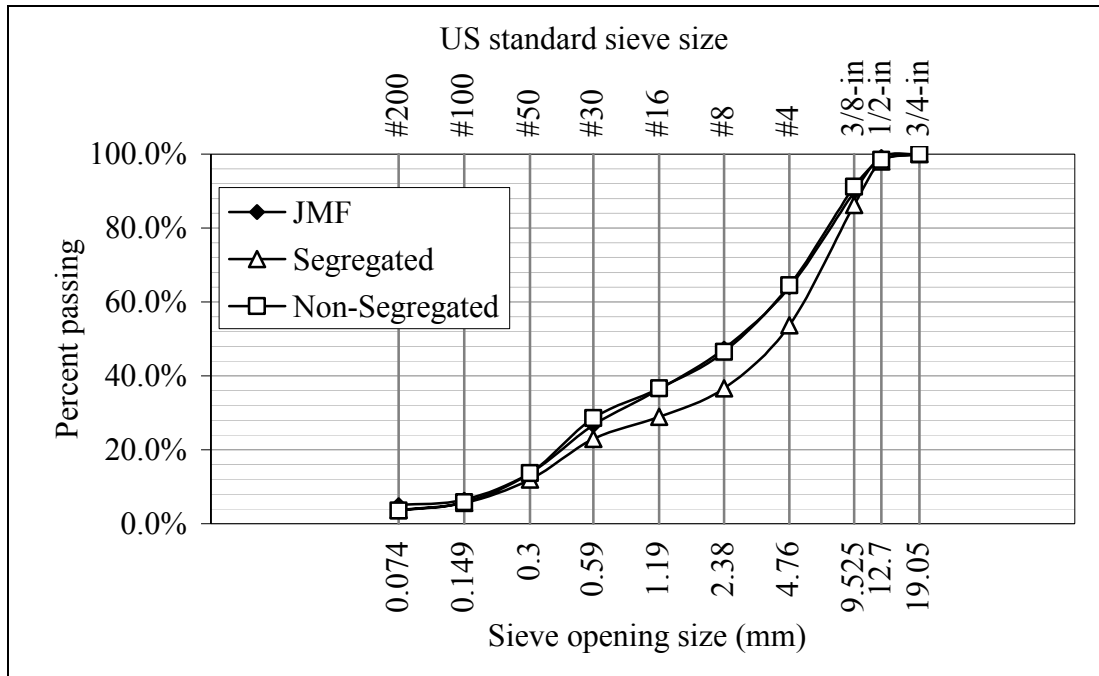Figure 4.37 Gradation analysis of US-41, test section 1
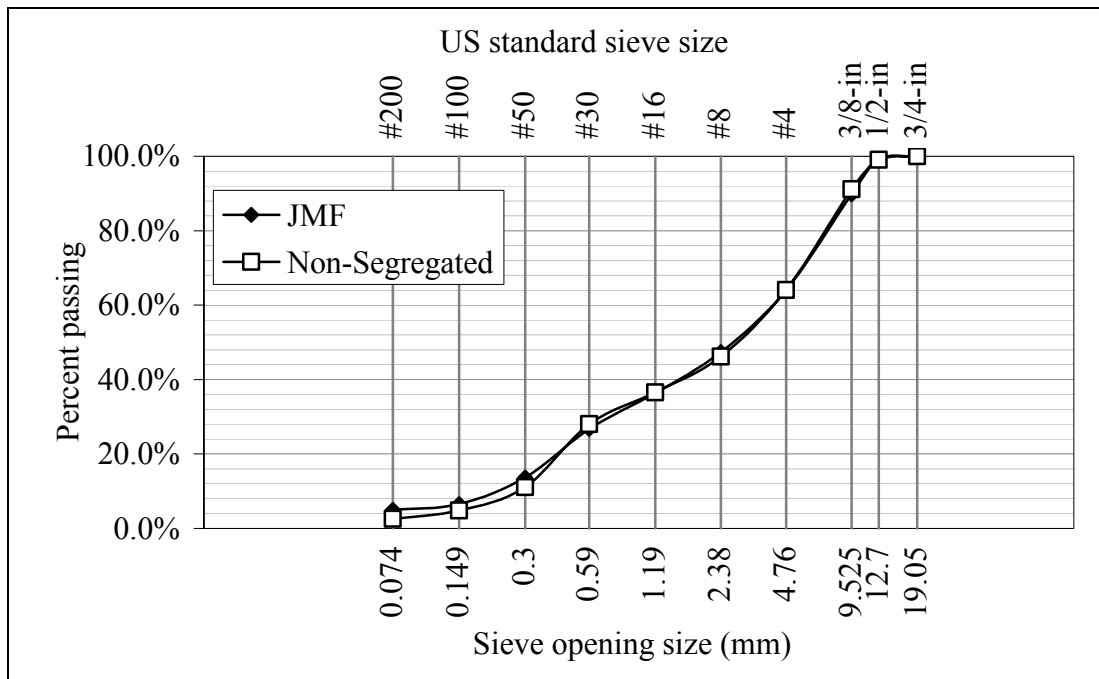
(a) Test site 1 (30202-11)

(b) Test site 2 (30202-12)

Figure 4.38 Gradation analysis of M-20, test section 1

(a) Test site 1 (30552-11)

(b) Test site 2 (30552-12)

Figure 4.39 Gradation analysis of M-55, test section 1

mainly used to aid in the mixing of laboratory test specimens as discussed in section 13.0 below.

It should be noted that the asphalt content data were obtained through incineration of the asphalt cores by weighing the sample before and after incineration. Loss of fines through the chimney may have contributed some errors in the data although the asphalt content data are very reasonable and consistent with MDOT specifications.

12.0   MOISTURE SUSCEPTIBILITY TESTING

The primary objective in the compacting of laboratory test specimens was to study the effect of segregation on the tensile strength of the mix. Several of the pavements exhibiting TDC also show segregation, the presence of which was confirmed by gradation analyses. Although the strength and hence the fatigue performance tends to decrease with increasing severity of segregation, researchers investigating the effects of segregation often use aggregate gradations that are much more extreme than those observed in this study.

Small changes in gradation, especially in the loss of fine materials as is often observed on segregated pavements can result in increases in the air void contents of the mix. This accelerates aging/hardening of the binder, and opens the surface of the pavement to environmental damage. To investigate the loss of tensile strength of segregated and non-segregated mixtures due to the impact of moisture, moisture susceptibility tests were conducted according to ASTM-4867M (1994 Annual Book of ASTM Standards).

Test specimens for moisture susceptibility tests were compacted in the laboratory according the procedure outlined in chapter 3, section 5.0. For each mix included in this

study, at least 14 specimens were made; half of those were representative of the JMF or non-segregated (control) mix in the field, and the other half were representative of segregated mix. The mass of each specimen was set at 1000-g of aggregate, plus asphalt cement to bring the total mass of each specimen to between 1040-g and 1065-g. This mass is consistent with a 100-mm diameter specimen compacted to about 60-mm in height. The 14 specimens were divided into five triplicate groups as follows:

1. Three specimens were made in accordance with the JMF gradation and asphalt content and were not subjected to moisture conditioning

2. Three specimens were made in accordance with the JMF gradation and asphalt content and were subjected to moisture conditioning

3. Three specimens were made in accordance with the segregated gradation and asphalt content and were not subjected to moisture conditioning.

4. Three specimens were made in accordance with the segregated gradation and asphalt content and were subjected to moisture conditioning.

5. Two specimens, one from the control or JMF gradation and asphalt content and the other from the segregated specimens, were used to determine the theoretical maximum specific gravity of the mix.

Each specimen was then subjected to an indirect tensile strength test. According to the test procedure, the mix is considered susceptible to moisture if the retained strength ratio falls below 90%. The calculation for retained strength is as follows:

$$\text{RSR} = \frac{S_c}{S} \times 100\% \tag{4.8}$$

Where: RSR = retained strength ratio;

           S = indirect tensile strength of the compacted mix; and

S_c = conditioned indirect tensile strength of the compacted mix.

The retained indirect tensile strengths of the non-segregated and segregated mixtures were compared to determine if segregation in the field was responsible for a significant loss in tensile strength. For these experiments, three different mixes were tested:

1. 4B mix, the gradations and asphalt contents were obtained from M-55. The 4B mix is prevalent among the test sites exhibiting TDC.

2. 4C mix which was obtained from a variety of sources. The 4C mix is also prevalent among test sites exhibiting TDC.

3. 4E10 , the gradations and asphalt contents were obtained from I-75. The 4E10 is a common surface course SUPERPAVE mixture used on rubblized pavements.

Figure 4.40 depicts the aggregate gradations of the three mixes. Results of the tests are shown in Figure 4.41. Figure 4.41a shows the average indirect tensile strengths of triplicates for three AC mixes, while Figure 4.41b shows the percent retained strength relative to the unconditioned specimens. These results are discussed for each mix in the following sections.

12.1 4B Mixture

The laboratory mix design for the 4B mix was obtained by incinerating field cores extracted from the pavement on M-55 and the quality control data. The mixes were designed according to the JMF, and to the segregated gradation and asphalt content
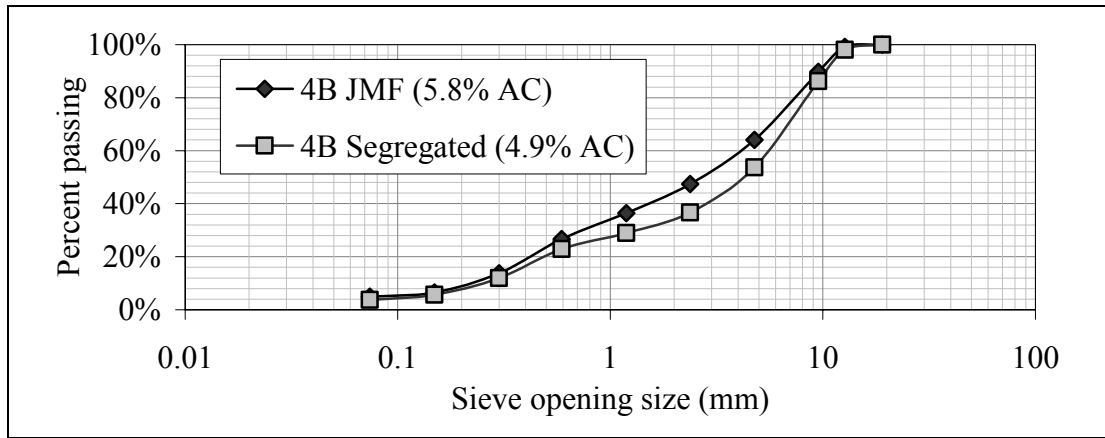
(a) 4B
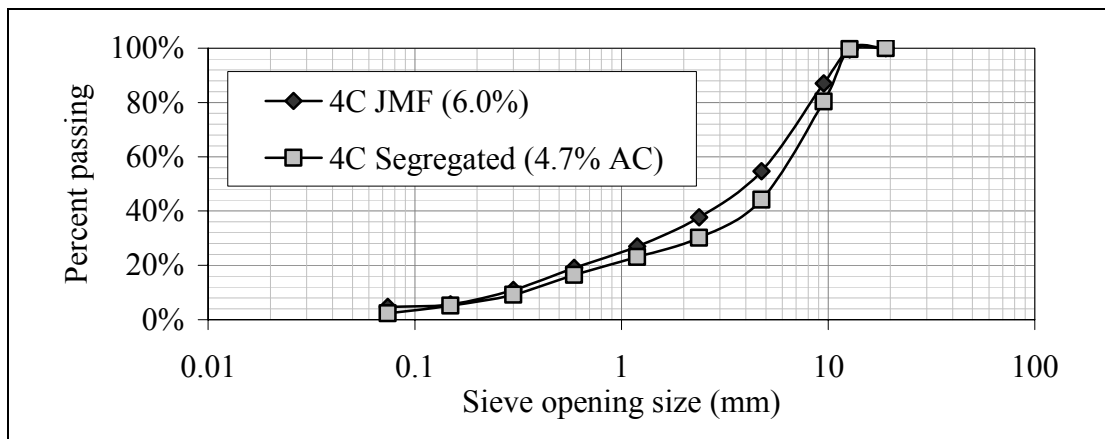
(b) 4C
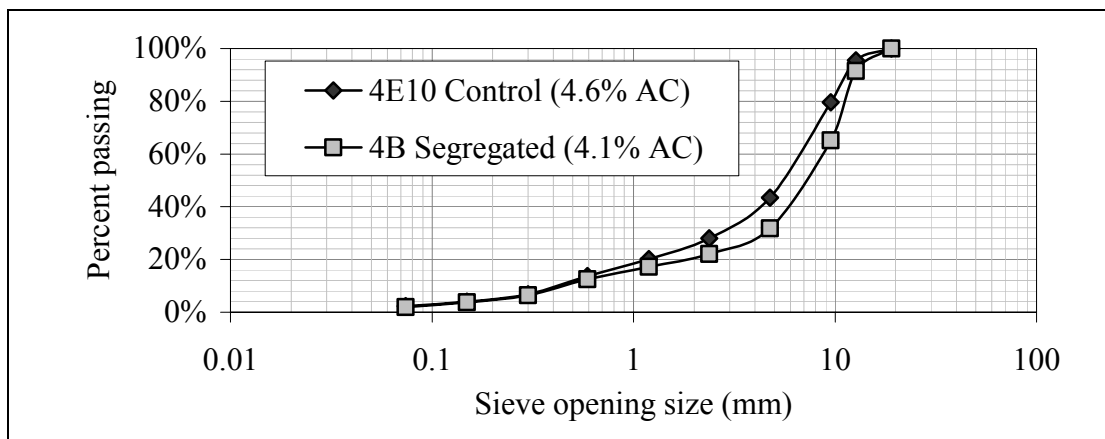
(c) 4E10

Figure 4.40 Gradations of mixtures used in moisture susceptibility tests
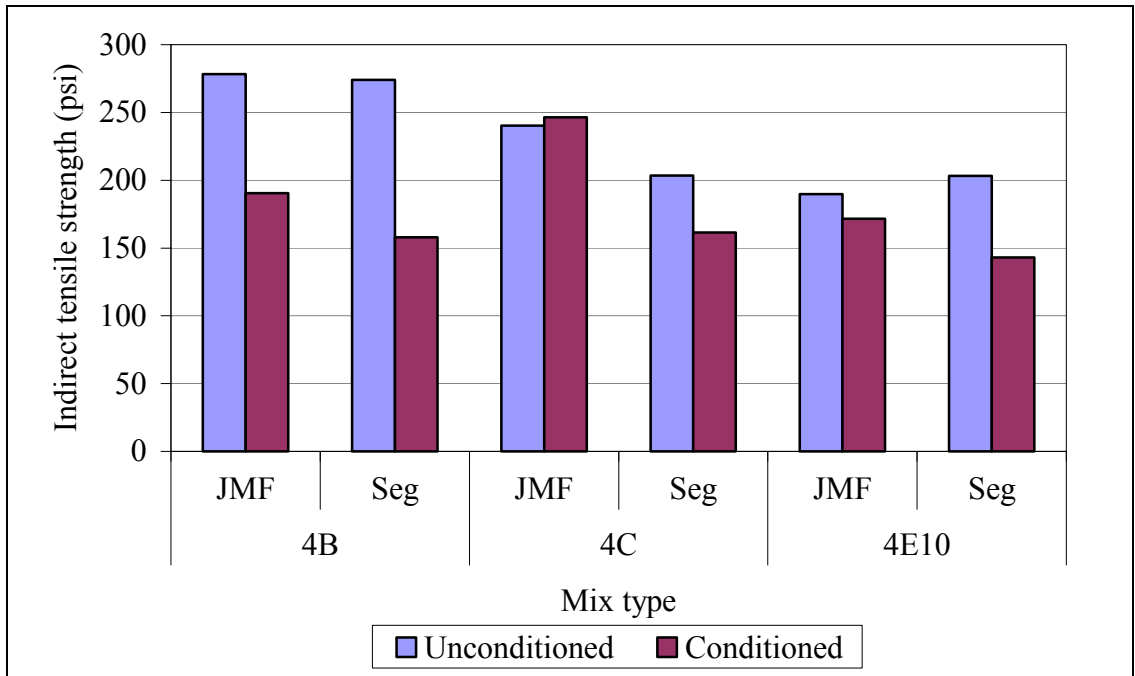
(a) Average indirect tensile strengths of triplicates
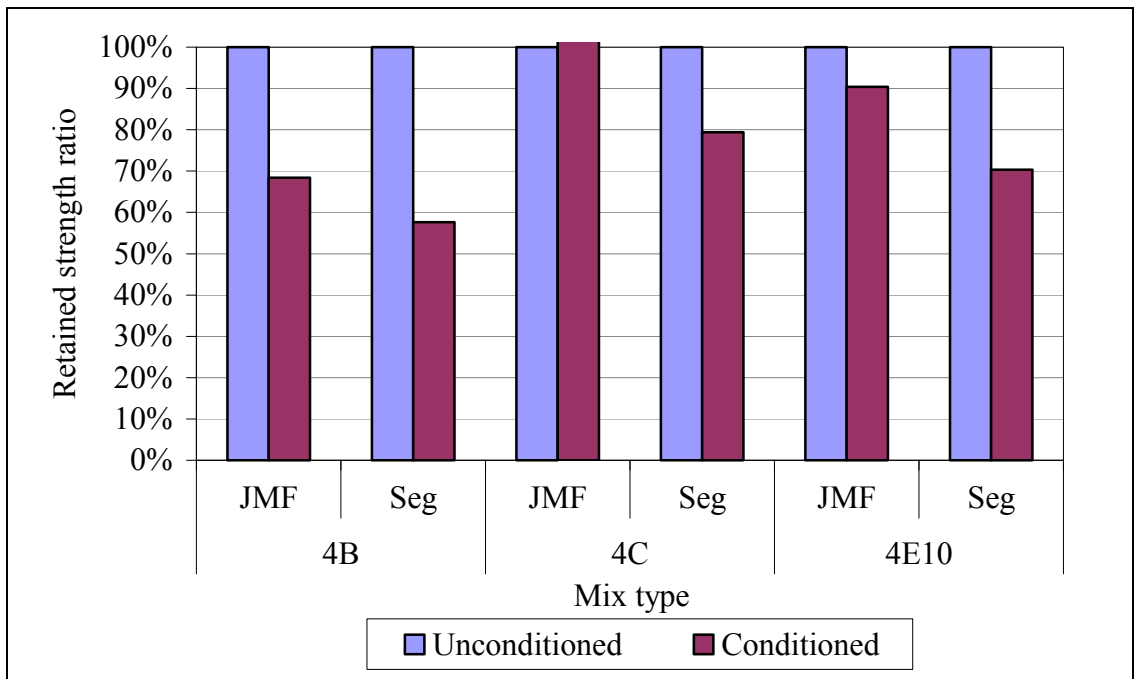
(b) Retained strength ratio of triplicates for 3 AC mixes

Figure 4.41 Average indirect tensile strength and averaged retained strength ratio of unconditioned and conditioned triplicates of 3 AC mixes

obtained by incinerating pavement cores. The two gradations used in this analysis are shown on Figure 4.40a.

Comparison between the test results can be seen in Figure 4.41. As can be seen, the unconditioned tensile strengths between the JMF and the segregated samples are for all purposes identical. This runs contrary to the results presented by Khedaywi and White and Brown et al. The gradations used by these researchers were extremely segregated, and cannot be regarded as representative of the segregation observed on M-55 and other pavements.

The data in Figure 4.41b indicate that after moisture conditioning, the retained strength of the JMF is about 68 percent of the unconditioned JMF. Whereas the retained strength of the segregated mix is about 58 percent relative to the unconditioned segregated mix. The two observations indicate that the 4B mix is moisture susceptible and segregation accelerated moisture damage. Therefore, even if the mixture on M-55 was not segregated to any degree, the strength of the mix, and therefore the fatigue resistance, would be compromised by the seasonal freeze-thaw cycles. This observation may explain why several pavements (M-20 in particular) show no segregation but exhibit TDC. The surface course on M-20 is also a 4B mix. Recall that the observed tensile strength of unconditioned specimens obtained from M-20 exhibited lower than typical tensile strengths (93.4-psi for test site 1 and 82.8-psi for test site 2). The results of the 4B indicate that moisture susceptibility is the likely cause of TDC.

12.2 4C Mixture

The laboratory mix design for the 4C mix was obtained from data collected by Chang and quality control data from Michigan Avenue in Jackson. The mix gradations were obtained from JMF and by incineration of recovered cores. The asphalt contents were obtained from the JMF and by equivalent binder film thickness calculations. The two gradations used in this analysis are shown on Figure 4.40b.

A comparison between the non-conditioned JMF and segregated samples are shown in Figure 4.41. Unlike the 4B mixture, there is a noticeable difference in strength (15%) between the JMF and segregated samples. Comparison of the JMF and segregated mixtures after moisture conditioning shows that the segregated and conditioned mixture has approximately 66% of the strength of the conditioned JMF mix. This indicates that the segregated mixture is more susceptible to moisture damage than the JMF, which was expected.

For the JMF and segregated mixtures subjected to moisture conditioning, the segregated mix shows a significant reduction in the tensile strength due to moisture conditioning. In this case, the tensile strength was reduced by an average of 21%. Unlike the 4B mixture, the tensile strength of the JMF mix before and after conditioning is essentially identical. This indicates that the 4C mixture is not susceptible to moisture damage. It has been shown however, that even relatively mild segregation in the 4C mix may result in a significant loss (33%) of strength over the JMF mixture.

12.3 4E10 Mixture

The laboratory mix design for the 4E10 mix was obtained from data collected by Chang and quality control measurements on I-75 near Rondo. The mix gradations were obtained from incineration of recovered cores. In this case, the JMF gradation was replaced by a control gradation observed in the field. This choice was made because significant differences occur in the small particles sizes between the JMF and the actual pavement. The asphalt contents were obtained from the JMF and by equivalent binder film thickness calculations. The two gradations used in this analysis are shown on Figure 4.40c along with the JMF gradation.

The behavior of the 4E10 mixture is similar to that of the 4C mixture, as is evidenced in Figures 4.41. The non-conditioned segregated mixture actually shows a higher tensile strength (7%) than the non-conditioned, non-segregated mixture but also shows a significantly higher loss of tensile strength due to moisture conditioning. The segregated mixture lost approximately 30% of its strength due to moisture damage, while the non-segregated mixture lost only about 10%. Hence, the test results indicate that the segregated mixture is susceptible to moisture damage.

13.0   SUMMARY OF DATA ANALYSES

Results of field and laboratory investigations and the results of the data analyses are presented and discussed. Field investigation includes distress survey, nuclear density and FWD testing, and pavement coring. The laboratory investigation includes specific gravity testing, ITCLT, ITST, incineration of field cores and the effects of segregation and moisture damage on the tensile strengths of three asphalt mixtures.

CHAPTER 5

SUMMARY CONCLUSIONS AND RECOMMENDATIONS

1.0   SUMMARY

Top-down cracks (TDC) are longitudinal and/or transverse cracks that initiate at the
pavement surface and propagate downward and outward. They have been
increasingly observed in flexible pavements throughout the state of Michigan. TDC
are usually manifested as longitudinal cracks appearing just outside the wheel paths.
Over time, they form an extensive network of longitudinal cracks connected by short
transverse cracks, which ultimately reduce the life of the pavement. Currently, no
pavement design method is capable of predicting or analyzing top-down cracking
potential although efforts are being made to include such model in the new
mechanistic-based AASHTO design procedure.

TDC adversely affect pavement performance. Hence, understanding the factors that
enhance their potential would be the first step that needs to be taken to improve the
service life of the pavements. This could be accomplished through seminars and short
courses as to differentiate between TDC and bottom-up cracks and to identify TDC in
the field. Pavements showing high TDC potential or exhibiting TDC initiation should
immediately be subjected to preventive maintenance actions. Such actions include
chip seal, micro-surfacing, thin overlay (about 1-inch), or mill and fill.

 To determine the causes of TDC, this study was initiated by the Michigan
Department of Transportation and the Pavement Research Center of Excellence at

Michigan State University under the auspices of the Thompson Scholars program, which is directed by the Michigan Asphalt Paving Association. The study included extensive field and laboratory investigations of various pavements exhibiting TDC. The main objective was to verify the hypothesis that TDC are fatigue cracks that are formed due to high tensile stress relative to the low tensile strength of the AC mix at the pavement surface.

Pavements suspected of exhibiting TDC were identified and were subjected to field investigation. Over the course of the study, eighteen test sites were investigated; twelve flexible and six rubblized pavements. For each test site, a manual distress survey was conducted and the pavement was subjected to FWD testing and coring to verify the existence of TDC. On some test sites, nuclear density tests were also conducted to verify the existence of segregation.

The manually collected distress data were analyzed against the various degrees of segregation. A TDC propagation model was developed and presented.

In the laboratory, the cores were carefully measured and the overall density of the core was determined. Then, the cores were subjected to ITCLT and ITST after which they were incinerated to determine the AC content and to recover the aggregates and determine their gradation. The data were examined against the nuclear density reading and the visual observations of segregation. For most cases, the three sets of data agreed.

Laboratory compacted test specimens of three asphalt mixes were made according to the JMF and to the asphalt content and aggregate gradation obtained from

incinerated cores. Some test specimens were subjected to moisture susceptibility and then to ITST while others were subjected to ITST directly.

The FWD data were used to backcalculate the pavement layer moduli using the new algorithm and procedure that were developed by Svasdisant. Results of the backcalculation were used as input to mechanistic analyses. The data were also used to examine the repeatability of the data and the linearity of the pavement response to load.

The 2-D and 3-D mechanistic analyses were conducted by Svasdisant to assess the sensitivity of the load-induced tensile stresses at the AC surface and bottom. Tire-pavement interaction data were obtained from the tire industry and used in the 3-D analyses to determine their impact on the lateral stresses induced at the AC surface and bottom.

Finally, Svasdisant obtained pavement temperature data from MDOT and used it to calculate daily and yearly variations in thermal stresses. His results are included in this dissertation for completion.

2.0   CONCLUSIONS

Based on the field and laboratory investigations, on data analyses and on the results of the 2-D and 3-D mechanistic analyses, the following conclusions were drawn:

1. TDC follows predictable patterns of development. The development can be divided into three phases as stated in Chapter 4 (page 106).

2. TDC can be divided into three different categories; longitudinal, transverse and in segregated areas. Each category has different causes (see chapter 2).

3. A TDC identification procedure was developed and verified. The procedure could be used by State highway agencies to identify TDC and to select proper pavement rehabilitation options.

4. Regardless of the mix type, segregation increases moisture damage potential. Moisture damage alone causes as much as 32 percent reduction in the tensile strength of the asphalt mix; whereas segregation alone causes as much as 15 percent reduction in strength. Finally, segregation and moisture damage cause as much as 42 percent reduction in the tensile strength.

5. Most TDC were observed in segregated pavements although few were found outside the segregated areas or in non-segregated pavements.

6. The main cause of TDC in segregated areas is the low tensile strength of the AC mix which is affected by segregation and moisture damage.

7. For non-segregated pavements, the main causes of TDC are the tensile stress induced by the tire-pavement interaction and relatively low tensile strength of the AC mix.

8. TDC are mainly caused by load coupled with strength reduction due to low asphalt contents (dry mix), segregation, moisture damage or combination thereof.

9. For segregated areas along flexible pavements, a TDC propagation model was developed and tested based on pavement surface age and degree of segregation.

10. Nuclear density tests can be used to confirm visual identification of segregation. On the other hand, the AC content was not a conclusive indicator of segregation in this study.

11. TDC initiation and propagation are independent of the pavement cross-section or the AC thickness.

12. Rubblized pavements show more variations in the FWD deflection than conventional flexible pavements. This is mainly due to variation in the structural capacity along and across the pavement. Said variation is the direct results of the rubblization operation which produce two distinct layers with variable thicknesses; a rubblized layer at the top and a fractured concrete layer at the bottom.

13. The depth to stiff layer used in backcalculation can be better estimated by using Bousinessq's equation and backcalculation of layer moduli using 3 and 4-layer systems.

14. Cyclic cold temperatures subject the asphalt binder to high tensile strength and hardening. Over time this causes transverse TDC, which are known as temperature cracks.

3.0   RECOMMENDATIONS

Based on the results and conclusions of this study, it is strongly recommended that:

1. Crack initiation and propagation be included in the design/build warranty standards.

2. In the PMS database, differentiate between TDC and regular cracks. This can be achieved by implementing the TDC identification criteria developed in this study. The reason for such differentiation is that preventive maintenance and rehabilitation actions for pavements exhibiting TDC are much different than those exhibiting regular cracks (bottom-up cracks).

3. All asphalt mixes should be evaluated regarding segregation, moisture susceptibility and asphalt contents (to prevent dry mixes).

4. Explore more in depth the effects of segregation and aging on the properties of the asphalt mixes.

REFERENCES

1. Annual Book of ASTM Standards - Section 4 - Construction, 1994, Vol. 04.03 Road and Paving Materials; Paving Management Technologies, The American Society for Testing and Materials, Philadelphia, Pennsylvania.

2. American Association of State Highway and Transportation Officials, "AASHTO Guide for Design of Pavement Structures", pp. 106-112, Washington D.C., 1993

3. Bensalem, A., A. J., Broen, M. E. Nunn, D. B. Merrill, and W. G. Lloyd, "Finite Element Modeling of fully Flexible Pavements: Surface Cracking and Wheel Interaction," *Proceedings of the Second International Symposium on 3D Finite Element For Pavement Analysis, Design, and Research,* West Virginia*,* 2000, pp. 103-121

4. Bonaquist, R., Surdahl, R., and W. Mogawer, "Effect of Tire Pressure on Flexible Pavement Response and performance," In *Transportation Research Record 1227*, TRB, National Research Council, Washington, D.C., 1989, pp 97-106.

5. Brown, E.R. and C.E. Bassett, "Effects of Maximum Aggregate Size on Rutting Potential and Other Properties of Asphalt-Aggregate Mixtures," In *Transportation Research Record 1259*, TRB, National Research Council, Washington, D.C., 1990, pp. 107-119

6. Brown, E.R., Ronald, C., and J.R. Brownfield, "Investigation of Segregation of Asphalt Mixtures in the State of Georgia," In *Transportation Research Record 1217*, TRB, National Research Council, Washington, D.C, 1989, pp. 1-8

7. Button , J.W., Perdomo, D., and R.L. Lytton, "Influence of Aggregate on Rutting in Asphalt concrete Pavements," In *Transportation Research Record 1259*, TRB, National Research Council, Washington, D.C., 1990, pp. 141-152

8. Chang, C.M., "Detecting Segregation in Bituminous Pavements and Relating its Effects to Performance," A Ph.D. Thesis, Department of Civil and Environmental Engineering, Michigan State University, 2000.

9. Chapuis, R.P. and A. Gatien, "Temperature Dependent Tensile strength of Asphalt Mixtures in Relation to field Cracking Data," ASTM STP 1265, 1995, pp. 180-193

10. Chatti, K., Kim, H.B., Un, K.K., Mahoney, J.P., and C.L. Monismith, "Field Investigation into Effects of Vehicle Speed and Tire Pressure on Asphalt Concrete Pavement Strains," In *Transportation Research Record 1539*, TRB, National Research Council, Washington, D.C., 1996, pp 66-71

11. Clark, S. M., Mechanics of Pneumatic Tires, U.S. Department of Transportation, National Highway Traffic Safety Administration, Washington, D. C., 1981

12. Dai, S.T., Van Deusen, D., Beer, M., Rettner D., and G. Cochran, "Investigation of Flexible Pavement Response to Truck Speed and FWD Load through Instrumented Pavements," Proceedings of the 8th International Conference on Asphalt Pavements, Seattle, 1997, pp. 141-160

13. Dauzats, M., and A. Rampal, "Mechanism of Surface Cracking in Wearing Courses," Proceedings of the 6th International Conference on Asphalt Pavements, Ann Arbor, 1987, pp. 232-247

14. De Beer, M. and C. Fisher, "Contact Stresses of Pneumatic Tires Measured with the Vehicle-Road Surface Pressure Transducer Array (VRSPTA) System for the University of California at Berkley (UCB) and the Nevada Automotive Test Center (NATC)", Volume 1 and 2, 1997

15. De Beer, M., Fisher, C., and F.J. Jooste, "Determination of Pneumatic Tyre/Pavement Interface Contact Stresses Under Moving Loads and Some Effects on Pavement with Thin Asphalt Surfacing Layers," Proceedings of the 8th International Conference on Asphalt Pavements, Seattle, 1997, pp. 179-227

16. Gerritsen, A.H., van Gurp, C.A.P.M., van der Heide, J.P.J., Molenaar, A.A.A., and A.C. Pronk, "Prediction and Prevention of Surface Cracking in Asphaltic Pavements," Proceedings of the 6th International Conference on Asphalt Pavements, Ann Arbor, 1987, pp. 378-391

17. Groenendijk, J., "Accelerated testing and Surface Cracking of Asphaltic Concrete Pavements," A PhD dissertation. Department of Civil Engineering, Delft University of Technology, the Netherlands, 1998.

18. Harichandran R. and G.Y. Baladi, "Integrated Material and Structural Design Method for Flexible Pavements," Volumes I and II, final report, FHWA/RD-88/109 and 110, Washington, D.C. September 1987

19. Harvey, J.T., and B.W. Tsai, "Effects of Asphalt Content and Air Void Content on Mix Fatigue and Stiffness." In *Transportation Research Record 1543*, TRB, National Research Council, Washington, D.C., 1996, pp. 38-45

20. Heukelom, W., "Observations on the Rheology and Fracture of Bitumens and Asphalt Mixes," Proceedings of the Association of Asphalt Paving Technologists, Volume 35, 1966, pp. 358-399

21. Hiltunen D.R. and R. Roque, "A Mechanics-Based Prediction Model for Thermal Cracking of Asphalt Concrete Pavements," Proceedings Association of Asphalt paving Technologists, Volume 63,1994, pp.81-117

22. Himeno, K., Ikeda, T., Kamijima, T., and T. Abe, "Distribution of Tire Contact Pressure of Vehicles and its Influence on Pavement Distress," Proceedings of the 8th International Conference on Asphalt Pavements, Seattle, 1997, pp. 129-139

23. Huang, Y.H., "Pavement Analysis and Design," Prentice-Hall Inc., New Jersey, 1993.

24. Hugo, F., and T.W. Kennedy, "Surface Cracking of Asphalt Mixtures in Southern Africa," Proceedings of the Association of Asphalt Paving Technologists, Volume 54, 1985, pp 454-501

25. Huhtala, M., Pihlajamaki, J., and M. Pienimaki, "Effects of tires and Tire Pressure on Roads Pavements," In *Transportation Research Record 1227*, TRB, National Research Council, Washington, D.C., 1989, pp. 107-114

26. Jacobs, M., de Bondt, A., Molenaar, A., and P. Hopman, "Cracking in Asphalt Concrete Pavements," Proceedings of the 7th International Conference on Asphalt Pavements, 1992, pp. 89-105

27. Jacobs, M.M.J., Hopman, P.C., and A.A.A. Molenaar, "Application of Fracture mechanics and Principles to Analyze Cracking in Asphalt Concrete (With Discussion)," Proceedings of the Association of Asphalt Paving Technologists, Volume 65, 1996, pp 1-39

28. Jung, D. and T. S. Vinson, "Thermal stress Restrained Specimen Test to Evaluate Low Temperature Cracking of Asphalt-Aggregate Mixtures." In *Transportation Research Record 1417*, National Research Council, Washington, D.C., 1993, pp. 12-20

29. Khedaywi, T.S. and T.D. White, "Development and Analysis of Laboratory Techniques for Simulating Segregation," In *Transportation Research Record 1492*, TRB, National Research Council, Washington, D.C., 1995, pp 36-45

30. Littlefield, G., "Thermal Expansion and Contraction Characteristics Utah Asphaltic Concrete," Proceedings of the Association of Asphalt Paving Technologists, Volume 36, 1967, pp. 673-702

31. Malan, G.W., Straus, P.J., and F. Hugo, "A Field Study of Premature Surface Cracking in Asphalt (With Discussion)," Proceedings of the Association of Asphalt Paving Technologists, Volume 58, 1988, pp 142-162

32. Markwick, A.H.D., and J.H. Starks, "Stresses Between Tire and Road." Journal of the Institution of Civil Engineers, Vol. 16, 1940-1941, pp 309-325

33. Marker, V., "Symposium-Compaction of Asphalt Concrete," *Proceedings of the Association of Asphalt Paving Technologists*, Volume 36, 1967, pp. 288-294

34. Matsuno, S., and T. Nishizawa, "Mechanism of Longitudinal Surface Cracking in Asphalt Pavement," Proceedings of the 7th International Conference on Asphalt Pavements, Nottingham, 1992, pp. 277-291

35. Mohammad, L.N. and H.R. Paul, "Evaluation of Indirect Tensile Test for Determining Structural Properties of Asphalt Mix," In *Transportation Research Record 1417*, TRB, National Research Council, Washington, D.C., 1993, pp. 58-63

36. Molenaar, A.A.A., "Fatigue and Reflective Cracking due to Traffic (With Discussion)," Proceedings of the Association of Asphalt Paving Technologists, Volume 53, 1984, pp 440-474

37. Myers, L.A., Roque, R., and B.E. Ruth, "Mechanisms of Surface-Initiated Longitudinal Wheel Path Cracks in High-Type Bituminous Pavements," Proceedings of the Association of Asphalt Paving Technologists, Volume 67, 1998, pp 401-432

38. Myers, L.A., Roque, R., Ruth, B.E., and C. Drakos, "Measurement of Contact Stresses for Different Truck Tire Types to Evaluate Their Influence on Near-Surface Cracking and Rutting," In *Transportation Research Record 1655*, TRB, National Research Council, Washington, D.C., 1999, pp. 175-184

39. Myers, L.A., Roque, R., and B. Birgisson, "Propagation Mechanisms for Surface-Initiated Longitudinal Wheel Path Cracks," In *Transportation Research Record 1778*, TRB, National Research Council, Washington, D.C., 2001, pp. 113-121

40. Myers, L. and R. Roque, "Top-Down Crack Propagation in Bituminous Pavements and Implications for Pavement management," *Proceedings of the Association of Asphalt Paving Technologists*, Volume 71, 2002, p 651-670

41. Niederquell, M.G., Baladi, G.Y., and K. Chatti, "Rubblization of Concrete Pavements: Field Investigation," In *Transportation Research Record 1730*, TRB, National Research Council, Washington, D.C., 2001, pp. 150-160

42. Pottinger M., "The Three-Dimensional Contact Patch Stress Field of Solid and Pneumatic Tires," Tire Science and Technology, TSTCA, volume 20 number 1, 1992, pp. 3-32.

43. Pottinger, M.G., and J.E. McIntrye, "Effects if suspension Alignment and Modest Cornering on the footprint Behavior of Performance Tires and Heavy Duty Radial Tires," Tire Science and Technology, TSTCA, volume 27 number 3, 1999, pp.128-160.

44. Rickards, I., Goodman, S., Pagani, J., Halim, A.O.A.E., and R. Haas, Practical Realization of a New concept for Asphalt Compaction," In *Transportation Research Record 1730*, TRB, National Research Council, Washington, D.C., 1999, pp. 27-35

45. Roque, R., and B. E. Ruth., "Mechanisms of Modeling of Surface Cracking in Asphalt Pavements," Proceedings of the Association of Asphalt Paving Technologists, Volume 59, 1990, pp. 396-421

46. Roque, R., Myers, L.A., and B. Birgisson, "Evaluating Measured Tire Contact Stresses to Predict Pavement Response and Performance." In *Transportation Research Record 1716*, TRB, National Research Council, Washington, D.C., 2000, pp 73-81

47. Schapery, R. A. and J. T. Tielking. Investigation of Tire-Pavement Interaction During Maneuvering, Vol. 1, Theory and Results, U.S. Department of Transportation, Fedearal Highway Admiistration, Washington, D.C., 1977

48. Schorsch, M., Chang, C.M., and G.Y. Baladi, "Effects of Segregation on the Initiation and Propagation of Top-Down Cracks," accepted for presentation at the TRB annual meeting, Washington, D. C., 2003

49. Shahin, Y., "Design System for Minimizing Asphalt Concrete Thermal Cracking," The 4th International Conference Structure Design of Asphalt Pavement, Ann Arbor, Volume 1, 1977, pp. 920-932.

50. Siddharthan, R.V. and P.E. Sebaaly, "Investigation of Asphalt Concrete Layer Strains from Wide-Base Tires," In *Transportation Research Record 1655*, TRB, National Research Council, Washington, D.C., 1999, pp 168-174

51. Siddharthan, R.V., N. Krishnamenon, M. El-Mously and P.E. Sebaaly, "Investigation of Tire Contact Stress distributions on Pavement Response," Journal of Transportation Engineering, Volume 128, No. 2, 2002, pp. 136-144

52. Soon, S. C., "Tire-Induced Surface Stresses in Flexible Pavements", Accepted for Publication in Transportation Research Record and Presented at TRB Annual meeting, Washington, D.C., 2003.

53. Svasdisant T., Schorsch, M., Baladi, G.Y., and S. Pinyosunun, "Mechanistic Analysis of Top-down Cracks in Asphalt Pavement," Accepted for presentation and publication by the Transportation Research Board, Washington DC, 2001

54. Svasdisant T., and G. Baladi, "Identify Causes for Under Performing Rubblized Concrete Pavement Projects Phase II" Research Report RC-1416, Michigan Department of Transportation, August 2002

55. Svasdisant T., "Analysis of Top-Down Cracking in Rubblized and Flexible Pavements," A Ph.D. Thesis, Department of Civil and Environmental Engineering, Michigan State University, 2003.

56. Tielking, J.T., and M.A. Abraham, "Measurement of Truck Tire Footprint Pressure." In *Transportation Research Record 1435*, TRB, National Research Council, Washington, D.C., 1994, pp 92-99

57. Teilking, J.T. and F.L. Roberts, "Tire Contact Pressure and Its Effect on Pavement Strain." Journal of Transportation Engineering ASCE, Vol. 113, 1987, pp. 56-83

58. Uhlmeyer, J.S., Willoughby, K., Pierce, L.M., and J. P. Mahoney, "Top-Down Cracking in Washington State Asphalt Concrete Wearing Courses," In *Transportation Research Record 1730*, TRB, National Research Council, Washington, D.C., 2000, pp. 110-116

59. Wambura, J.H.G., Maina, J., and H.R. Smith., 'Kenya Bituminous Materials Study," In *Transportation Research Record 1681*, TRB, National Research Council, Washington, D.C., 1999, pp. 129-137

60. Williams, R.C., Duncan, G., and White, T.D., "Hot-Mix Asphalt Segregation: Measurement and Effects." In *Transportation Research Record 1543*, TRB, National Research Council, Washington, D.C., 1996, pp. 97-105

61. Yoder, E.J., and M.W. Witczak, "Principles of Pavement Design 2nd Edition", J. Wiley and Sons, N.Y. NY, 1975

62. Zubeck, H. K. and T. S. Vinson, "Prediction of Low-Temperature Cracking of Asphalt Concrete Mixtures with Thermal Stress Restrained Specimen Test Results," In *Transportation Research Record 1545*, TRB, National Research Council, Washington, D.C., 1996, pp. 50-58